Scour Protection of Offshore Wind Farms

Nielsen, Anders Wedel

Publication date:
2011

Document Version
Publisher's PDF, also known as Version of record

Scour Protection of Offshore Wind Farms

Anders Wedel Nielsen

August 2011

Ph.D. thesis
Section of Coastal, Maritime and Structural Engineering
Department of Mechanical Engineering
Technical University of Denmark
Kgs. Lyngby, Denmark

Contents

Nomenclature

Greek Characters

α	Empirical coefficient
β_0	Inclination of beach
β	Empirical coefficient
ϵ	Dissipation of turbulent kinetic energy
η_b	Equilibrium bed elevation with pile
$\eta_{b,u}$	Equilibrium bed elevation without pile
γ	Empirical coefficient
μ	Dynamic viscosity
ν	Kinematic viscosity
Ω	Mobility number for sediment underneath a scour protection
ω	The angular frequency of the oscillatory flow
Ω_c	Critical mobility number for sediment underneath a scour protection
Φ_b	Dimensionless bed load discharge
ψ	Mobility number
ρ	Density of fluid
σ_U	Root-mean-square of the orbital velocity
τ_0	Bed shear stress
θ	Shields parameter
τ	Shear stress

θ_c Critical Shields parameter

ξ Surf similarity parameter

ζ Mobility number for breaking waves

Roman Characters

A Empirical coefficient

a Empirical coefficient

B Empirical coefficient

b Empirical coefficient

D_p Pile diameter

d_{15} Size of stones (15% fraction)

D Pile diameter, Chapter 4

D Height of armour blocks, Chapter 5

d_{50} Mean size of sediment or particle

$D_{c,15}$ Size of cover stones (15% fraction)

D_c Mean size of cover stones

d_{85} Size of stones (85% fraction)

d Particle size

$D_{c,85}$ Size of cover stones (85% fraction)

D Mean size of cover stones, Chapter 5

D_{cover} Mean size of cover stones

D Mean size of stones, Chapter 3

$D_{c,15}$ Size of filter stones (15% fraction)

D_f Mean size of filter stones

$D_{c,85}$ Size of filter stones (85% fraction)

D_{stone} Mean size of cover stones

e Sinking of cover stones

e_{max}	Maximum sinking of cover stones
f	Emperical coefficient
G	Gap between armour blocks
g	Acceleration of gravity
H	Wave height
h	Water depth at pile
H_0	Deep water wave height
H_b	Wave height at breaking
H_s	Significant wave height
I	Approach pressure gradient
k	Turbulent kinetic energy
KC	Keulegan-Carpenter number
L	Wave length
L_0	Deep water wave length
L_s	Size of scour hole
L_b	Wave length at breaking
L_p	Wave length corresponding to peak period
n	Porosity
N_w	Number of waves
n_c	Porosity of cover layer
N_P	Number of pores
N_c	Number of cover layers
N_f	Number of filter layers, $N_f = t_f/D_f$
n_f	Porosity of filter layer
q	Discharge of water
q	Discharge of sediment (Chapter 6)

Re	Reynolds number
S	Scour depth
s	Specific weight of sediment
S_{max}	Maximum scour depth
S_{eq}	Equilibrium scour depth
SWL	Still Water Level
T	Time scale of sinking (Chapter 2)
T	Wave period
t	Time
T^*	Dimensionless time scale of sinking
t_f	Thickness of filter layer
t_{SP}	Total thickness of scour protection
T_p	Peak period
T_s	Time scale of the scour process
u'	Streamwise velocity fluctuation
U_{m0}	Maximum orbital velocity at the base bottom
U_m	Maximum orbital velocity at the at the bed (Chapter 4)
U_m	Maximum orbital velocity at the top of the armour stones (non-breaking waves)
$\tilde{u}$	Ensamble average of waves
U_{fb}	Friction velocity at the base bottom
U_f	Friction velocity
u	Streamwise velocity
$U_{D/2}$	Velocity a half pile diameter above the bed
U_s	Pore-averaged, phase-resolved r.m.s value of the streamwise fluctuating velocity
U_∞	Undisturbed velocity

U_{fc}	Critical friction velocity
V	Depth averaged current velocity
v'	Crossflow velocity fluctuation
w'	Vertical velocity fluctuation
w_c	Plan-view extension of the scour protection (from upstream to downstream)
w_{cover}	Plan-view extension of the scour protection (from upstream to downstream)
w_s	Plan-view extension of the scour protection (from upstream to downstream)
x	Streamwise coordinate (0 in centre of the pile, positive in the flow direction)
x_b	Distance from breaking point to pile (Chapter 4)
x_{bt}	Distance from breaking point to bar (Chapter 4)
x_p	Distance from top of slope to pile (Chapter 4)
y	Vertical coordinate (0 at the base bottom, positive upwards) (Chapter 6)
y^+	Dimensionless distance from wall
z	Vertical coordinate (0 at the base bottom, positive upwards) (Chapters 2, 3 and Appendix A)

Preface

The present Ph.D. thesis is submitted as part of the requirement for obtaining a Ph.D. degree from the Technical University of Denmark. The Ph.D. has been conducted at the Department of Mechanical Engineering under the main supervision of Professor B. Mutlu Sumer.

I am grateful for the guidance and supervision from Mutlu Sumer, who has excelled in giving a clear goal for the Ph.D. study in its entity, however, still within wide boundaries.

I would also like to thank all other staff in the section of Coastal, Maritime and Structural Engineering for help and interesting discussions throughout the project. Among these special thanks should be given to the co-supervisors professor Jørgen Fredsøe (DTU) and professor Erik Damgaard Christensen (DTU, DHI to September 2010), Assistant Professor Xiaofeng Liu at University of Texas at San Antonio (UTSA) for his help during my visit at UTSA and with the numerical simulations. I will also give special thanks to Adriana Hudecz, Pau Calsapeu, Sebastian Schjelde Ebbe, François Roignant and Ph.D. Martin Dixen who have conducted parts of the experiments reported in this thesis. I will also thank the Ph.D.-students and Post docs. in the Coastal Group: Nilas Mandrup Hansen, Ph.D. Özgür Kirca, Thor Ugelvig Petersen, Ph.D. Niels Gjøl Jacobsen, Kasper H. Kærgaard, Sten Esbjørn Kristensen and Bjarne Jensen, the staff in the laboratorium Henning Jespersen and Jan Larson, the draftsman in the group Liselotte Norup and Helle Christensen who has corrected my English in parts of the thesis. Finally, I would like to thank Statkraft, DHI and Danish Council for Strategic Research (DSF)/Energy and Environment under the programme "Seabed Wind Farm Interaction" (sagnr. 2104-07-0010) for the financial support.

31st of August 2011, Kgs. Lyngby

Anders Wedel Nielsen

This edition of the thesis includes minor corrections to the original thesis used for the assessment for the Ph.D degree. The changes are limited to corrections of spelling, gramma and references. A major part of the thesis consists of manuscripts for journal articles. These manuscripts are now published or in print, some of them with important revisions. The relevant chapters are listed below and details are added in the beginning of the chapters. Chapter 2 was published in December 2011 and a revised version of chapter 5 was published in September 2012. Revised versions of chapter 3 and 4 are accepted for publication and in print. It should be noted that the manuscripts have been improved during the review processes and it is highly recommended to use the published journal articles rather than the manuscripts found in this thesis. This is especially the case for Chapter 5.

15^{th} of October 2012, Charlottenlund

Anders Wedel Nielsen

Abstract

Scour Protection of Offshore Wind Farms

One of the first large offshore wind farms is the Horns Rev 1 Wind Farm in the Danish part off the North Sea. It is located around 20 km of the coast in relatively shallow water. The wind farm was installed and commissioned during 2002. In 2005 a control survey of the scour protections around the foundations showed that the scour protections adjacent to the mono piles sank by up to 1.5 m. This was unexpected and shortly after the survey in 2005 the holes were repaired by adding additional stones. The aim of the thesis is to give an explanation of the sinking at Horns Rev 1 Wind Farm and to describe the processes causing the sinking.

In Chapters 2 and 3, a description of the main processes causing the sinking of a scour protection around a pile if exposed to a current is given, based on results of physical and numerical models. Using the results it is possible to make designs of the scour protection to prevent or estimate sinking of scour protections around mono piles. It is shown that the horseshoe vortex at the base of the pile will penetrate into the scour protection and if strong enough mobilize the base sediment and transport it out of the scour protection where it will be removed by the outer flow. The equilibrium sinking of the scour protection is found for various conditions. It is also found that a fine filter layer can prevent the mobilization of the sediment and therefore the sinking.

In Chapter 4, the scour around mono piles in breaking waves is studied. The scour is found to depend on two parameters: (1) The distance between the breaking point and the pile normalized by the wave length and (2) the breaking wave height normalized by the pile diameter. The maximum scour is found to be approximately 0.65 times the pile diameter. It can be larger than the scour generated by non-breaking waves especially for small KC-numbers. The main reason for the increased scour is found to be turbulence generated by the breaking and is forced to the bottom by the pile.

In Chapter 5, the onset of suction from between armour stones under breaking waves is studied. The critical conditions for onset of suction are determined for several different conditions, regarding wave height and period,

slope of the bed, sediment and cover stone size and number of cover layers. The oblique descending eddies generated by the breaking waves are found to be the main mechanism regarding suction of the base sediment.

In Chapter 6, the flow in and the bed shear stresses under a stone cover under an oscillatory flow is described. The flow velocities and the turbulence are measured in case of one, two and three layers of stones in several pores. The tests showed that the horizontal velocities in the pores are affected by the outer flow approximately one stone diameter into the stone cover. Under this level the horizontal velocities become constant. The bed shear stresses are much smaller than at a smooth bed without stone cover and large variations are observed.

In Chapter 7, the effect of waves on sinking of the scour protection around a mono pile is studied. It is found that the sinking will increase for increasing KC-numbers for a given diffraction parameter. The magnitude of the sinking is found to be comparable with the scour observed around an unprotected pile exposed the same wave conditions.

Resumé

Erosionsbeskyttelse af Havvindmølleparker

En af de første store havvindmølleparker er Horns Rev 1 Vindmøllepark i den danske del af Nordsøen. Den er bygget omkring 20 km fra kysten på relativt lavt vand. Vindmølleparken blev bygget og sat i drift i løbet af 2002. I 2005 viste en kontrol opmåling af erosionsbeskyttelserne rundt om fundamenterne, at erosionsbeskyttelserne nær monopælene havde sat sig op til 1.5 m. Det var ikke forventet og kort efter opmålingen i 2005 blev hullerne repareret med ekstra sten. Formålet med denne afhandling er at give en forklaring på sætningerne på Horns Rev 1 Vindmøllepark og at beskrive processerne der fører til sætningerne.

I Kapitel 2 og 3 er der givet en beskrivelse af de væsentlige processer der fører til sætning af en erosionsbeskyttelse omkring en pæl i tilfælde af strøm, baseret på fysiske og numeriske modeller. Ved hjælp af resultaterne er det muligt at udføre design af erosionsbeskyttelser hvor sætningerne af erosionsbeskyttelsen omkring monopælen undgås eller forudsiges. Det er blevet vist at hesteskohvirvlen ved bunden af pælen vil trænge ind i erosionsbeskyttelsen og, hvis den er stærk nok, mobilisere bund sedimentet og transportere det ud af erosionsbeskyttelsen, hvor det vil blive fjernet af den ydre strømning. Ekvilibrium sætningen er fundet for forskellige forhold. Det er også fundet at et fint filterlag kan forhindre sætninger.

I Kapitel 4, er erosionen omkring monopæle i brydende bølger undersøgt. Det er fundet at erosionen afhænger af to parametre: (1) Afstanden mellem brydningspunktet og pælen normaliseret med bølgelængden, og (2) højden af den brydende bølge normaliseret med pælens diameter. Den største erosion blev fundet til at være omkring 0,65 gange pælens diameter. Den kan blive større end erosionen fra ikke brydende bølger, specielt for små KC-tal. Hovedårsagen til den øgede erosion skyldes turbulens dannet af den brydende bølge og tvunget mod bunden af pælen.

I Kapitel 5 er begyndelsesbetingelserne for fjernelse af sediment mellem dæksten under brydende bølger bestemt. De kritiske betingelser for fjernelse af sediment er bestemt for mange forskellige forhold, som bølgehøjde og -periode, bundhældning, størrelse af sediment og dæksten samt antal dæk-

stens lag. De skrående hvirvelpar dannet af de brydende bølger er fastslået til at være hovedårsagen til fjernelsen af sedimentet.

I kapitel 6 er strømningen i og bundforskydningsspændingerne under et stenlag i en oscillerende strøm beskrevet. Strømningshastighederne og turbulensen er målt for et, to og tre stenlag i adskillige porer. Forsøgene viste at de horisontale hastigheder i porerne er påvirket omkring en stendiameter ind i stenlaget. Under dette niveau bliver de horisontale hastigheder konstante. Bundforskydningsspændingerne er meget mindre end for en glat bund uden stenlag og store variationer er observeret.

I Kapitel 7 er effekten af bølger på sætningen af erosionsbeskyttelsen omkring en pæl studeret. Det er fundet at sætningen øges for et øget KC-tal for en given diffractionsparameter. Størrelsesorden af sætningen er sammenlignelig med erosionen observeret omkring en ubeskyttet pæl påvirket af den samme bølgeforhold.

Chapter 1

Introduction

Over the last decades more and more offshore wind turbines have been installed all over the world - most of them in Northern Europe. The first offshore wind turbines were erected in protected, very shallow waters and close to the shore. The first offshore wind turbine was in Norgersund in Sweden (1990) 300 m offshore at 7 m of water (Offshore Center Danmark, 2011). One year later the first actual offshore wind farm with more than one turbine was commissioned. It is located 1.5 to 3.0 km offshore in the Great Belt (Denmark) at 2 to 6 m of water and has a total capacity of approximately 5 MW (Offshore Center Danmark, 2011).

The next major step in the development of offshore wind energy was the development of the Horns Rev 1 (2002) and Rødsand 1 (2003, also known as Nysted) Offshore Wind Farms. Both wind farms were erected as full-scale demonstration projects as part of the programme for offshore wind farms in the Danish waters (Elselskabernes og Energistyrelsens Arbejdsgruppe for Havmøller, 1997). The large-scale demonstration projects were initiated to obtain new knowledge about technical, economical and environmental issues regarding large offshore wind farms.

The Rødsand 1 Offshore Wind Farm (72 turbines, 165.6 MW in total) is located in the Danish part of the Baltic Sea, while Horns Rev 1 (80 turbines, 160 MW in total) is located in much harder environment in the Danish part of the North Sea (Offshore Center Danmark, 2011). The Rødsand 1 Wind Farm (6 to 9.5 m water depth) is founded on gravity based concrete structures, while the Horns Rev 1 Wind Farm (6.5 to 13 m water depth) is founded on the, for offshore wind turbines, much more common mono pile foundation (Offshore Center Danmark, 2011). To ensure the stability of the foundations, scour protections were applied for the foundations in both farms Horns Rev Webpage (2011) and Rødsand Webpage (2011). While no problems were reported for the scour protections at Rødsand 1, Hansen *et al.* (2007) reported unexpectedly large sinking of the scour protections at Horns

Rev 1, up to 1.5 m.

Scour around mono piles has been studied extensively over the last decades. Most of the available results are compiled in Breusers and Raudkivi (1991); Hoffmanns and Verheij (1997); Whitehouse (1998); Melville and Coleman (2000) and Sumer and Fredsøe (2002). Scour protection of piles has not been studied nearly as much and the mechanism of failure of scour protections around a mono pile has only been described briefly. Chiew (1995); Chiew and Lim (2000); Lauchlan and Melville (2001); Chiew (2002); De Vos (2008) among others have studied the scour protection around mono piles, however, except De Vos (2008), these studies have focused on bridge piers in rivers, where large bed forms are common and much more important than at Horns Rev. Lauchlan and Melville (2001) and De Vos (2008) main attention was the stability of the stones in the scour protection (disintegration of the scour protection), Chiew (1995); Chiew and Lim (2000) and Chiew (2002) both focused on the sinking/embedment and the total disintegration of the scour protection. Chiew (1995) and Chiew and Lim (2000) presented an empirical method for prediction of the failure mode of a scour protection around a mono pile, but not the magnitude of the sinking.

This thesis presents results of detailed measurements of the flow inside a scour protection around a mono pile in current. Based on these results, a detailed description of the mechanism causing the sinking of the scour protection observed by Chiew (1995); Chiew and Lim (2000); Lauchlan and Melville (2001); Chiew (2002) and at Horns Rev 1 Wind Farm is given. Equilibrium sinking of the scour protection is found experimentally for various conditions, including scour protections with and without filter layer. A threshold for the motion of sediment underneath the scour protection is found, which makes it possible to determine whether the bed sediment will move or not and the scour protection eventually sink.

1.1 Horns Rev 1 Wind Farm

The study leading to this thesis was initiated as an attempt to give a detailed explanation of the sinking of the scour protections at Horns Rev 1 Wind Farm and to make it possible to make use of the new knowledge in future projects, either by preventing sinking or by incorporating the sinking in the design. This section will provide basic information on the Horns Rev 1 Wind Farm with special focus on the foundations and scour protections.

The Horns Rev 1 Wind Farm is located in the Danish part of the North Sea, see Fig. 1.1. The farm is located 14 to 20 km off the Danish west coast on relatively shallow water: 6.5 to 13.5 m water depth, see Fig 1.2. In total four detailed surveys of the area are available (1998, 1999, 2000 and 2001),

these surveys can be seen in Appendix B. The environment at Horns Rev is harsh: Large waves and tidal currents. Waves with a return period of one year are more than 6 m (Horns Rev Webpage, 2011). The waves are frequently breaking during storm conditions, at least in parts of the wind farm, which has caused severe problems for access platforms and ladders (Nielsen and Jacobsen, 2007). The tidal current is around 0.5 m/s, but the total current speed can reach as much as 0.8 m/s during storm conditions (Horns Rev Webpage, 2011).

Figure 1.1: *The North Sea. The location of Horns Rev 1 Wind Farm is indicated by wind turbine signs. Map by Halava [CC-BY-SA-3.0 (www.creativecommons.org/licenses/by-sa/3.0) or GFDL (www.gnu.org/copyleft/fdl.html)], via Wikimedia Commons.*

1.1.1 Scour Protections at Horns Rev 1 Wind Farm

The scour protections at Horns Rev 1 Wind Farm are traditional scour protections made of stones. Descriptions of the protections are found in Hansen *et al.* (2007) and Horns Rev Webpage (2011): They consist of a 0.5 m thick filter layer and two stones thick cover layer, in total approximately 1.3 m thick. The filter layer was made of sea material in the range of 3 to 20 cm, with a mean size of 10 cm. The cover layers are made of quarry run in the range of 35 to 55 cm, with a mean size of 40 cm. The natural seabed at Horns Rev consists of sand in the range of 0.1 to 1.0 mm, depending on the location.

The procedure of the installation was (Horns Rev Webpage, 2011):

1. Installation of the filter layer.
2. Installation of the mono pile, driven through the filter layer.
3. Installation of the transition piece, including J-tubes and ducts for cables.
4. Installation of the cover layer.
5. Installation of the turbine, cables, etc.

An extensive survey programme of the seabed surrounding each foundation was conducted previous to, during and after the installation, Nielsen (2007). Four surveys of the entire area were carried out before the installation: August 1998, June 1999, April 2000 and 2001, see Appendix B. Several surveys were conducted during the installation (all in 2002):

1. Before installation of filter layer.
2. After installation of filter layer.
3. After installation of cover layer.
4. After extra filter stones were placed.
5. After extra cover stones were placed.

The last survey is used as reference for the sinking. It was made during November 2002, around 6 to 9 months after the installation of the filter layers and around 4 to 8 months after the installation of the mono piles (Horns Rev Webpage, 2011).

Time evolution monitoring surveys were conducted in April 2005 and fall 2006 (Nielsen, 2007). The 2005 survey is used as reference for the sinking of the scour protection as additional cover stones were placed after the

2005 survey (Nielsen, 2007), to fill the holes caused by sinking of the scour protections.

1.1.2 Sinking of the Scour Protections at Horns Rev 1 Wind Farm

After the 2005 survey it was clear that the scour protections were lowered by up to 1.5 m adjacent to the piles (Hansen *et al.*, 2007). The survey data is given in Nielsen (2007) for all turbines, except one (Turbine 34, 2002 survey). There is no clear correlation between the lowering of the scour protection and the location of the turbine foundation within the farm. In the present study Turbine 44 has been used as an example (see Chapter 3). This turbine is found to represent the average turbine: (1) It is located in the middle of the farm; (2) there is no extreme bathymetry nearby; (3) it is not extraordinarily exposed or protected from the dominating waves from westerly directions; (4) the local water depth is approximately 10 m as the average in the farm (see Fig. 1.2) and (5) the sinking is significant, but not extreme. The results of the surveys of Turbine 44 are shown in Fig. 1.3. The scour protection has clearly sunk by at least 1 m. The scour protection is around 1.5 m lower east and west of the foundation. This might be because of some extra cover stones on top of the actual scour protection. These stones will be more exposed than the rest and might have been relocated during a storm.

1.1.3 The Reason for the Sinking

The reason for the lowering of the scour protections adjacent to the foundations could be: (1) Damage to the cover layer; (2) winnowing of the filter layer through the cover layer and (3) removal of the base sediment through the filter and cover layers. Hansen *et al.* (2007) showed that options one and two were very unlikely, while the third option was possible, as simplified calculations showed that the base sediment underneath the scour protections might be mobile during storm conditions.

Three different hydrodynamic conditions could play a role in the sinking of the scour protection and removal of the base sediment (see sec. 1.1):

- Tidal current.
- Non-breaking waves.
- Breaking waves.

All three hydrodynamic conditions are considered in this thesis. The effect of current is described in detail in Chapters 2, 3 and Appendix A. The effect of the interaction between non-breaking waves and scour protection

with and without a pile is given in Chapters 6 and 7. The scour around a pile in breaking waves and the onset of scour in a stone cover without structure are given in Chapter 4 and 5.

1.2 Outline

The present thesis is, except for Chapter 7, compiled of articles published, accepted or submitted to journals and conferences. Details about the status of the papers are stated at the beginning of each relevant chapter.

Chapter 2 presents results of physical experiments with scour protections without filter layer around a pile exposed to a current. This includes detailed measurements of the flow velocities and turbulence inside the scour protections with various configurations and sediment bed experiments with equilibrium sinking of the scour protections and the time scale of the process. The chapter gives guidelines to determine the expected sinking and the time-scale of the sinking for a coarse scour protection with sediment transport underneath. The chapter is an extended version of a conference paper (Nielsen *et al.*, 2010), see Appendix A.

Chapter 3 presents results of the physical and numerical experiments with scour protections with a filter layer around a pile exposed to a current. This includes detailed measurements and numerical simulations of the flow velocities, turbulence and bed shear stress in scour protections of different configurations. Sediment bed experiments have been used to find the sinking of different scour protection with filter layer and to study the effect of the filter layer. The chapter gives guidelines to determine the necessary filter stone size to prevent motion of the sediment underneath the scour protection. Chapter 3 shows that there was motion of the sediment underneath the scour protection at Horns Rev 1 Wind Farm under extreme current conditions and Chapter 2 shows that a sinking of up to 1.4 m can be anticipated, based on the physical model tests. This corresponds to the observations from Horns Rev 1 Wind Farm described above.

Chapter 4 presents the results of physical model tests of scour around unprotected mono piles in breaking waves. The result is that the scour is smaller than the expected equilibrium scour for current alone, but the scour in some cases is up to 0.6 times the diameter of the pile. It was found that the scour caused by breaking and non-breaking waves was almost the same for higher KC-numbers (~ 35), while the scour caused by breaking waves was much larger than the scour caused by non-breaking waves in the case of small KC-numbers (~ 5). In the latter case the scour was up to $O(10)$ times larger than the scour caused by non-breaking waves. However, the most important result in relation to scour protection is that the scour

in breaking waves is caused by turbulence generated by the wave breaking and transported to the bottom. The results in Chapters 2, 3 and Appendix A showed that scour protections made of stones are effective against scour generated by turbulence and similar flow structures, like vortices caused by vortex shedding. More stationary pressure gradients, like the adverse pressure gradient causing the horseshoe vortex, can generate critical flows in the scour protection and causes sediment transport underneath the scour protection. Given the relatively small maximum scour generated by breaking waves and that it is caused mainly by turbulence, which is found not to penetrate into the scour protection in other cases it is most likely that the breaking waves at Horns Rev 1 Wind Farm have no or very little effect on the sinking of the scour protections.

Chapter 5 presents the results of physical model tests with scour protection of sloping beds under breaking waves. The critical wave conditions are found for varying different conditions: Slopes, sediment sizes, armour layer sizes, armour layer thicknesses and specific weights of sediment. The critical conditions for onset of suction from between the armour blocks are given for one and two layers of armour stones and for one layer of armour blocks (cubes). The most important finding in relation to scour protection of mono piles is that the oblique descending eddies (Nadaoka *et al.*, 1989) are the most important reason for mobilizing the sediment under the scour protection. The oblique descending eddies are strong turbulent structures generated by breaking waves. They agitate the water in the pores between the stones and thereby mobilize the sediment. As seen in Figs. 5.5 and 5.6 the required mobility number to causes suction is increased around 3 times when the number of stone layers is increased from one to two. Based on this it is unlikely that descending eddies will be able to cause suction through scour protections like those installed at Horns Rev 1 Wind Farm.

Chapter 6 presents the results of physical model tests with a stone covered bed under an oscillatory flow. The streamwise and vertical velocities were measured in the pores of the stone cover in case of one, two and three layers of stones. The magnitude of the streamwise bed shear stress was measured in different pores under three layers of stones. The results show that the boundary layer of the outer flow penetrates approximately 4 cm (or one stone size) into the scour protection. Below this level the averaged pore velocities are constant. The bed shear stress under three layers of cover stones is found to be more than ten times smaller than in case of a smooth bed without stone cover, but the turbulence level is, on the other hand, much higher. The low bed shear stress shows that the stone cover is effective to prevent scour, but the high level of turbulence will, on the other hand, causes a much higher bed load discharge of sediment in the case of onset of motion

in between the stones.

Chapter 7 presents results of physical model tests with a scour protection around a pile exposed to waves. The experiments were made on sediment beds as those used in Chapter 2 and 3 and the experiments gave the equilibrium sinking of the scour protection. The results showed that the sinking increased for increasing KC-number for a given diffraction parameter (D_p/L). The results also showed that the magnitude of the sinking was comparable to the scour expected around an unprotected pile under the same conditions, and for very low KC-numbers the sinking apparently exceeded the expected scour, two to three times. Based on the limited available data it has not been possible to give a detailed description of the mechanisms causing the sinking in waves, but based on the pattern of the scoured and deposited sediment in the scour protection it is concluded that a reverse flow takes place at the offsohre side of the pile at very low KC-numbers. However, all the results showed a significantly lower sinking than in case of a current (Chapters 2, 3 and Appendix A). Based on this it was decided to focus on the current case.

It can be concluded that the sinking of the scour protections at Horns Rev 1 Wind Farm is mainly caused by the current at Horns Rev. The waves might have caused a minor part of the sinking. Breaking waves have most likely not contributed to the sinking as the primary reason for scour caused by breaking waves is found to be turbulent structures which hardly penetrate deep into the scour protections. Combined waves and current have not been studied in this thesis, but it is likely that this combination will cause at least some sinking, and it may increase the period of time where significant sinking takes place.

If the sinking should have been avoided the filter stones used for the scour protections should have been smaller than those actually applied. If the filter stones had been small enough it would have reduced the velocity in the filter layer to be below the critical velocity for onset of motion of the base sediment. Fig. 3 can be used to determine the required filter stone size. It should be noted that the figure is only valid for current alone. Combined waves and current might be able to cause onset of motion of the base sediment at lower mobility numbers.

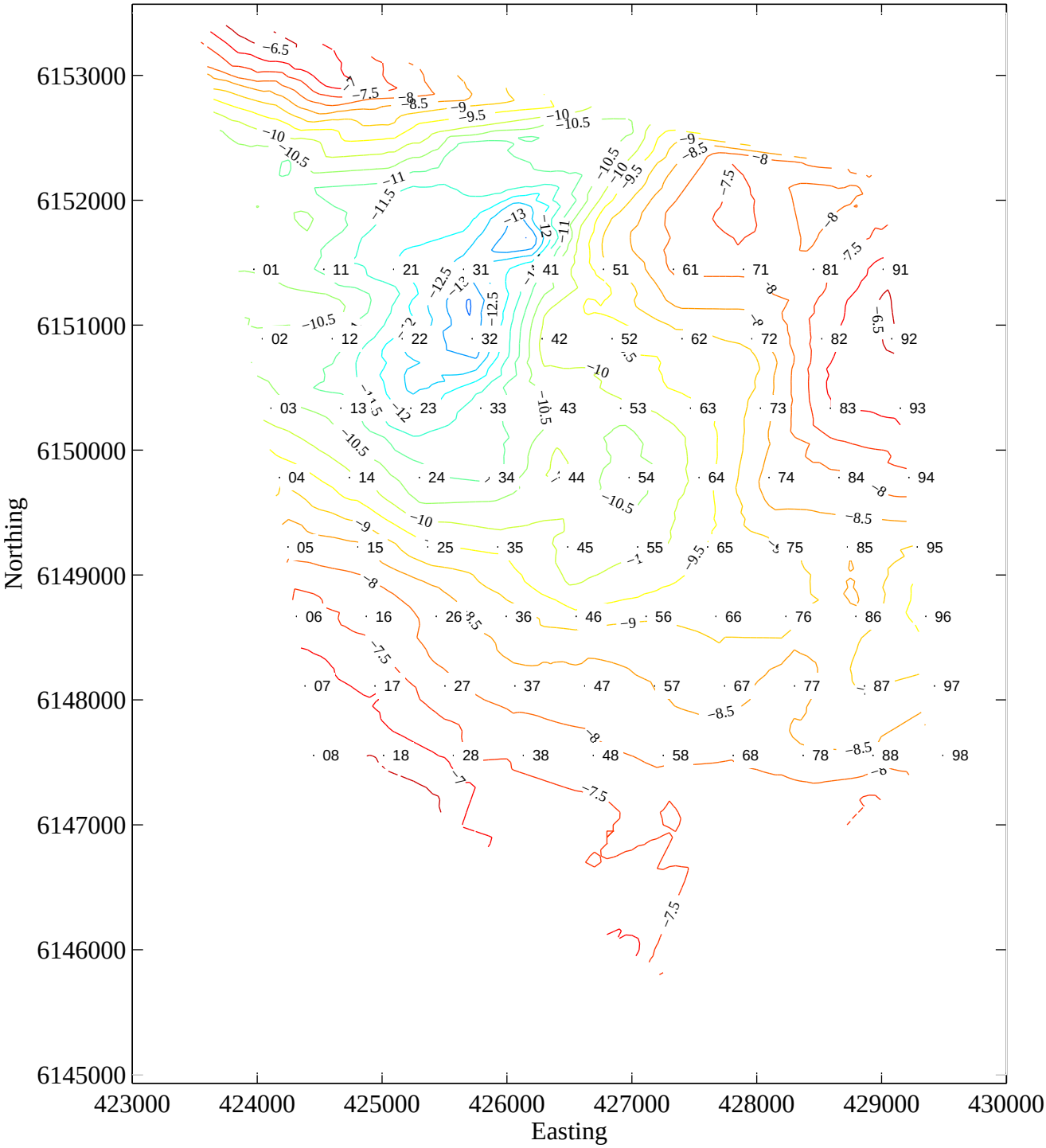

Figure 1.2: *Bathymetry of the Horns Rev 1 Wind Farm area (2001 survey). The coordinates are UTM zone 32U. Adapted from Nielsen (2007). Courtesy of Vattenfall and DONG Energy.*

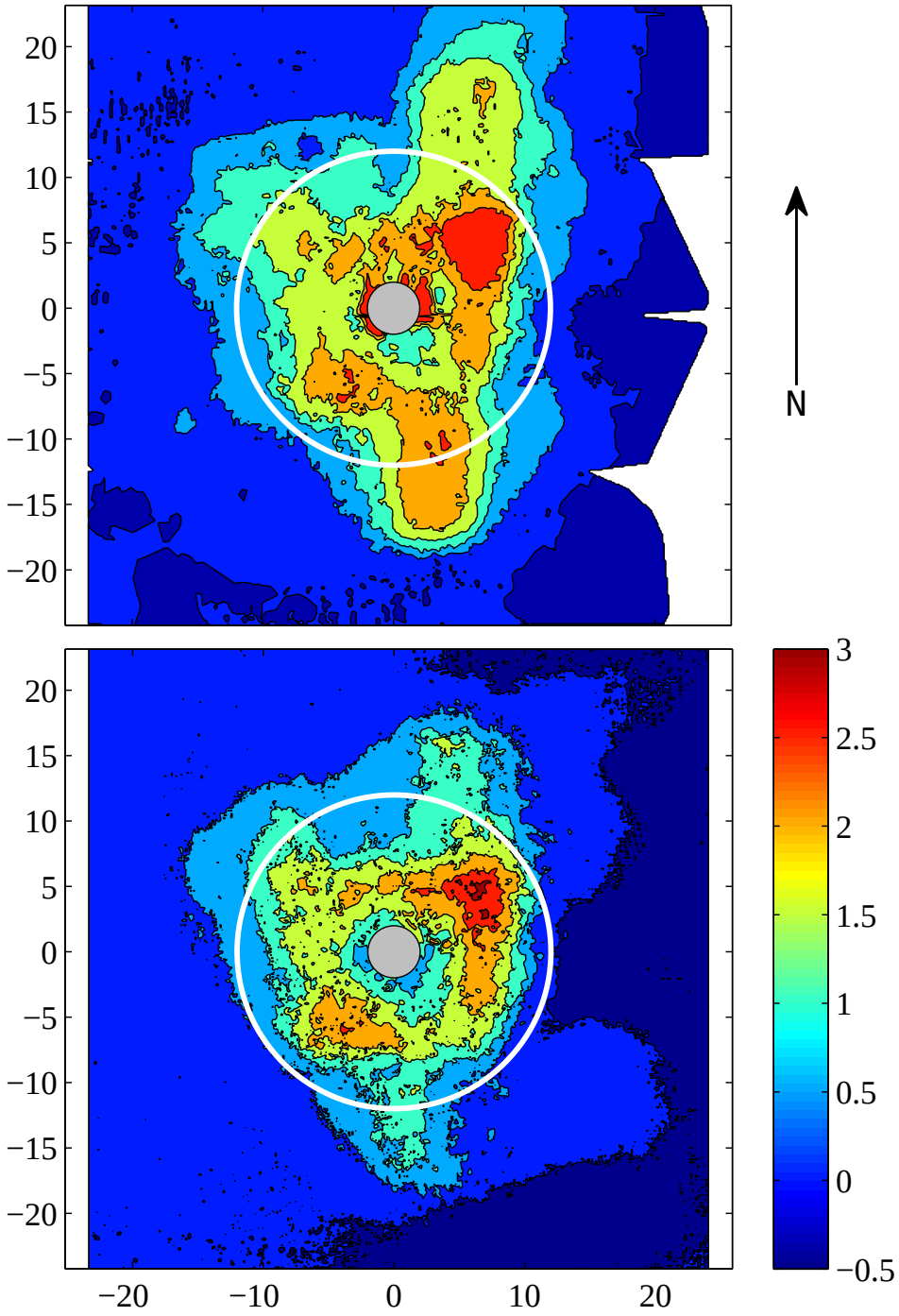

Figure 1.3: *Results of the surveys of Turbine 44. The upper panel is the last 2002 survey and the lower panel is the 2005 survey. The white circles are the design limits of the scour protection. Adapted from Nielsen (2007).*

Chapter 2

Sinking of Armour Layer around a Cylinder exposed to a Current

This chapter will appear in Institution of Civil Engineers (ICE) Maritime Engineering:
Nielsen, A.W., Sumer, B.M., Fredsøe, J. and Christensen, E.D.: "Sinking of armour layer around a cylinder exposed to a current"

Published article: The final reference is: Nielsen, A.W., Sumer, B.M., Fredsøe, J. and Christensen, E.D. (2011). Sinking of armour layer around a cylinder exposed to a current. *Proceedings of the ICE - Maritime Engineering*, **164**(4), 159-172 (doi: 10.1680/maen.2011.164.4.159).

Abstract

The flow processes in a scour protection around a mono-pile in steady current are described in relation to transport of sediment in the scour protection based on physical model tests. The scour protection consisted of a uniformly distributed coarse stones without filter layer.

Transport of sediment in the scour protection may cause sinking of the scour protection. This may reduce the stability of the mono-pile and change for instance the natural frequency of the dynamic response of an offshore wind turbine in an unfavourable manner. The most important flow process with regard to transport of sediment and sinking of the scour protection is found to be the horseshoe vortex.

It is found that a larger pile diameter relative to the size of the protection stones will cause a larger sinking and that two layers of stones will decrease the sinking relative to one layer of stones with the same size.

Keywords: Renewable energy, foundations, offshore engineering

2.1 Introduction

During the last decade more and more wind farms have been erected offshore. One of the first larger offshore wind farms is the Horns Rev I. The Horns Rev I is located in relatively shallow water (6.5 to 13 m water (MSL)) about 20 km off the Danish West Coast in the North Sea. This area is exposed to strong tidal currents and large waves from the North Sea. The wind turbines are founded on mono-piles with a scour protection made of a two-layer cover (quarry run from around 350 mm to 550 mm) and a 0.5 m thick filter layer (sea stones from around 30 mm to 200 mm) between the armour layer and the seabed. The wind farm was installed in the summer 2002. A control survey in 2005 showed that the scour protections adjacent to the mono-piles sank up to 1.5 m, Hansen *et al.* (2007). This was unexpected and shortly after the survey in 2005 the holes were repaired by adding additional stones.

Scour around unprotected piles have been studied extensively over the last decades. Most of the available results are compiled in Breusers and Raudkivi (1991); Hoffmanns and Verheij (1997); Whitehouse (1998); Melville and Coleman (2000) and Sumer and Fredsøe (2002). This work has in recent years made it possible to develop numerical models for long-term prediction of the development of scour holes around monopiles (Nielsen and Hansen, 2007; Raaijmakers and Rudolph, 2008; Harris *et al.*, 2010). Scour protection of piles has not been studied nearly as much and the mechanism of failure of scour protections around a mono-pile has only been described briefly. In order to gain an understanding of the mechanisms that cause the sinking of the scour protection, an extensive program of physical model tests with steady current has been carried out in the present study, in an attempt to contribute to the knowledge obtained recently by Chiew and Lim (2000); Lauchlan and Melville (2001); Chiew (2002); De Vos (2008) among others. The model tests showed that the horseshoe vortex, the key element to cause scour around unprotected piles, see e.g. Dargahi (1989) and Roulund *et al.* (2005), is a key flow feature governing the sinking process of the scour protection.

This study address the live-bed situation where the horseshoe vortex is strong enough to penetrate the entire thickness of the scour protection and generate bed shear stresses at the base bottom high enough to cause sediment transport.

2.2 Experimental Setup

The tests were conducted in two different current flumes. (1) a 2 m wide, 23 m long and 0.5 m deep flume; and (2) a 4 m wide, 28 m long and 1.0 m deep flume. The flumes were equipped with recirculation pumps providing mean current speeds of more than 60 cm/s. Three different setups were used for the tests in the 2 m wide flume: (1) a fixed bottom setup used for flow visualizations and velocity profiles measurements, (2) a fixed bottom setup with a half pile mounted on a vertical transparent wall, and (3) a sediment bed test setup with a 10 m long and 0.15 m deep sand section. At both ends of the sand section were plywood ramps inclined towards the sand section. The ramps in both ends of the sand section had an inclination of 1:10.

In the case of the 4 m wide flume only sediment bed tests were conducted. The sand section was around 10 m long and 0.35 m deep, with a 3 m long ramp at the upstream end, with a core of concrete blocks covered with at least one layer of stones ($d_{50} = 4$ cm). In some of the tests in the 4 m wide flume, two piles were tested at the same time, in order to save time. The piles were placed at the same distance from the inlet and the distance between the piles was 1.75 m, which was large enough to ensure no interference. The setups used in both flumes are, for the most part, described in details in Nielsen *et al.* (2010).

In the case of the fixed-bottom experiments an approximately 0.5 cm thick, 2.9 m long, white plastic plate, with 15 cm long tapered upstream end, was placed on the base bottom over the entire width of the flume enabling a good contrast for the flow visualizations. For the velocity profile measurements (using Laser Doppler Anemometry, LDA) the plate was painted matt black to reduce reflections of the laser beams. The pile with an outer diameter of 14.0 cm was placed 2.0 m downstream of the upstream end of the plastic plate (approximately 15 m from the inlet section). In the case of the half pile a semi-circular pile with an outer diameter of 15.0 cm was mounted on a transparent vertical wall, see Fig. 2.1. The latter wall was 10 mm thick, 1.75 m long and surface piercing. The upstream edge of the plate was tapered to both sides with an angle of 1:6. The half pile was mounted at the middle of the transparent plastic wall in the streamwise direction. The half pile and wall was placed so that the half pile was at the same position as the previous mentioned full pile and the plastic wall was parallel with the side walls of the flume. In all setups the bottom end of the piles were completely sealed.

The flow velocity was measured in two different ways: A small propeller (3 cm in diameter) was used in the case of the sediment bed tests and a submerged pen size LDA probe was used in the case of the fixed-bottom tests. The pen-size LDA probe was a two component probe, approximately

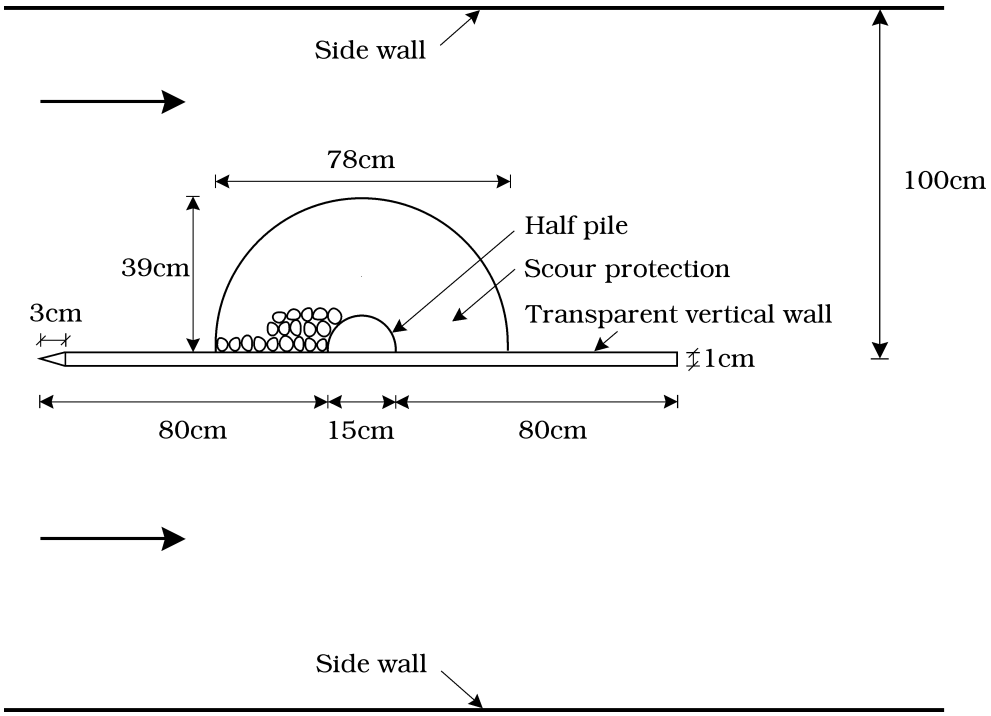

Figure 2.1: *Sketch of the half pile setup.*

1 cm in diameter and 15 cm long. It had a focal length of 80 mm (in water), a beam spacing of 8 mm and a beam diameter of 0.27 mm. The probe was placed vertically pointing downwards, when used to measure velocities in between the stones and placed horizontally when used outside the stones and through the transparent wall in the case of the half pile.

The sinking of the stones in the sediment bed experiments was determined by measuring the vertical displacement of the stones adjacent to the pile. To avoid disturbances due to the irregularities of the stones the sinking was measured with reference to the same point marked on the stone. In case of large rotations or if the stone was covered by other stones the measured sinking of that stone was disregarded. In the case when a disregarded stone was likely to be the stone with maximum sinking the entire test was abandoned. Based on the results of the tests it was found that the maximum sinking always occurred for the stone upstream of the pile or on the sides of the pile. The number of stones where the sinking was measured around the pile was between three and eight for each test. In the case were only three stones were measured, these were placed in front and on the sides of the pile. Along with the sinking of the stone adjacent to the pile, the scouring and deposition of sand in the area around the pile was measured using measuring

pins (3 mm in diameter) with scales in the form of coloured strips. The pins were placed in and around the scour protection.

2.3 Test Conditions

One sand size was used for the experiments, $d_{50} = 0.18$ mm. The pile diameter, D_p, was changed in the range 7.5 cm to 20.0 cm. The plan-view extension of the scour protection from upstream edge to downstream edge, w_c, was kept in the interval of 20 to 90 cm giving a relative extension of the scour protection, w_c/D_p, of 2.0 to 4.5. The size of the cover stones, D_c, was in the interval 1.9 cm to 10.3 cm (d_{50}) and applied in one to three layers. The water depth, h, was maintained at 29 cm to 30 cm and at 56 cm, giving a relative water depth, h/D_p, of 2.1 to 5.1. The depth-averaged velocity, V, was kept within the interval 34 cm/s to 55 cm/s giving a mobility parameter from 35 to 105 defined as:

$$\psi = \frac{V^2}{g(s-1)d_{50}} \tag{2.1}$$

where V, is the depth-averaged velocity associated with the far field, calculated using the Colebrook-White equation based on a single point measurement. This range of the mobility number is within the live-bed regime, corresponding to $0.08<\theta<0.21$, based on the roughness of the sand grains. Three different materials were used for the scour protection: (1) Round stones with a mean diameter (d_{50}) of $D_c = 10.3$ cm with $d_{15} = 9.0$ cm and $d_{85} = 11.2$ cm. They were used in one layer with a mean thickness of 7.6 cm; (2) crushed stones with a mean size of $D_c = 4.3$ cm with $d_{15} = 3.7$ cm and $d_{85} = 4.9$ cm and. They were used in one, two and three layers with a mean thickness of 3.2, 6.2 and 9.0 cm, respectively; (3) crushed stones $D_c = 1.9$ cm with $d_{15} = 1.6$ cm and $d_{85} = 2.8$ cm, the stones were used in one and two layers with a mean thickness of 1.8 and 3.3 cm, respectively.

In the case of the fixed bottom experiments only the $D_c = 4.3$ cm stones were used, but with up to 7 layers. The thickness of the scour protection with 4, 5, 6 and 7 layers was: 12.3, 15.4, 17.8 and 20.4 cm, respectively. The size of the stones was defined as the average length of three sides of the stone, perpendicular to each other. The thickness of the scour protection was defined as the average distance from the base bottom to the top of the stones.

2.4 Results

2.4.1 Fixed-Bed Results

The flow around and within the scour protection around the monopile has been investigated using flow visualization and velocity measurements (LDA). The flow visualizations were made by injecting blue and green dye at the edge of the scour protection and in between the stones adjacent to the upstream side of the pile. Only one layer of 4 cm stones was used in order not to block the view of the flow near the base bottom and to keep the overall view relatively simple.

The flow visualizations showed that the flow pattern around the monopile with scour protection is very similar to the pattern around an unprotected monopile. The flow around an unprotected pile has been studied extensively and the results are compiled in, for example, Sumer and Fredsøe (2002). In relation to scour development the most important flow feature is the horseshoe vortex, see for example Roulund *et al.* (2005).

The present flow visualization showed that the horseshoe vortex is still the main reason for the removal of sediment close to the upstream side of the pile, see Fig. 2.2: When adding dye at the top of the stones adjacent to the upstream side of the pile, the dye was transported down into the stones and then upstream in between the stones. Around 10 to 15 cm from the upstream edge of the pile and 10 to 15 cm from the upstream edge of the scour protection these two, oppositely directed flows met at a separation line. At the separation line they were forced upwards into the main flow and transported away.

By adding dye at the upstream edge of the scour protection two important flow patterns were observed: Small horseshoe vortices were generated in front of the protection stones (as sketched in Fig. 2.2) while water was able to flow into the scour protection in the gaps between the stones.

Flow visualizations were made at different positions at the side of the pile and downstream of the pile. These flow visualizations showed no important flow features in relation to the sinking of the scour protection. The flow at the side of the pile was dominated by the downstream part of the horseshoe vortex. A flow into the scour protection at the downstream edge of the scour protection was observed, but this flow was weak and it has not been possible to relate it to any important effect in relation to the sinking of the scour protection. The most important flow feature at the downstream side of the cylinder is the vortex shedding, see Fig. 2.2. The sediment bed tests, however, showed that the vortex shedding was not causing any significant sinking. Velocity profiles in between the stones have been measured from approximately 1.5 cm above the base bottom to the surface using LDA. The

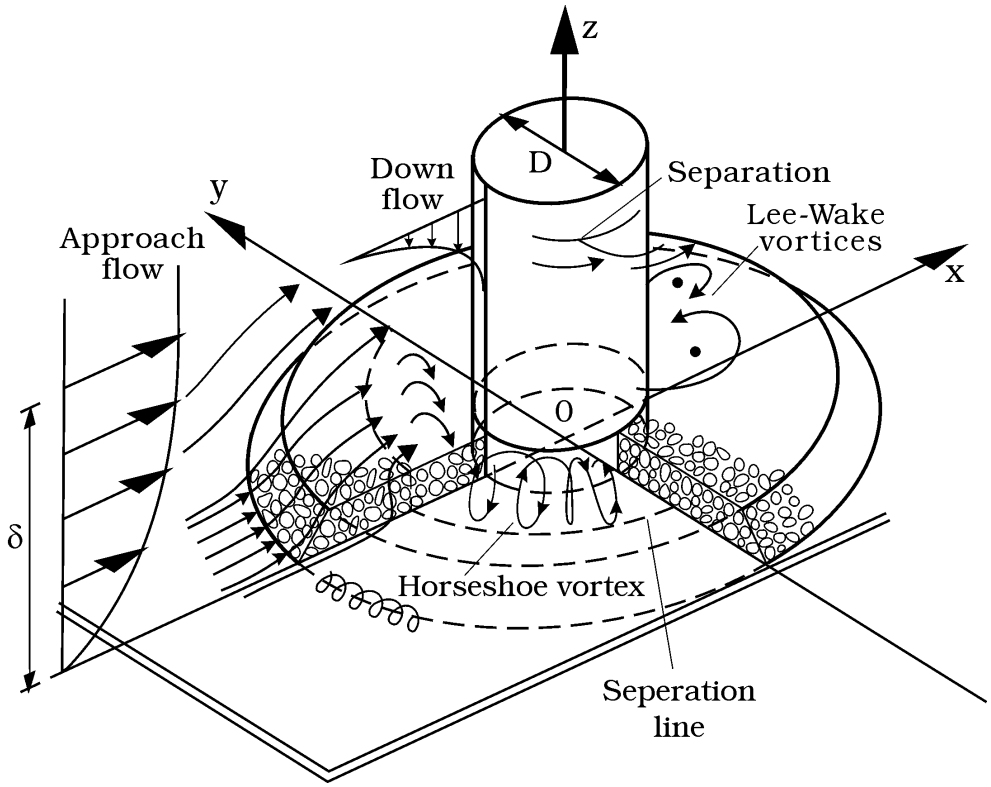

Figure 2.2: *Sketch of the flow around a mono-pile with scour protection.*

reason for the relatively large distance from the base bottom to the lowest measuring point was that the LDA probe needed to be vertical in order to measure in between the stones. This caused some heavy reflections from the base bottom which made it impossible to measure closer to the bottom with the available equipment.

The velocity profiles upstream of the pile are shown in Fig. 2.3. It is clearly seen that a significant return flow is present in between the stones up to around 10 cm from the edge of the pile. This is consistent with the results of the flow visualizations. Fig. 2.4 shows the velocity profiles downstream of the pile. The velocities are in general 3 to 4 times lower than the velocities measured upstream of the pile. The mean flow in between the stones 7.7 cm downstream of the pile centre is directed upstream, while it is directed downstream 21.5 and 38.0 cm downstream of the pile centre. This overall flow pattern is in good agreement with the flow pattern observed by e.g. Graf and Yulistiyanto (1998) and Roulund *et al.* (2005) for an unprotected pile. Note that the results in Graf and Yulistiyanto (1998) were made with a flow with Froude number 0.5 while the present study has a Froude number

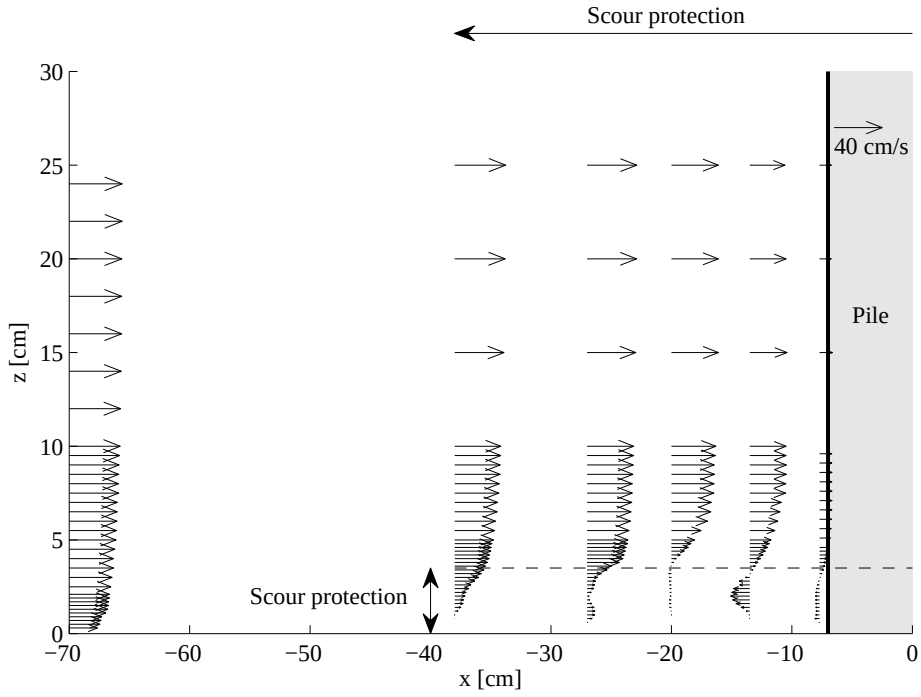

Figure 2.3: *Velocity profiles at different distances upstream of the mono-pile with one layer of 4.3 cm stones.*

of 0.35.

The turbulent kinetic energy, k, defined as:

$$k = \frac{1}{2}(\overline{u'^2} + \overline{v'^2} + \overline{w'^2})$$

where u' is the streamwise velocity fluctuation, v' is the crossflow velocity fluctuation and w' is the vertical velocity fluctuation. The turbulent kinetic energy is the other important quantity in relation to sediment transport. Sumer *et al.* (2003) showed that the sediment transport can be increased by a factor of 6 when the turbulence level near the bottom is increased by 20%. The turbulent kinetic energy measured at the same locations as the velocity profiles given in Fig. 2.3 and 2.4 are shown in Fig 2.5 and 2.6. The turbulent kinetic energy shown in the figures is determined using the measured data and the following relationship (Nezu and Nakagawa (1993)):

$$\frac{\overline{u'^2}}{2k} = 0.55, \qquad \frac{\overline{v'^2}}{2k} = 0.28, \qquad \frac{\overline{w'^2}}{2k} = 0.17 \tag{2.2}$$

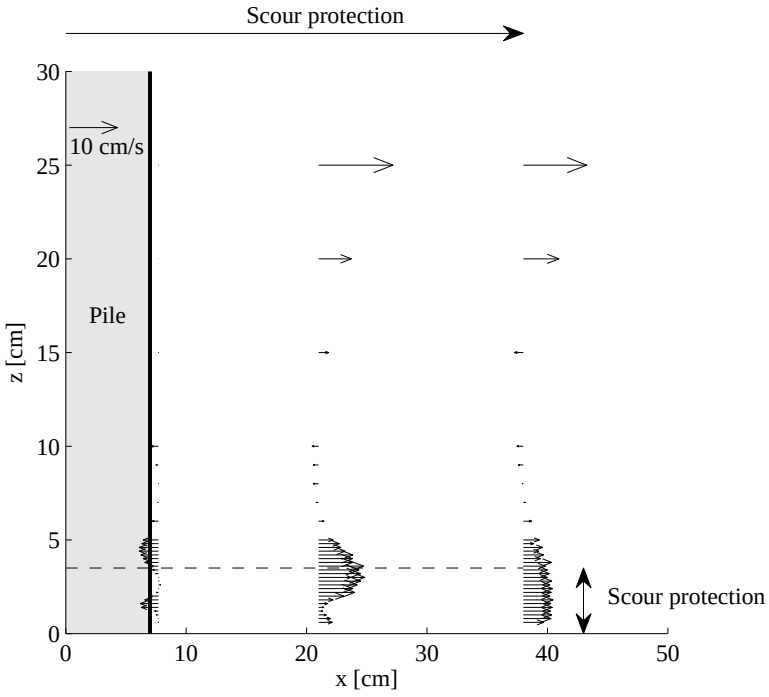

Figure 2.4: *Velocity profiles at different distances downstream of the mono-pile with one layer of 4.3 cm stones.*

For z smaller than approximately 10 cm the two horizontal components were measured and for z larger than approximately 5 cm the streamwise and vertical component were measured. Only the streamwise and vertical components were measured in the far field ($x = -70$ cm).

Fig. 2.5 and 2.6 show a large increase in the turbulent kinetic energy compared to the undisturbed flow, $x = -70$ cm. The maximum turbulent kinetic energy at the upstream side of the pile is approximately two times larger than the maximum undisturbed value. This is consistent with the measurement made by Graf and Yulistiyanto (1998) for an unprotected pile.

At the downstream side of the pile Graf and Yulistiyanto (1998) measured the maximum turbulent kinetic energy approximately at $x = 1.5D_p$. In the present case the maximum turbulent kinetic energy was measured further downstream. However, comparing the maximum turbulent kinetic energy in $x = 1.5D_p$ shows that the turbulent kinetic energy for the unprotected pile was approximately 35 times higher than what was measured in the present study. The reason for this is the higher Froude number used by Graf and

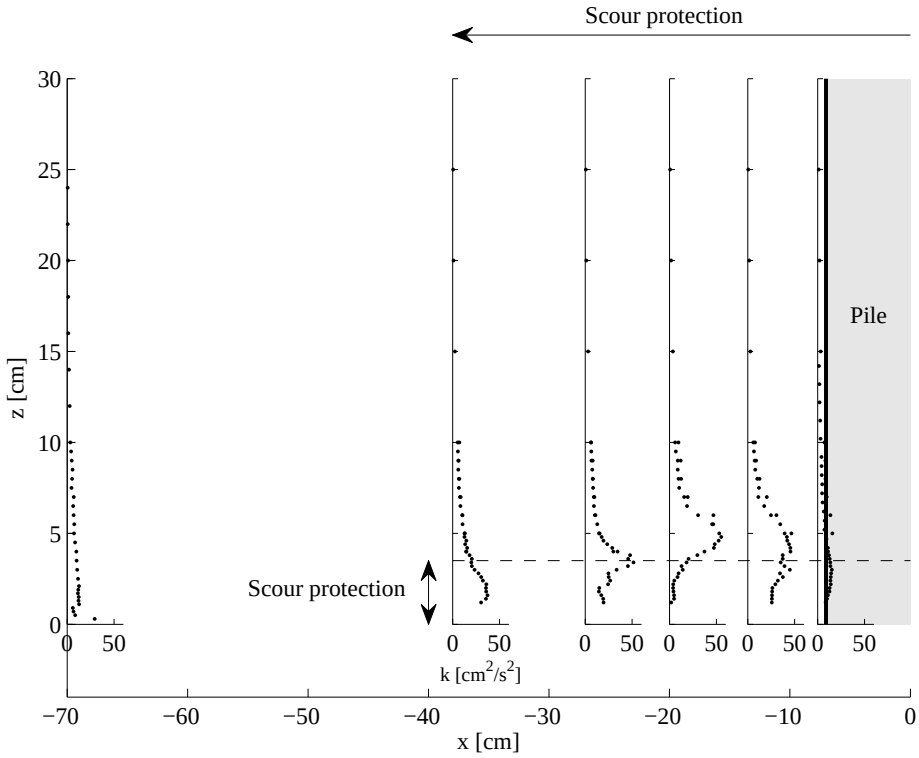

Figure 2.5: *Turbulent kinetic energy profiles at different distances upstream of the mono-pile with one layer of 4.3 cm stones.*

Yulistiyanto (1998). Roulund *et al.* (2005) showed that the high Froude number had an important influence on the flow at the side and downstream of the pile and for that reason a comparison of the two sets of data is only indicative.

Downstream of the pile the turbulence level is around 3 times higher at $z = 3.0$ cm, but the turbulence level is rapidly decreasing to be less than the undisturbed situation approximately 1 cm above the base bottom. In Graf and Yulistiyanto (1998)) the turbulence level was always the same or larger downstream of the pile compared with the undisturbed turbulence level.

By comparing Fig. 2.3-2.6 it is seen that sinking of the protection layer will take place upstream of the pile where the velocities and turbulence levels are relatively high due to the horseshoe vortex penetrating into the protection layer, while no sinking or even deposition of sediment will take

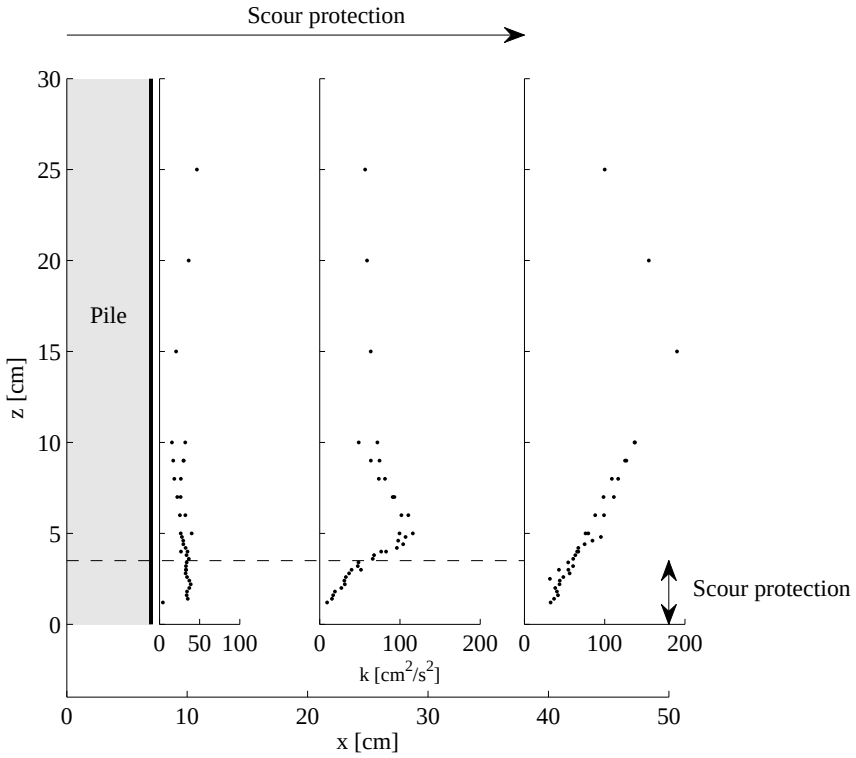

Figure 2.6: *Turbulent kinetic energy profiles at different distances downstream of the mono-pile with one layer of 4.3 cm stones.*

place on the downstream of the pile due to the low velocities and turbulence levels near the base bottom under underneath the protection layer. Fig. 2.3-2.6 have shown the velocity and turbulence around a pile with a single layer scour protection. However, most placed rock scour protection consists of more than one layer and for that reason the effect of the scour protection thickness has been studied. Upstream of the pile at $x = -12.0$ cm, where the maximum velocity within the stones was measured in the case of one layer of stones, the two horizontal components of the flow were measured for one to seven layers of stones ($D_c = 4.3$cm). The velocities were measured using the pen-size LDA-probe described earlier. The probe was placed vertically and was measuring through a vertical hole in between the stones. This vertical hole was around 1.5 cm in diameter. The measuring hole could have an influence on the kinematic in the scour protection. First of all the, diameter

of the hole is the same size as the natural cavities in between the stones so the only difference is that it extends from the base bottom to the top of the scour protection. For this reason the largest influence, if any, should be on the vertical velocity at this particular location. The vertical velocity is not measured in the present case, but it was measured above the stones in the case of one layer of stones (same test as the measurement shown in figs. 2.3 to 2.6). In this case the vertical velocity was measured to 3.5 cm/s (downwards) just above the protection layer. This should be compared to horizontal velocities typically up to around 10 to 15 cm/s inside the scour protection, so even if the measuring hole allowed a larger vertical inflow of water to the scour protection at this particular location the influence on the horizontal velocities will be small.

The depth-averaged approach velocity was kept constant at 40 cm/s. In the case of the tests undertaken with 1 to 3 layers of stones the water depth was maintained at 30 cm, and was increased to 45 cm for the tests with 4 to 7 layers of stones. An additional test with 30 cm water depth was conducted in the case of 4 layers of stones. This test showed no significant difference compared to the test with a water depth of 45 cm. A new layer of stones was added for each test, so that the stone configuration of the lower layers was preserved for all the tests. The streamwise velocities are plotted in Fig. 2.7 and the turbulent kinetic energy, determined as described earlier, is plotted in Fig. 2.8.

Fig. 2.7 a to c shows the same tendency as seen in Fig. 2.3, the horseshoe vortex is penetrating into the stone layers generating an upstream directed flow near the base bottom. When the thickness of the scour protection is increased up to 3 layers this upstream directed flow is decreased (Fig. 2.7.a-c). When adding 4 to 7 layers of stones the near-bed flow speed starts to increase, but now it is directed downstream (Fig. 2.7.d-g). When seven layers of stones are applied, the near-bed velocity increases to approximately the same value as in case of one layer, but in the opposite direction. The horseshoe vortex has a limited size, determined by the pile diameter and cannot penetrate deeper than the size of the vortex. In the present case the horizontal size of the horseshoe vortex is approximately 13 cm, see Fig. 2.3. The vertical size of the horseshoe vortex is limited to be approximately the same as the horizontal size. In the case of 4 layers of stones, which gives a total thickness of protection of 12.3 cm, therefore the horseshoe vortex should be almost completely embedded in the scour protection. This is not possible and the horseshoe vortex remains in the top layers of the scour protection and leaves space for a second vortex below the upper vortex and creates a double horseshoe system. The lower vortex is driven by the upper vortex and is rotating in the opposite direction (Fig. 2.7.d-g).

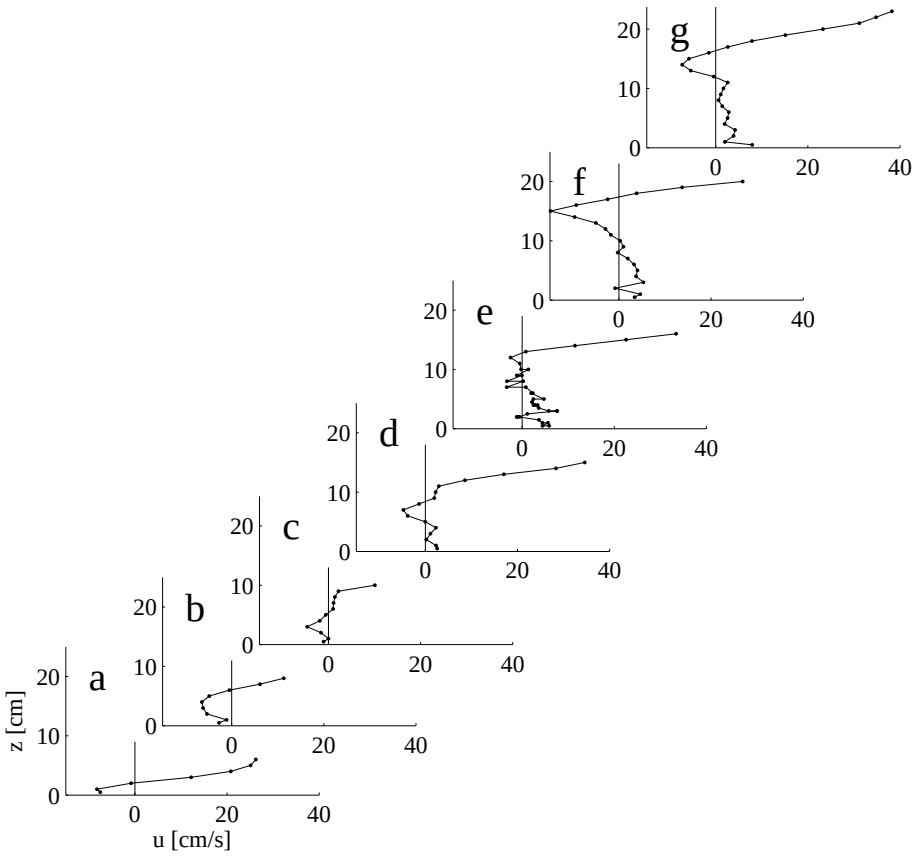

Figure 2.7: *Streamwise velocity profiles for one to seven layers of 4.3 cm stones. Panel a is for one layer of stones, b for two layers etc. The profiles were measured 12 cm upstream of the pile centre.*

Although the near-bed speed is approximately the same in the case of one and seven layers of stones, the potential of sinking of the scour protection is smaller in the case of seven layers of stones compare to one layer. Fig. 2.8 shows the turbulent kinetic energy for the different tests and it is clear that the turbulence decreases rapidly with increased thickness of the scour protection, although it has a slight tendency to increase for six and seven layers of stones. The figure shows that the near bottom turbulence is approximately halved for each additional layer until three layers is added. When the fourth layer is added the near-bed turbulence suddenly drops to approximately 1/5 of the turbulence obtained in the three layer case.

In addition to the measurements described above, the velocities inside the scour protection with one, two and three layers of stones without a pile

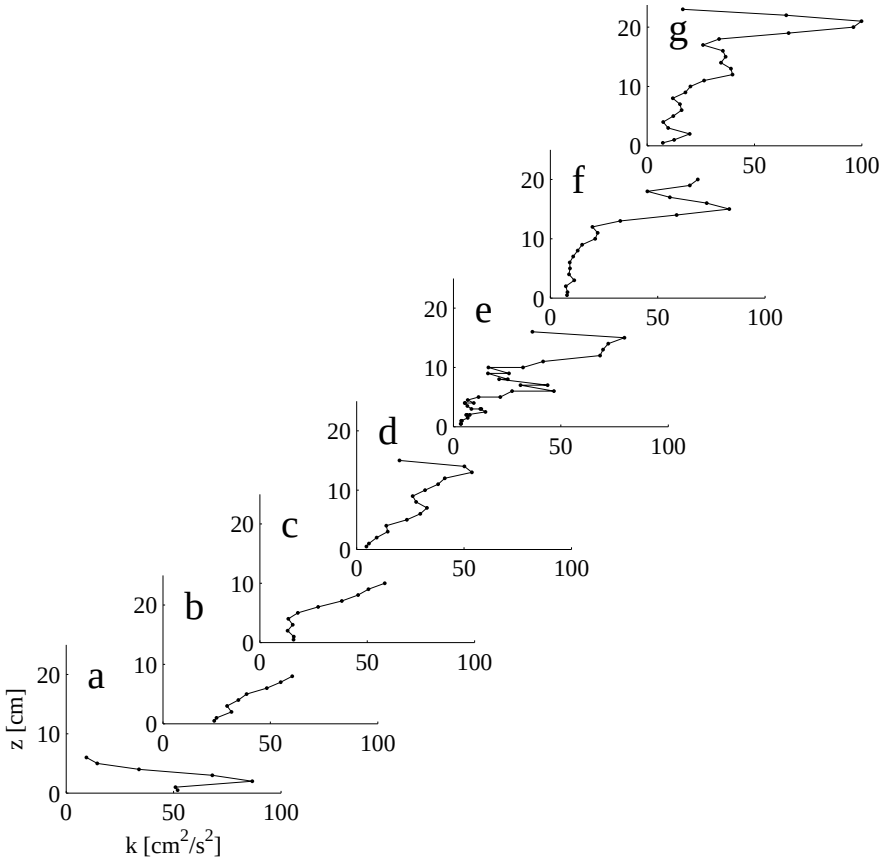

Figure 2.8: *Turbulent kinetic energy profiles for one to seven layers of 4.3 cm stones. Panel a is for one layer of stones, b for two layers etc. The profiles were measured 12 cm upstream of the pile centre.*

were measured. All three measurements showed very low velocities near the base bottom, $z = 1.0$ cm. In the one layer case the velocity was around 2 cm/s while in the two and three layer cases the velocity was O(1 mm/s). This shows that the flows around the pile are caused by the adverse pressure gradient of the pile.

In order to obtain a more detailed picture of the flow in between the stones in the case of the double horseshoe vortex system the half pile setup described earlier was used. This setup allowed a detailed measurement of the flow in the pores, see Fig. 2.9, without creating measuring holes from the top of the scour protection. The disadvantage of the setup is the presence of the transparent vertical wall. When the full pile is replaced by a half pile and a vertical wall the flow in the wake at the downstream side of the pile

is completely changed as the vortex shedding cannot take place under these conditions. For this reason the downstream side of the cylinder has not been investigated using this setup. Another disadvantage is the development of a boundary layer along the vertical wall. This boundary layer was measured to be approximately 2 cm thick at 13.0 cm upstream of the pile centre. This is a relatively thin and undeveloped boundary layer and it will develop further until the separation point at the half pile. As the boundary layer is thin the energy loss can be neglected. The effect of this boundary layer on the flow through the pores of the protection layer will for this reason be minimal. We note that Fig. 2.9 should only be used qualitatively as an example of the flow pattern in a scour protection upstream of a mono-pile since the pile in the present setup is not a full pile, but rather a half pile.

Fig. 2.9 shows the situation after the breakup of the single horseshoe vortex system. The new system consists of two significant vortices: One at the base bottom adjacent to the pile and one at the top of the scour protection with centre around $x = -16$ cm. Both vortices are rotating clockwise. Between the upper vortex and the pile a strong downflow takes place. Just under the top of the scour protection this flow splits up in two. One branch is following the pile surface to the base bottom where it is driving the lower vortex. The other branch is flowing down between the two vortices, partly driving the upper vortex and partly continuing to the base bottom where it flows in the streamwise direction and seems to flow in the crossflow direction when it meets the lower vortex. A sketch of the flow is shown in Fig. 2.10.

2.4.2 Sediment-Bed Results

Based on the results of the flow visualizations and the velocity measurements the flow pattern around the pile causing the sinking of the scour protection can be described as follows: The horseshoe vortex penetrates into the scour protection and causes removal of sediment adjacent to the upstream side of the pile. This leads to the sinking of stones due to the exceedance of the bearing capacity of the soil, or re-arrangement of stones e.g. by tilting. The scoured material is transported by the horseshoe vortex either upstream to the separation line or to the sides. The material will in both cases be deposited in between the stones, relatively far from the pile or, if the horseshoe vortex is strong enough, sucked/winnowed up into to the main body of the flow and transported downstream. The reason for the suctioning/winnowing out of the sand from the scour protection is a combination of suction by the main flow, as described in Sumer *et al.* (2001), and the upward directed flow at the separation line between the incoming flow and the horseshoe vortex of which the mean flow and turbulence characteristics are given in Figs. 2.7-

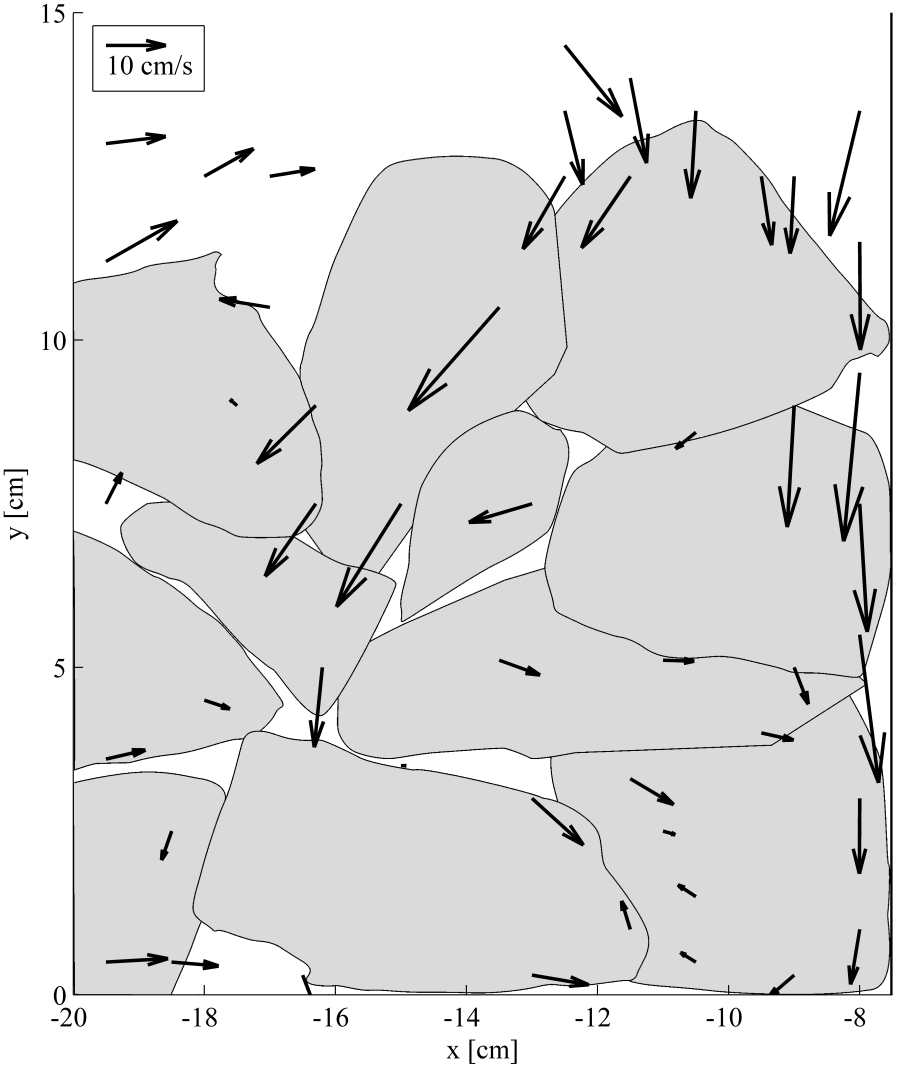

Figure 2.9: *Pore velocities upstream of the pile in case of 4 layers of stones. The velocities were measured through a transparent wall with a half pile mounted on.*

2.8. The tests have shown that the deposition inside the scour protection is very limited on the upstream side of the pile, and for this reason most of the sediment must be sucked out from the scour protection and transported away. Sumer *et al.* (2001) used the parameter e/D_c as the non-dimensional parameter for the sinking of an undisturbed protection layer. The process for a scour protection around a pile is in many ways similar to that described

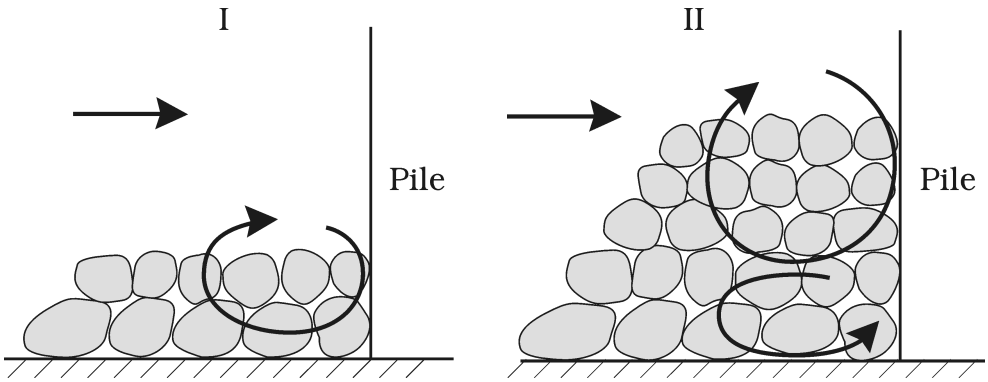

Figure 2.10: *Sketch of the flow plotted in Fig. 2.9.*

above and the parameter e/D_c is also adopted for the present process as well.

The size and strength of the horseshoe vortex is determined by the flow velocity and the pile size. The horseshoe vortex causes the removal of the sediment and a larger pile/horseshoe vortex will, in absolute terms, cause a larger sinking. On the other hand, for a given pile diameter, the larger the ratio D_p/D_c, the larger the penetration of the agitating forces. Therefore, the sinking, e_{max}/D_c, should be larger for larger values of D_p/D_c. If the ratio $D_p/D_c = 0$ the situation is the undisturbed protection, Sumer *et al.* (2001). In this case Sumer *et al.* (2001) showed that the ratio $e_{max}/D_c = 0.1$ for one layer of stones is in agreement with the trend seen in Fig. 2.11. The velocity is indirectly included in the mobility number.

Fig. 2.11 shows the non-dimensional sinking relative to the non-dimensional pile size. The data given in Fig. 2.11 are a slightly extended version of the data first reported in Nielsen *et al.* (2010). The caption of the figure includes the range of the mobility number, Eq. 2.1. The latter was given in Nielsen *et al.* (2010) in terms of the Shields parameter, θ, the mobility number is adopted in the present paper in favour of θ for its convenience when implementing the present data in engineering applications.

There is a clear trend, indicating that the larger the pile diameter, the larger the sinking. This is linked to the horseshoe vortex; the larger the pile diameter, the larger the horseshoe vortex, and the larger the scour underneath the stones, and, therefore, the larger the sinking. The sinking decreases for increasing number of layers. This result is also valid for large piles as there is a one-to-one relationship between the horseshoe vortex size (normalized by pile diameter) and the water depth-to-pile-diameter ratio (Sumer and Fredsøe (2002), p 158).

When the number of layers is increased from one to two the sinking is

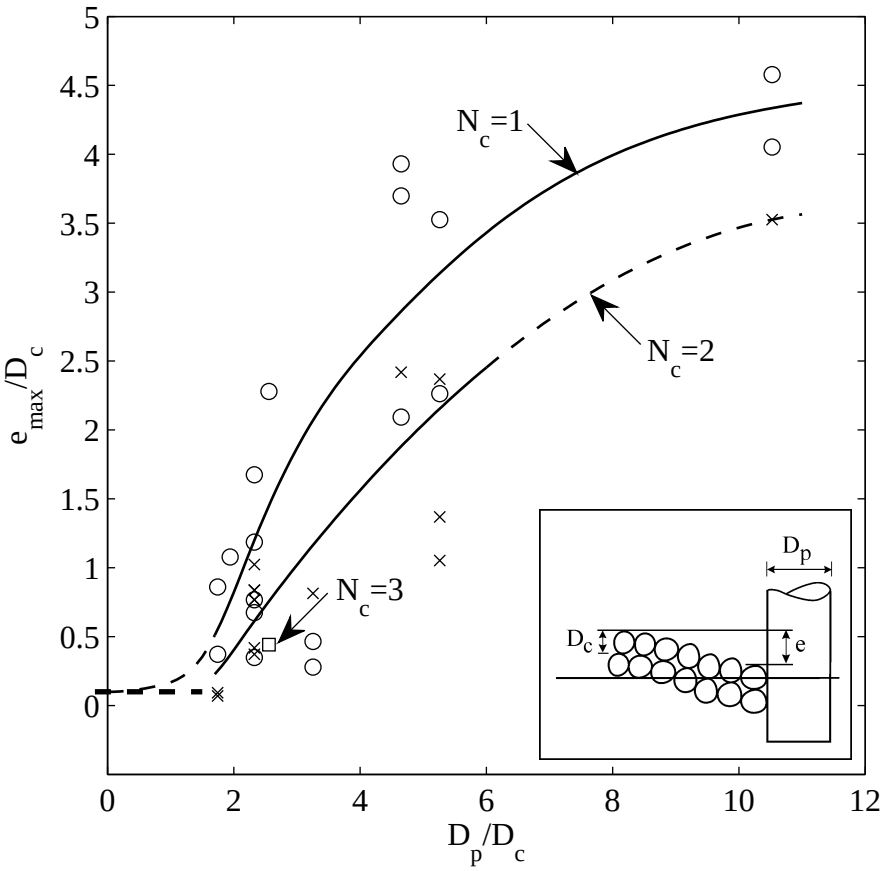

Figure 2.11: *Equilibrium sinking of the scour protection. The range of the mobility number is 35<ψ<105 (live bed) and the range of h/D_p is 1.5≤ h/D_p ≤5.1.* ◯*:* $N_c = 1$, ×*:* $N_c = 2$, □*:* $N_c = 3$. *Thick dashed line: No pile and* $N_c = 1$ *(Sumer* et al. *(2001)).*

decreased with around a factor of two for D_p/D_c smaller than around 5, however, the effect is much smaller for $D_p/D_c = 10$. Only one test has been carried out with three layers and considering the scatter of the results with one and two layers it is not clear if the third layer provides any significant extra protection.

Regarding the scatter in the data in Fig. 2.11, this may be attributed to the way in which the stones are laid around the model pile, considering the fact that the stone size in the tests was relatively large.

The time-scale of the sinking process is the other important quantity.

The concept of time-scale has been used for many different scour problems e.g. scour under pipelines and around piles, see e.g. Sumer and Fredsøe (2002) and also for sinking of cover stones, see Sumer and Fredsøe (2002) and Dixen *et al.* (2008). The non-dimensional time-scales of the sinking as function of the mobility number in case of one and two layers of stones are shown in Fig 2.12-2.13. The non-dimensional time-scale is defined in the same way as for scour around piles:

$$T^* = \frac{\sqrt{g(s-1)d_{50}^3}}{D_p^2} T \tag{2.3}$$

From dimensional considerations, the non-dimensional time-scale is a function of two parameters:

$$T^* = f\left(\psi, \frac{D_p}{D_c}\right) \tag{2.4}$$

This is because the larger the mobility number the more vulnerable the sediment will be to be to the agitation of the flow, and, therefore, the smaller the time-scale. If D_p/D_c is large the relative penetration distance will be small and the sediment will be more exposed and the time-scale will be shorter. The time-scale is decreasing with increasing mobility number, this is consistent with previous studies of scouring and sinking of stone covers, e.g. Sumer *et al.* (2001) and Sumer and Fredsøe (2002).

The relatively large scatter of the time-scale data presented in Fig. 2.12-2.13 might be explained by the fact that the data covers a large range of h/D_p. Sumer *et al.* (1992) reported a strong influence of h/D_p on the time-scale in the case of an unprotected pile, and it is likely that this will be the case for a pile with scour protection as well.

2.5 Horns Rev I - an Example

The sinking of the scour protections at the Horns Rev I Wind Farm (Denmark) is well documented, see Hansen *et al.* (2007). Horns Rev I consists of 80 turbines founded on mono-piles in the Danish part of the North Sea. The wind farm is located at approximately 5 to 15 m water depth and is exposed to strong tidal current and large waves, including breaking waves. The foundations are 4.2 m in diameter and the scour protection consists of a 0.5 m thick filter layer of stones with a mean size of 10 cm. The filter layer is covered by 2 layers of stones with a mean size of 40 cm. According to Hansen *et al.* (2007) the scour protections have sunk up to 1.5 m adjacent to the foundations three years after installation. Hansen *et al.* (2007) concluded,

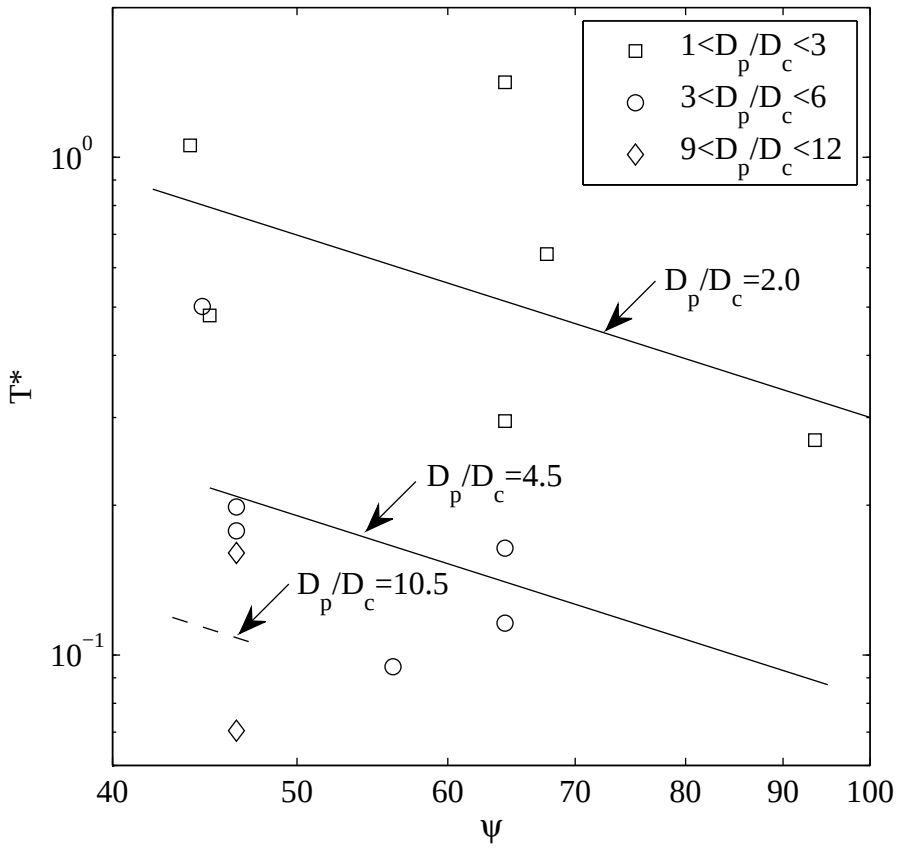

Figure 2.12: *Time-scale as function of the mobility number in case of one layer of protection stones. For the range of h/D_p is 1.5$\leq h/D_p \leq$5.1.*

based on simple calculations that the sinking of the scour protections was most likely caused by ineffective filter layers.

Although the present study does not include the effects of filter layers and waves it will still be interesting to compare the observations from Horns Rev with the results of this study. For Horns Rev I Wind Farm $D_p/D_c = 10.5$. This will give an expected sinking of around $e_{max}/D_c = 3.5$ or $e_{max} = 1.4$ m for two layers of cover stones, see Fig. 2.11. The latter figure (1.4 m) is apparently not radically different from the observed value at Horns Rev I, i.e. 1.5 m. Presumable this result supports that the effect of the filter layers at Horns Rev I Wind Farm seems to be not very significant.

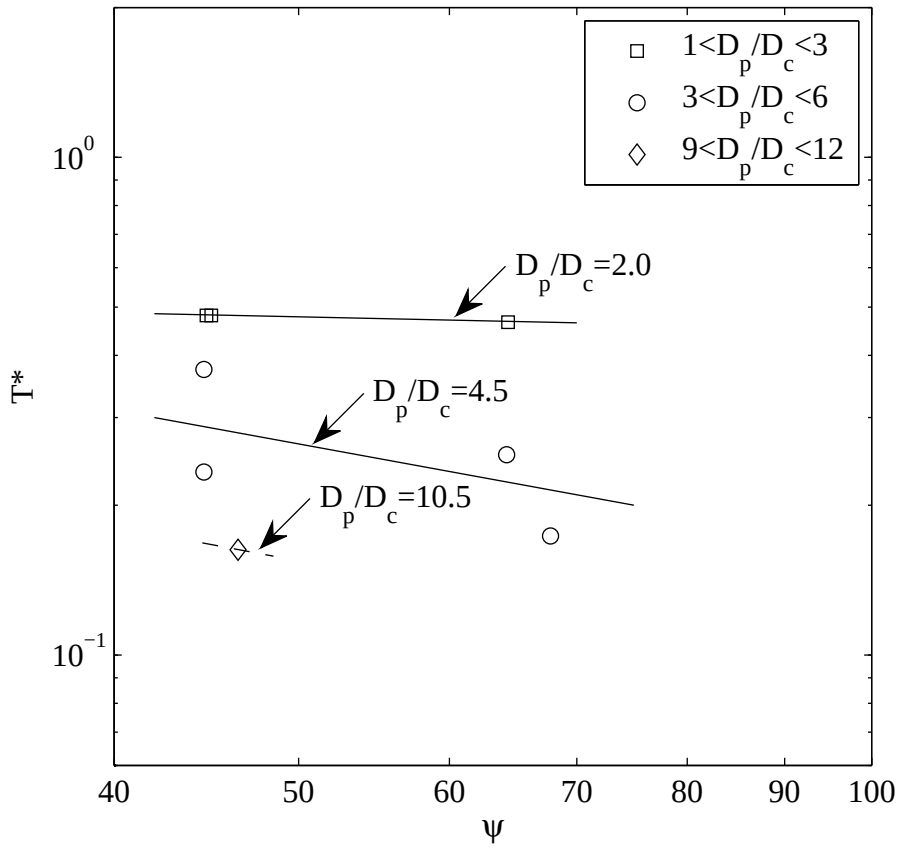

Figure 2.13: *Time-scale as function of the mobility number in case of two layers of protection stones. For the range of* h/D_p *is* $1.5 \leq h/D_p \leq 5.1$.

2.6 Conclusion

It is found that the horseshoe vortex caused by the adverse pressure gradient at the upstream edge of the pile can penetrate into the scour protection and cause high flow velocities and levels of turbulence near the base sediment under the scour protection. It is shown that the horseshoe vortex system consists of one dominating vortex (single horseshoe vortex system) for relatively thin protection layers up to little less than one pile diameter thick. For thicker protection layers, the single horseshoe vortex system will break up into a system of two dominating vortices on top of each other. It is shown that the near bed velocities can be equally high in case of the single horse-

shoe vortex system and the double horseshoe vortex system. However, the turbulence level decreases in the case of a double horseshoe vortex system.

The mechanism causing sinking of the scour protection adjacent to the mono-pile has been identified as the horseshoe vortex penetrating into the scour protection. When the horseshoe vortex penetrates into the scour protection it transports the sediment adjacent to the pile upstream, where it is winnowed and transported away by the main flow.

It is found that a larger pile diameter relative to the size of the protection stones will cause a larger sinking. The maximum sinking is found to be approximately 4 to 4.5 times the diameter of the cover stones in case of one layer of stones and approximately 3 to 3.5 in case of two layers of stones.

Two layers of stones will decrease the sinking relative to one layer of stones with the same size. For values of D_p/D_c smaller than approximately 5 the sinking seems to be reduced by a factor of two if the number of layers is increase from one to two.

Acknowledgement

This research was carried out as part of the Statkraft Ocean Energy Research Program, sponsored by Statkraft (www.statkraft.no). The study was partially supported by the Danish Council for Strategic Research (DSF)/Energy and Environment under the program Seabed Wind Farm Interaction (http://sbwi.dhigroup.com, sagsnr. 2104-07-0010) and DHI (www.dhigroup.com). Part of the fixed-bottom experiments and a major part of the sediment bed experiments were conducted by MSc Adriana Hudecz. Part of the sediment bed experiments were conducted by François Roignant.

Chapter 3

Flow and bed shear stresses in scour protections around a pile in a current

This chapter is submitted to Coastal Engineering:
Nielsen, A.W., Liu, X., Sumer, B.M. and Fredsøe, J.: "Flow and bed shear stresses in scour protections around a pile in a current"

Published article: A revised version of this chapter was accepted for publication on the 5th of September 2012. The reference is: Nielsen, A.W., Liu, X., Sumer, B.M. and Fredsøe, J. (2013). Flow and bed shear stresses in scour protections around a pile in a current. *Coastal Engineering*, **72**, 20-38 (doi: 10.1016/j.coastaleng.2012.09.001).

Abstract

Transport of bed sediment inside and beneath the scour protection may cause deformation and sinking of the scour protection for pile foundations. This may reduce the stability of the mono pile and change the natural frequency of the dynamic response of an offshore wind turbine installed on it in an unfavourable manner. Using physical models and 3D computational fluid dynamic (CFD) numerical simulations, the velocity and bed shear stresses are investigated in complex scour protections around mono piles in steady current. In the physical model the scour protections consisted of an upper cover layer with uniformly distributed coarse stones and a lower filter layer with finer stones. For the numerical simulations, the Flow-3D software was used. The scour protection layers were simulated with different numerical approaches, namely regularly arranged spheres, porous media, or their combinations (hybrid models). Numerical simulations with one or four layers

of cover stones without filter layer were first computed. Three additional simulations were then made for a scour protection with a cover layer and a single filter layer. Finally, a simulation of a full scale foundation and scour protection was made with porous media approach.

Based on the physical and numerical results, a method to determine the critical stones size to prevent motion of the base sediment is established and compared to a full scale case with sinking of scour protection (Horns Rev I Offshore Wind Farm, Denmark). It is also found that the CFD simulations are capable of calculating the flow velocities when the scour protection is represented by regular arranged spheres, while the turbulence in general is underestimated. The velocity can also be calculated using porous media flow approach, but the accuracy is not as good as for spheres. The deviation is more severe for more complex scour protections. In general, computational models provide valuable information for the prediction and design of scour protections for offshore wind farms.

Keywords: Scour Protection; Mono pile; foundations; bridge piers; offshore wind turbines.

3.1 Introduction

During the last decade more and more wind farms have been erected offshore. One of the first larger offshore wind farms is the Horns Rev I in Denmark. The Horns Rev I is located in relatively shallow water (6.5 to 13 m water (MSL)) about 20 km off the Danish West Coast in the North Sea. This area is exposed to tidal currents (around 0.5 m/s, up to 1 m/s during storm situations) and large waves from the North Sea. The wind turbines are founded on mono piles with a scour protection made of a two-layer cover (quarry run from around 350 mm to 550 mm) and a 0.5 m thick filter layer (sea stones from around 30 mm to 200 mm) between the armour layer and the seabed. The wind farm was installed in the summer of 2002. A control survey in 2005 showed that the scour protections adjacent to the mono piles sank up to 1.5 m (Hansen *et al.*, 2007). This was unexpected and shortly after the survey in 2005 the holes were repaired by adding additional stones.

Whitehouse *et al.* (2011) compiled the experience of scour and scour protections from several offshore wind farms and other piled foundations. In at least one other case, Egmond aan Zee Offshore Wind Farm, has sinking of the scour protection been observed adjacent to the pile. One year after the installation the scour protection had sunk 0.2 to 0.8 m adjacent to the pile, somewhat more than the general sinking of the scour protection, (Raaijmakers *et al.*, 2007). Whitehouse *et al.* (2011) reported that the scour protection at Arklow Offshore Wind Farm might have sunk, although

the scour protection was installed in an already developed scour hole. The possible sinking might be because of irregular placement of the rocks, some places with noticeable voids between the place rocks.

Scour around unprotected piles have been studied extensively over the last decades. Most of the available results are compiled in Breusers and Raudkivi (1991); Hoffmanns and Verheij (1997); Whitehouse (1998); Melville and Coleman (2000) and Sumer and Fredsøe (2002). This work has in recent years made it possible to develop numerical models for long-term prediction of the development of scour holes around mono piles (Nielsen and Hansen, 2007; Raaijmakers and Rudolph, 2008; Harris *et al.*, 2010). Also numerical studies of unprotected piles have been performed successfully over the last decades, see e.g. Roulund *et al.* (2005); Liu and García (2008). Scour protection of piles has not been studied nearly as much and the mechanism of failure of scour protections around a mono pile has only been described briefly. In order to understand the mechanisms that cause the sinking of the scour protection, an extensive program of physical model tests with steady current has been carried out in the present study, in an attempt to contribute to the knowledge obtained recently by Chiew (1995); Chiew and Lim (2000); Lauchlan and Melville (2001); Chiew (2002); De Vos (2008) among others. The first results of this extensive program of physical model tests were presented in Nielsen *et al.* (2010, 2011). This study showed that the horseshoe vortex was the main reason for the sinking of scour protections around mono piles. It was postulated that current at Horns Rev I could have caused the sinking of the scour protection if the horseshoe vortex was strong enough to caused sediment transport in the scour protection. However, no direct evidence has been obtained to prove sediment motion in the scour protection.

To test the hypothesis and improve design criteria, this study aims at investigating the velocity distribution, coherent turbulent flow structure, and most importantly critical bed shear stress under a scour protection around a mono pile in steady current using physical and numerical model tests. The structure of this paper is the following. First, the setup and test conditions for the physical model tests are introduced. Three different facilities were used: (1) a 2 m wide, 0.5 m deep flume for measuring flow velocities inside the scour protection, (2) a 3 m wide and 1 m deep flume for determine the critical bed shear stress underneath the scour protection and (3) a 4 m wide and 1 m deep flume for sediment bed experiments to determine the equilibrium sinking of the scour protection. Then the details about the numerical modelling will be presented. Three different representations of the scour protection have been used for the numerical models: (1) The individual stones represented as regularly arranged spheres, (2) the scour protection

represented as one or in case of a filter layer two different porous media and (3) a hybrid model, which is a combination of the two previous methods, where the individual stones are represented by regularly arranged spheres at locations of special interest and by porous media at other locations. The numerical models will be validated against the results of the physical model tests in the present paper and results reported in Nielsen *et al.* (2011). These two parts will be followed by a discussion where a new mobility number for the sediment underneath a scour protection (Eq. 3.5) is introduced and validated against the results of the physical model tests. The mobility number can be used to determine whether sediment underneath the scour protection will be mobile or not, given the approach current velocity, the pile diameter, and filter stone size. Also the results of the different numerical models are discussed in relation to the results of the physical model tests.

It is found that the sediment underneath the scour protections at the Horns Rev I Wind Farm has been mobile during extreme current events and the actual observed sinking of the scour protection is caused by the current, as postulated in Nielsen *et al.* (2011).

3.2 Physical model setup

Three different kinds of experiments were conducted. (1) Velocity measurements; (2) measurements of the critical bed shear stress underneath the scour protection; (3) measurements of stone sinking in the scour protection. All the experiments were for the most part made with a mono pile and a scour protection of one filter layer and a cover layer.

3.2.1 Velocity Measurements in the Scour Protection

The tests where the velocities inside the scour protection were measured, were conducted in a 2 m wide, 23 m long and 0.5 m deep flume. An approximately 0.5 cm thick, 2.9 m long, plastic plate, with 15 cm long tapered upstream end, was placed on the base bottom over the entire width of the flume to obtain a smooth bed. The plate was painted matt black to reduce reflections of the laser beams from the Laser Doppler Anemometer, LDA, used for the velocity measurements.

The flow velocity was measured with a submerged pen size LDA probe. It was a two component probe, approximately 1 cm in diameter and 15 cm long. It had a focal length of 80 mm (in water), a beam spacing of 8 mm and a beam diameter of 0.27 mm. The probe was placed vertically and was measuring through a vertical hole in between the stones. This vertical hole was around 1.5 cm in diameter in the cover layer and 0.5 to 1.0 cm in the filter layer. The pile with an outer diameter of 14.0 cm was placed 2.0 m

downstream of the upstream end of the plastic plate (approximately 15 m from the inlet section). The bottom ends of the piles were completely sealed. The scour protection consisted of a 2 cm thick filter layer with stone size of 1.1 cm covered by one, two and four layers of cover stones with a mean stone size of 4.3 cm. The plan-view extension of the scour protection was 75 cm. The setup was the same as that used to measure the velocities inside scour protections without filter layer, see Nielsen *et al.* (2010) and Nielsen *et al.* (2011). The setup is described in details in Nielsen *et al.* (2010).

3.2.2 Measurements of the Bed Shear Stresses underneath the Scour Protection

The tests to determine the bed shear stress underneath the scour protection were conducted in a 3 m wide, 35 m long and 1 m deep flume. The flume was equipped with recirculation pumps providing mean current speeds up to approximately 50 cm/s.

Two different pile sizes were tested: (1) a pile with a diameter, D_p, of 1.0 m and (2) a pile with a diameter of 0.55 m. The bed shear stress was estimated using small plastic particles: The particles (size of approximately 0.5 to 3 mm) were placed on the base bottom in between the filter stones and were observed through the transparent base bottom. The particles were placed in the filter layer via a thin, rigid, and surface piercing plastic tube (inner diameter 5 mm and outer diameter 7 mm). The end of the tube was placed at the top of the lowermost filter stones, 12.5 and 25 cm upstream of the upstream edge of the pile for the 55 cm and 1.0 m pile, respectively. In both cases the tube was placed 4 to 6 cm off the centre line of the pile (Fig. 3.1), the offset was introduced because a support beam blocked the view through the transparent bottom at the centre line.

In the case of 1.0 m pile a scour protection of round stones was applied. Four different scour protections were tested. The plan-view extension of the scour protection was in all cases 3 m and consisted of a filter layer with $d_{50} = 2.3$ cm stones and a cover layer of $d_{50} = 9.0$ cm stones (stone nos. 3 and 5, Table 3.1). The four scour protections were: (1) a 20 cm thick filter layer under two layers of cover stones, (2) a 20 cm thick filter layer under one layer of cover stones, (3) a 20 cm thick filter layer without cover and (4) a 10 cm thick filter layer without cover.

In the case of 0.55 m pile two scour protections were applied: A scour protection of crushed stones with a plan-view extension of 1.5 m. It consisted of a 10 cm thick filter layer of stones with $d_{50} = 1.1$ cm and a cover layer of two layers of $d_{50} = 4.3$ cm stones (stones no. 1 and 4, Table 3.1).

The second setup had the same overall dimension, but the scour protection consisted of three layers of filter stones, $d_{50} = 4.3$ cm, and one layer of

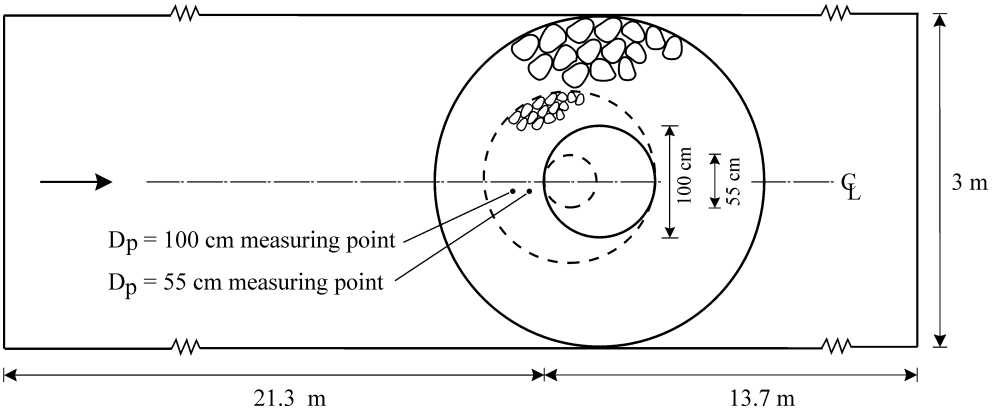

Figure 3.1: *Setup for the physical experiments to determine the bed shear stress underneath the scour protection. The fully drawn lines are the $D_p = 1.0$ m pile and corresponding perimeter of scour protection and the dashed lines are the $D_p = 0.55$ m pile and corresponding perimeter of scour protection.*

cover stones, $d_{50} = 9.0$ cm (stones no. 4 and 5, Table 3.1).

The flow velocity was measured using a propeller, 5.0 cm in diameter. The setup is shown in Fig. 3.1.

3.2.3 Sediment Bed Experiments

The sediment bed experiments used to determine the equilibrium sinking of the scour protection with filter layer were conducted in a 4.0 m wide, 28 m long and 1.0 m deep flume. An around 10 m long and 0.35 m deep sand section, with a 3 m long ramp at the upstream end was installed. The ramp was made with a core of concrete blocks covered by at least one layer of stones ($d_{50} = 4.3$ cm). Two piles were tested at the same time, in order to save time. The piles (11.0 and 20.0 cm in diameter) were placed at the same distance from the inlet and the distance between the piles was 1.75 m, which was large enough to ensure no interference. The setup was the same as the setup used to measure the sinking of the scour protections without filter layer, see Nielsen *et al.* (2010) and Nielsen *et al.* (2011). The setup is described in details in Nielsen *et al.* (2010).

3.3 Test conditions

Six different kinds of stones were used for the experiments. The type, size, grading of the stones and the porosity, n, are listed in Table 3.1.

Table 3.1: *Different kinds of stones used for the experiments.*

Stone no.	Type	d_{15} [cm]	d_{50} [cm]	d_{85} [cm]	n
1	Crushed	0.9	1.1	1.3	0.47
2	Crushed	1.6	1.9	2.8	0.45
3	Sea stones	1.8	2.3	3.1	0.45
4	Crushed	3.7	4.3	4.9	0.43
5	Sea stones	7.7	9.0	12.5	-
6	Sea stones	9.0	10.3	11.2	-

3.3.1 Flow velocities inside the scour protection

For the measurements of the flow velocities inside the scour protection in the 2 m wide flume stone no. 1 was used for filter layer and stone no. 4 for cover layers. The filter layer was 2 cm thick and a cover layer with a thickness of one, two and four layers was tested. This gave a total thickness of the scour protection of 5.2, 8.4 and 13.7 cm for one, two and four cover layers, respectively. During these experiments the depth averaged approach velocity was kept constant at 0.4 m/s. The water depth was 30 cm in case of one and two layers of cover stones and 45 cm in the case of four layers of cover stones.

3.3.2 Bed shear stress underneath the scour protection

For the bed shear stress experiments in the 3 m wide flume with a pile diameter of 1.0 m the filter layer consisted of stone no. 3 and the cover was made of stone no. 5. In the case of a pile diameter of 0.55 m two different filters and cover layers were tested: (1) stone no. 1 as filter layer and stone no. 4 as cover layer and (2) stone no. 4 as filter layer and stone no. 6 as cover layer. The water level of 90 cm to the base bottom was maintained.

The bed shear stress was determined by placing small plastic grains underneath the scour protection upstream of the pile. Two different plastic materials were used: (1) a plastic material with specific density, $s = 1.045$. The particles were cut from cylindrical shaped plastic particles with a diameter of 1.2 to 1.5 mm. A 0.2 to 0.4 mm thick slide was cut from the end of the cylinder and divided into "cake pieces"; 1/1, 1/4, 1/8 and 1/16 of the cylinder. Based on the volume of these pieces the corresponding spherical diameter was calculated. (2) A plastic material with specific density of $s = 1.31$. In this case the particles were cut into cube shaped particles. The size of these particles was approximately the same as for the previous material.

It was not possible to use the more dense material than $s = 1.045$ in the case of the 1.0 m pile as the required approach velocity was too high considering the blockage effect caused by the structure size relative to the flume size.

The test was conducted by increasing the approach velocity in small increments, approximately 3 cm/s, until the particle (placed underneath the scour protection) was removed; a particle was defined "as removed" if it (1) was moved through a narrow channel between two stones to another pore or (2) was moved to the side of the original pore where it was stuck.

The results and main test conditions of the physical model tests to determine the bed shear stress underneath the scour protection are listed in Table 3.2. Where D_p is the pile diameter, D_c is the mean cover stone size, D_f is the mean filter stone size, N_c is the number of cover layers, t_f is the thickness of the filter layer, U_∞ is the undisturbed depth averaged velocity, d is the particle size, θ_c is the critical Shields number underneath the scour protection, Ω_c is the critical mobility number (Eq. 3.5) and Re is the Reynolds number (Eq. 3.7).

3.3.3 Equilibrium sinking of the scour protection with filter layer

Four different materials were used for the sediment bed experiments in the 4 m wide flume: Stone no. 1 (filter layer), stone no. 2 (filter layer), stone no. 4 (filter and cover layer) and stone no. 6 (cover layer). The thickness of the filter layer was kept in the interval from approximately 1.5 cm to 5.5 cm corresponding to approximately 1 to 3 layers of stones. The total thickness of the scour protection was in the interval from approximately 3 to 10 cm corresponding to a relative thickness, D_p/t_{SP}, from 1.3 to 6.1. From Nielsen *et al.* (2011) it can be seen that the flow in the scour protection changes significantly for a scour protection without filter layer if D_p/t_{SP} is smaller than approximately 2; this is also the case when a filter layer is introduced, see Figs. 3.18 and 3.19; however, only one test was made with D_p/t_{SP} smaller than 2 (the only test with two cover layers) for the rest for the tests D_p/t_{SP} was 2 or larger.

For all the sediment tests, the depth averaged velocity was kept constant at $V = 0.4$ m/s and the water depth was 56 cm. One sediment size of $d_{50} = 0.18$ mm was used for all the experiments. The overall extension of the filter layer from the upstream edge to the downstream edge was approximately 5 times the diameter of the pile while, for the cover layer, it was 4.5 times the diameter of the pile.

The results and main test conditions of the physical model tests to determine the equilibrium sinking of the scour protection are listed in Table 3.3.

Table 3.2: *Test conditions and results of the bed shear stress tests.*

Test no.	D_p [m]	D_c [cm]	D_f [cm]	N_c	t_f [cm]	U_∞ [cm/s]	d [mm]	s	θ_c	Ω_c	Re
1	0.55	4.3	1.1	2	10.0	16.5	0.85	1.045	0.06	1.3	141
2	0.55	4.3	1.1	2	10.0	25.2	0.49	1.045	0.08	5.2	124
3	0.55	4.3	1.1	2	10.0	20.9	0.62	1.045	0.07	2.8	130
4	0.55	4.3	1.1	2	10.0	15.5	0.62	1.045	0.07	1.6	96
5	0.55	4.3	1.1	2	10.0	22.1	0.46	1.045	0.09	4.3	102
6	0.55	4.3	1.1	2	10.0	28.4	0.62	1.045	0.07	5.2	176
7	0.55	4.3	1.1	2	10.0	44.2	0.62	1.31	0.04	2.3	274
8	0.55	4.3	1.1	2	10.0	45.6	0.62	1.31	0.04	2.5	283
9	0.55	4.3	1.1	2	10.0	52.9	0.62	1.31	0.04	3.3	328
10	1.00	9.0	2.3	2	20.0	20.1	0.44	1.045	0.09	3.9	88
11	1.00	9.0	2.3	2	20.0	18.5	0.53	1.045	0.08	2.8	98
12	1.00	9.0	2.3	2	20.0	22.3	0.53	1.045	0.08	4.0	118
13	1.00	9.0	2.3	2	20.0	22.3	0.53	1.045	0.08	4.0	118
14	1.00	9.0	2.3	2	20.0	19.3	0.61	1.045	0.07	2.6	117
15	1.00	9.0	2.3	2	20.0	19.9	0.66	1.045	0.07	2.5	132
16	1.00	9.0	2.3	2	20.0	24.6	0.77	1.045	0.06	3.4	188
17	1.00	9.0	2.3	2	20.0	18.7	0.84	1.045	0.06	1.8	157
18	1.00	9.0	2.3	2	20.0	24.4	1.10	1.045	0.05	2.3	267
19	1.00	9.0	2.3	2	20.0	25.7	1.92	1.045	0.04	1.5	493
20	1.00	9.0	2.3	2	20.0	26.1	1.94	1.045	0.04	1.5	506
21	1.00	9.0	2.3	2	20.0	23.1	2.21	1.045	0.04	1.0	510
22	1.00	9.0	2.3	2	20.0	21.7	2.44	1.045	0.04	0.8	530
23	1.00	9.0	2.3	2	20.0	22.1	2.45	1.045	0.04	0.9	541
24	1.00	9.0	2.3	1	20.0	20.1	2.40	1.045	0.04	0.7	481
25	1.00	9.0	2.3	1	20.0	23.9	2.40	1.045	0.04	1.0	575
26	1.00	9.0	2.3	1	20.0	28.2	1.74	1.045	0.04	1.9	489
27	1.00	9.0	2.3	1	20.0	26.4	0.99	1.045	0.05	3.0	261
28	1.00	9.0	2.3	1	20.0	23.4	0.54	1.045	0.08	4.3	127
29	1.00	9.0	2.3	1	20.0	20.7	0.80	1.045	0.06	2.3	166
30	1.00	9.0	2.3	1	20.0	26.9	0.64	1.045	0.07	4.9	171
31	1.00	9.0	2.3	1	20.0	20.7	1.01	1.045	0.05	1.8	209
32	1.00	9.0	2.3	1	20.0	26.9	0.52	1.045	0.08	6.0	139
33	1.00	9.0	2.3	1	20.0	23.6	0.65	1.045	0.07	3.7	153
34	1.00	9.0	2.3	1	20.0	19.4	0.52	1.045	0.08	3.1	100
35	1.00	9.0	2.3	0	20.0	25.2	2.38	1.045	0.04	1.1	601
36	1.00	9.0	2.3	0	20.0	19.5	2.31	1.045	0.04	0.7	450
37	1.00	9.0	2.3	0	20.0	22.0	2.66	1.045	0.04	0.8	584
38	1.00	9.0	2.3	0	20.0	20.8	1.77	1.045	0.04	1.0	368
39	1.00	9.0	2.3	0	20.0	27.0	1.46	1.045	0.04	2.1	392
40	1.00	9.0	2.3	0	20.0	29.9	1.11	1.045	0.05	3.4	330
41	1.00	9.0	2.3	0	20.0	23.7	0.70	1.045	0.07	3.4	165
42	1.00	9.0	2.3	0	20.0	22.3	0.88	1.045	0.06	2.4	197
43	1.00	9.0	2.3	0	20.0	20.8	0.54	1.045	0.08	3.4	111
44	1.00	9.0	2.3	0	20.0	26.4	0.67	1.045	0.07	4.4	179
45	1.00	9.0	2.3	0	20.0	25.7	1.88	1.045	0.04	1.5	483
46	1.00	9.0	2.3	0	10.0	19.2	2.31	1.045	0.04	0.7	444
47	1.00	9.0	2.3	0	10.0	23.8	0.85	1.045	0.06	2.8	202
48	1.00	9.0	2.3	0	10.0	26.8	2.31	1.045	0.04	1.3	619
49	0.55	9.0	4.3	1	8.0	44.9	1.42	1.31	0.03	2.7	637
50	0.55	9.0	4.3	1	8.0	28.2	0.62	1.31	0.04	2.5	175
51	0.55	9.0	4.3	1	8.0	34.1	0.87	1.31	0.03	2.6	296
52	0.55	9.0	4.3	1	8.0	32.6	1.24	1.31	0.03	1.7	404
53	0.55	9.0	4.3	1	8.0	49.9	3.23	1.31	0.04	1.5	1611
54	0.55	9.0	4.3	1	8.0	52.1	1.86	1.31	0.03	2.8	970
55	0.55	9.0	4.3	1	8.0	46.3	1.86	1.31	0.03	2.2	861
56	0.55	9.0	4.3	1	8.0	49.5	0.99	1.31	0.03	4.8	491
57	0.55	9.0	4.3	1	8.0	26.7	1.86	1.31	0.03	0.7	498
58	0.55	9.0	4.3	1	8.0	46.3	0.99	1.31	0.03	4.2	459

Where D_p is the pile diameter, D_c is the mean cover stone size, D_f is the mean filter stone size, N_c is the number of cover layers, t_f is the thickness of the filter layer, N_f is the number of filter layers, w_c is the is the overall extension of the cover layer, w_f is the overall extension of the filter layer, e_{max} is the maximum sinking of the scour protection adjacent to the pile and Ω is the mobility number (Eq. 3.5).

Table 3.3: *Test conditions and results of the equilibrium sinking tests.*

test	D_p [cm]	D_c [cm]	D_f [cm]	N_c	t_f [cm]	$N_f = t_f/D_f$	w_c [cm]	w_f [cm]	e_{max} [cm]	D_p/D_c	e_{max}/D_c	Ω
1	20.0	4.3	1.1	1	2.5	2.3	110	120	0.7	4.7	0.2	2.7
2	20.0	1.9	1.1	1	1.5	1.4	90	100	2.9	10.5	1.5	2.7
3	11.0	4.3	1.9	1	2.5	1.3	45	55	6.5	2.6	1.5	7.8
4	20.0	10.3	1.9	1	2.5	1.3	90	100	6.0	1.9	0.6	4.3
5	11.0	4.3	1.9	2	2.5	1.3	45	55	2.6	2.6	0.6	7.8
6	20.0	4.3	1.9	1	5.5	2.9	90	100	0.8	4.7	0.2	4.3

3.4 Numerical modelling

Simulations of 3D flow through the scour protection around a mono pile were performed using FLOW-3D v9.4.2 (Flow3D User Manual, 2011). FLOW-3D is a CFD code solving the fully 3D transient Navier-Stokes equations using a finite-volume-finite-difference method in a fixed Eulerian grid. The reason that this code was chosen for this study is its flexibility and the functionality for porous media flows. Obstacles inside the flow domain are modelled through a method similar to the immersed boundary method (IBM), which allows an easy setup for complex structures and multiple discrete elements (in the order of hundreds). Alternatives to immersed boundary method exist. For example, one can use a mesh which resolves all the geometries of the stones and impose proper boundary conditions. This approach sounds ideal. However, it is a tedious and daunting task for a complex system like the scour protection layers.

The code also provides the functionality to model the effects of porous media inside the flow domain. From the microscopic view of point, fluid can flow through the highly irregular interstitial voids between scour protection stones. Layers of spheres, which have similar size characteristics of the protection stones used in the physical tests, were positioned in the simulation domain according to the experiment arrangement. As will be demonstrated by the simulation results, the use of spheres, instead of real geometry of the individual stones, is a reasonable and economical approximation. However, even with this simplification, it still requires tremendous computational power and time to fully resolve the detailed geometry of all the spheres. To alleviate this drawback, this study experimented with the volume average approach where the macroscopic effect of the porous media is integrated into the governing Navier-Stokes equations as an extra forcing term. In this approach, the bulk of the scour protection layers were modelled as porous media with porosity and hydraulic conductivity. These parameters were estimated according to the stones used in the experiment which will be detailed in the following sections.

3.4.1 Computational domain and setup

A fixed Eulerian mesh combined with a multiblock technique was used to represent the domain. The multiblock domain was used to reduce the total number of cells by using coarse meshes in less relevant areas and keeping high resolution in the scour protection. The first set of runs was made with a coarse mesh without pile and scour protection to obtain a logarithmic velocity profile in the entire domain. After this initial run pile and scour protection were added using a relative coarse mesh. Then the mesh reso-

lution was increased until there was no significant difference between two consecutive solutions of mean velocities and turbulence quantities. All the results shown in this paper are from the finest resolution runs. In the final run, the vertical resolution near bed was kept fine enough to ensure at least one cell in the vertical direction within the viscous sublayer ($y^+ \leq 10$) in regions where the bed shear stress was of interest (not relevant for the cases with porous media). The fine resolution allowed the bed shear stress to be calculated based on the strain rate alone as the Reynolds stresses are neglectable within the viscous sublayer (Grass, 1971).

Three different types of setups have been used for simulations of the scour protection: (1) spheres arranged in a regular pattern, (2) porous media, and (3) a hybrid model with a combination of porous media and spheres. In the latter case, the spheres were placed in the regions where a precise calculation of velocities and strain rates were required. The first setup using spheres was used to get a good representation of the stones in the scour protection. As pointed out in the previous section, this requires a high resolution in the area around the spheres. The cell size should be no more than 0.1 times the diameter of the spheres to obtain a result fully independent of the grid size (note: this was not fulfilled in model 5 in Table 3.4 due to computational limitations; the cell size for that case was around 0.2 times the diameter of the spheres, which was still giving reasonable results). The porous media were introduced to reduce the required number of cells to resolve the scour protection. However, the porous media cannot predict the flow velocities and strain rates as precise as the setup using spheres. As a compromise to have a reasonable simulation time and a good prediction of the near bed strain rate, a hybrid model (combination of the sphere model and the porous media model) was used.

Eight different models have been used in the present study, see Table 3.4. All eight models are described in details below.

Table 3.4: *Main properties of the numerical setups.*

Model number	D_p [cm]	Type [cm]	h [cm]	w_s [cm]	D_c [cm]	N_c	D_f	N_f	Domain length [m]	Domain width [m]	Domain height [m]	Approx. number of cells 10^6
1	14	Spheres	30	81.7	4.3	1	-	-	4.5	2.0	0.35	7.1
2	14	Porous medium	30	80.0	4.3	1	-	-	4.5	2.0	0.35	2.2
3	14	Hybrid	45	81.7	4.3	4	-	-	4.5	2.0	0.5	5.5
4	14	Porous medium	45	80.0	4.3	4	-	-	4.5	2.0	0.5	2.9
5	55	Hybrid	90	155.0	4.3	2	1.1	9	2.2	3.0	1.0	3.4
6	55	Porous medium	90	155.0	4.3	2	1.1	9	4.2	3.0	1.0	0.8
7	55	Porous medium	90	155.0	9.0	1	4.3	3	4.2	3.0	1.0	0.8
8	400	Porous medium	1000	2700	40	2	10	5	28.0	50.0	5.0	0.9

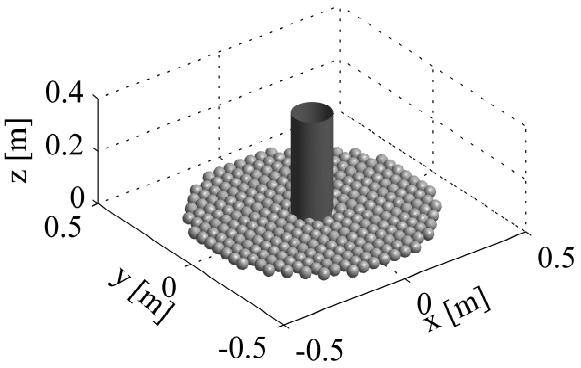

Figure 3.2: *Model 1: $D_p = 14$ cm with a one layer of stones scour protection modelled with spheres. The approach flow is in the positive x-direction.*

Models 1 and 2 were models of a laboratory flume: 2 m wide, 0.3 m water depth and 23 m long. The models were used to do numerical calculations of flow in a scour protection consisting of one layer of stones as reported in Nielsen *et al.* (2011). The scour protection was circular with a 14 cm in diameter pile in the centre. The scour protection in the model was represented by spheres or by a porous medium, Models 1 and 2, respectively. The models are shown in Figs. 3.2 and 3.3.

Models 3 and 4 were the same basic setup as Models 1 and 2, but with a scour protection of 4 layers of stones. In this case a hybrid model with a layer of spheres at the bed and the top with a porous medium in between was tested together with a model with only porous medium. The setups are shown in Figs. 3.4 and 3.5.

Models 5, 6 and 7 were also models of a laboratory flume: 3 m wide, 0.9 m water depth and 35 m long. The pile was 0.55 m in diameter and two different scour protections were applied: A 5 cm thick filter consists of 1.1 cm large stones (d_{50}) and a two stone thick cover layer ($D_c = 4.3$ cm) (models 5 and 6) and a 12 cm thick filter consists of 4.3 cm large stones (d_{50}) and a one stone thick cover layer ($D_c = 9.0$ cm) (model 7). Model 5 was a hybrid model and models 6 and 7 were porous media models. The models were made with two different layers of porous media. The lower one at the bed representing the filter layer and an upper one at the top of filter layer representing the cover layer. In the case of the hybrid model a 11.0 cm wide (crossflow), approximately 30.5 cm long (from the upstream edge of the pile) and 1.1 cm thick box of the porous medium was replaced by one layer spheres with a diameter of 1.1 cm. The spheres were placed at the bed.

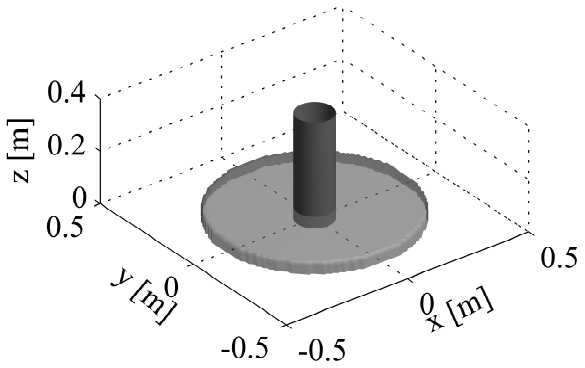

Figure 3.3: *Model 2: D_p = 14 cm with a one layer of stones scour protection modelled with porous medium. The approach flow is in the positive x-direction.*

A 12.9 cm wide (crossflow), approximately 31.9 cm long (from the upstream edge of the pile) and 4.3 cm thick box of the porous medium was replaced by one layer of spheres with a diameter of 4.3 cm. The top of the spheres was flush with the top of the porous media. All the spheres were arranged in a regular pattern. The setups are shown in Figs. 3.6 and 3.7. Fig. 3.6 shows the hybrid model while Fig. 3.7 shows the porous media models.

Model 8 was a model of a Horns Rev I wind turbine (turbine 44). The turbine is located at 10 m of water (MSL) in the middle of the farm. 10 m (MSL) is approximately the average water depth for the turbines in the Horns Rev I Wind Farm. The wind turbines are founded on individual mono piles ($D_p = 4.0$ m) placed in a regular grid with a distance of 500 m. The scour protection consists of a 0.5 m thick filter layer (30 to 200 mm, $d_{50} = 100$ mm) and a two stone thick cover layer (350 to 550 mm, $d_{50} = 400$ mm). The overall diameter of the filter layer is 25 m (plus approximately 2 m slope). The cover layer is 19 m (plus approximately 2-3 m slope) in diameter. The scour protection was represented as porous media, see Table 3.4 for the actual applied stone sizes. The domain used for the calculations was 50 m wide and 11 m deep. The model is shown in Fig. 3.8.

3.4.2 Boundary conditions

For all the setups the inlet boundary condition was a steady state velocity profile obtained from a preparation run. This run simulated an open channel with the same cross sectional dimensions as the actual model and free surface model activated. The free surface in FLOW-3D is captured using the volume

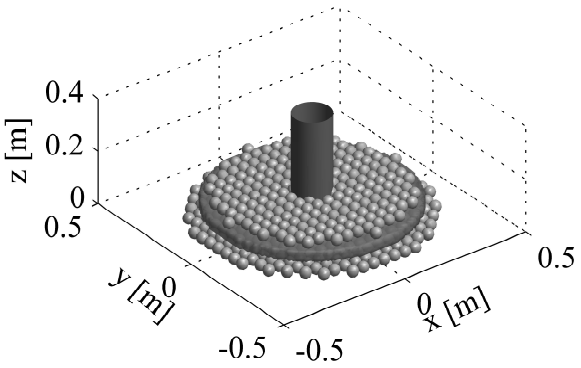

Figure 3.4: *Model 3: D_p = 14 cm with a four layers of stones scour protection modelled with a hybrid model. The approach flow is in the positive x-direction.*

of fluid (VOF) method (Hirt and Nichols, 1981). The use of a preparation run insured a correct incoming velocity profile within a reduced computational domain. For the setups modelling laboratory flumes (models 1-7) the bottom and side walls was as smooth no-slip walls. The downstream outlet was modelled as zero gradient boundary which minimize reflections. For the Horns Rev model the side boundaries (parallel to the incoming flow) were set to be symmetry planes and the bottom was assumed to be a smooth, horizontal, and no-slip wall. The outlet was also modelled as zero gradient.

3.4.3 Turbulence closure model

The turbulence was modelled using a renormalization group (RNG) modified version of the $k-\epsilon$ turbulence closure model. This model is mainly useful near solid boundaries and in regions with rapid distortions (Yakhot and Orszag, 1986; Yakhot and Smith, 1992). It has been used for similar applications with and without structures in steady current, see Lane *et al.* (1999); Ferguson *et al.* (2003); Rodriguez *et al.* (2004); Abad *et al.* (2008) among others. Others have, however, successfully modelled similar problems using a standard $k-\epsilon$ model, for example Kocaman *et al.* (2010) (flow around bridge piers) and Lai *et al.* (2010) (breaking waves over spheres on a sloping beach), among others. Kocaman *et al.* (2010) tested in one case both a traditional $k-\epsilon$ model and the RNG model and found the results similar.

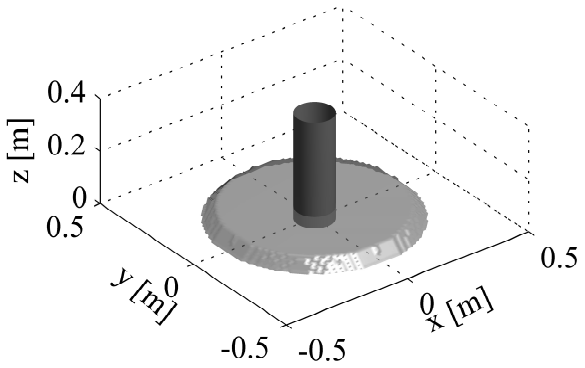

Figure 3.5: *Model 4: D_p = 14 cm with a four layers of stones scour protection modelled with porous medium. The approach flow is in the positive x-direction.*

3.4.4 Porous media modelling

There exist several ways to take account for the porous effects, i.e. the functional form the extra forcing term in Navier-Stokes equation could depend on porosity, saturation, or Reynolds number. Among them, the Reynolds dependant form is suitable for cases where the porous medium is composed of coarse particles and the microscopic velocity might be significant (Flow3D User Manual, 2011). This is the case for our scour protection problem and it is chosen for this study. The forcing term in the Reynolds number dependant porous media model has the form:

$$F_d = \frac{\mu}{\rho}\frac{1-n}{n}\left(A\frac{1-n}{n} + B\frac{Re_p}{D}\right) \tag{3.1}$$

where μ is the dynamic viscosity, ρ is the density of water, n is the porosity, D is the mean size of the stones, $Re_p = Du/\nu$ where ν is the kinematic viscosity and u is the mean velocity, equivalent to the Darcy velocity. A and B are coefficients related to the stone size with $A = \alpha/D^2$ and $B = \beta/D$. Flow3D User Manual (2011) recommends $\alpha = 180$ and β in the interval 1.8 to 4.0 depending on the roughness of the stones. β was calibrated to have a value of 2.9 for all the porous media in the present study. The flow in the scour protection is found to be turbulent, which means that B in Eq. 3.1 is the determining parameter of A and B. Burcharth and Andersen (1995) reported similar values of β for fully turbulent flow. The porosity was kept constant at $n = 0.5$.

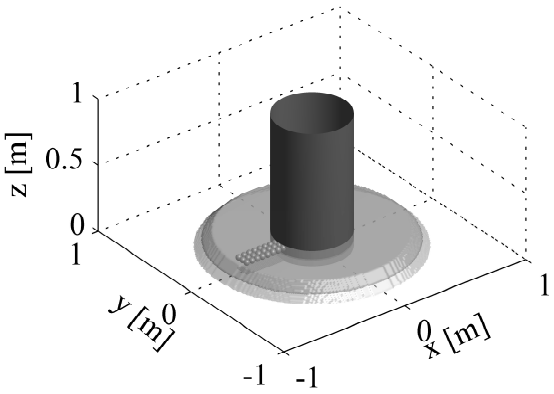

Figure 3.6: *Model 5: $D_p = 55$ cm modelled with a hybrid model. The approach flow is in the positive x-direction.*

3.5 Results of the physical model tests

3.5.1 Flow velocities in the scour protection

Nielsen *et al.* (2011) reported the velocity profiles measured inside a scour protection of cover stones around a mono pile. The velocities were measured in the case of one to seven layers of cover stones. In the present study similar profiles are measured in the case of a 2 cm thick filter layer (two layers) and one, two and four cover layers. The filter layer consisted of 1.1 cm large stones (stone no. 1, Table 3.1). The cover stones, pile diameter, measuring location and flow conditions were the same as used in Nielsen *et al.* (2011) ($D_c = 4.3$ cm (stone no. 4), $D_p = 14$ cm, 12 cm upstream of the pile centre, $V = 40$ cm/s and $h = 30$ (one and two layers of cover stones) or 45 cm (four layers of cover stones)). Fig. 3.9 shows the measured velocity profiles inside the scour protection. For comparison the velocity profiles without filter layer are plotted as well. It is seen that the overall velocity distribution and magnitude are similar in the case with and without a filter layer. A vertical offset of around 2 cm is observed for the velocity profiles with and without filter layer in the case of one cover layer. This vertical offset is much less pronounced for two and four layers of cover stones. The reason for this is that the near bed velocity is much higher in the case of one layer of cover stones than in the case of two and four layers: As the flow capacity in the filter layer, given the pressure gradient, is much smaller than in the cover layer a larger fraction of the water must flow above the filter layer in the case of one layer of cover stones (high near bed velocity) than in the case of two and four layers of cover stones, where the near bed velocity is already

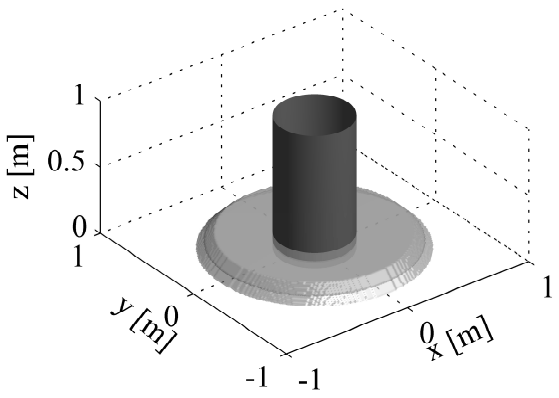

Figure 3.7: *Model 6 and 7: $D_p = 55$ cm modelled with porous media. The approach flow is in the positive x-direction.*

low without a filter layer.

Fig. 3.10 shows the turbulent kinetic energy profiles for the same cases as seen in Fig. 3.9. It is seen that there is a significant reduction in the turbulent kinetic energy in the case of one and two layers of cover stones. There is a local increase in the turbulent kinetic energy around 6 cm above the base bottom in the case of two cover layers. This is associated with a significant change in the velocity (see Fig. 3.9) and it is probably caused by the actual stone configuration, however, it has not been possible to identify the actual reason. In the case of four layers of cover stones the turbulent kinetic energy is almost the same with and without filter layer. This is because the near bed velocity is already very low without a filter layer so the reduced flow capacity caused by the filter layer has no influence on the overall flow pattern.

The turbulent kinetic energy, k, is found in the same way as in Nielsen *et al.* (2011):

$$k = \frac{1}{2}(\overline{u'^2} + \overline{v'^2} + \overline{w'^2}) \tag{3.2}$$

where u' is the streamwise velocity fluctuation, v' is the crossflow velocity fluctuation and w' is the vertical velocity fluctuation. The turbulent kinetic energy is the other important quantity in relation to sediment transport. The turbulent kinetic energy shown in the figures is determined using the measured data and the following relationship (Nezu and Nakagawa (1993)):

$$\frac{\overline{u'^2}}{2k} = 0.55, \qquad \frac{\overline{v'^2}}{2k} = 0.28, \qquad \frac{\overline{w'^2}}{2k} = 0.17 \tag{3.3}$$

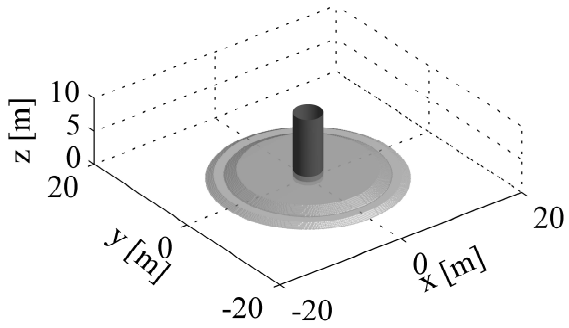

Figure 3.8: *Model 8: The Horns Rev case using porous media. The approach flow is in the positive x-direction.*

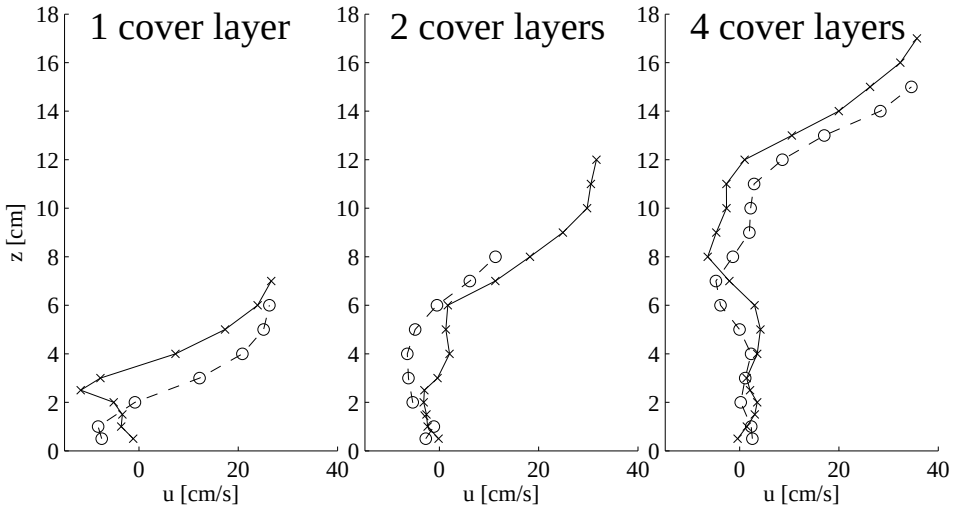

Figure 3.9: *Velocity profiles inside the scour protection 12 cm upstream of the pile centre. The × is with a 2 cm filter layer, while the ∘ is without filter layer, the latter is taken from Nielsen* et al. *(2011).*

This method was also used for the same purpose in Nielsen *et al.* (2011), in this case it was shown that the method gave the same results if u' and v' or if u' and w' were measured just above the scour protection.

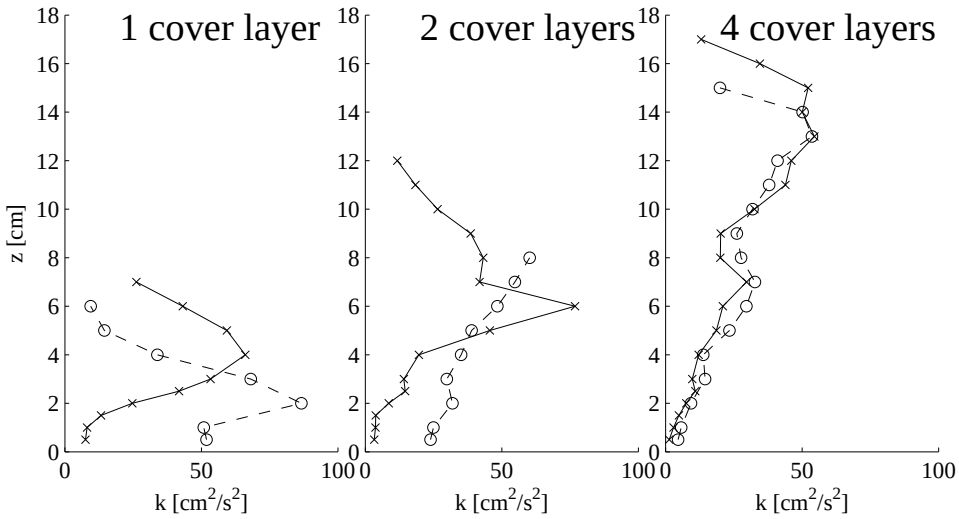

Figure 3.10: *Turbulent kinetic energy profiles inside the scour protection 12 cm upstream of the pile centre. The* × *is with a 2 cm filter layer, while the* ∘ *is without filter layer, the latter is taken from Nielsen* et al. *(2011).*

3.5.2 Critical flow under the scour protection

A filter layer can reduce the near bed turbulence significantly and the near bed velocity to some degree as seen in section 3.5.1. A reduced level of turbulence and, if it is the case, low velocity will decrease the bed shear stress (Sumer *et al.*, 2003). The reduction is due to the reduced flow capacity in the filter layer compared to the coarser cover layer. The flow capacity in a porous media like a stone cover is governed by several quantities:

$$U_{SP} = f(I, D_c, D_{c,15}, D_{c,85}, N_c, n_c, D_f, D_{f,15}, D_{f,85}, N_f, n_f, \nu) \qquad (3.4)$$

where I is the approach pressure gradient, D_c is the mean cover stone size, $D_{c,15}$ is the 15% fraction of the cover stones, $D_{c,85}$ is the 85% fraction of the cover stones, N_c is the number of cover layers, n_c is the porosity of the cover layer, D_f is the mean filter stone size, $D_{f,15}$ is the 15% fraction of the filter stones, $D_{f,85}$ is the 85% fraction of the filter stones, N_f is the number of filter layers, n_f is the porosity of the filter layer and ν is the viscosity of the water.

Based on dimensional considerations the Shields parameter (Eq. 3.8) can be extended to a mobility number for the sediment underneath the scour protection:

$$\Omega = \frac{U_\infty^2}{g(s-1)d}\frac{1}{D_p}D_f\frac{n_f}{1-n_f} \tag{3.5}$$

The friction velocity, U_f is replaced by the approach velocity, U_∞^2 as they are proportional and the friction velocity underneath the scour protection is usually unknown. $1/D_p$ gives, together with U_∞^2 are proportional to the pressure gradient caused by the approached velocity and $D_f n_f/(1-n_f)$ is counting for the friction in the filter layer, Engelund (1953).

As in the case of unprotected sediment transport, the critical mobility number for the sediment underneath a scour protection depends on the grain Reynolds number. In the case of the Shields diagram the grain Reynolds number is defined as:

$$Re = \frac{U_f d_{50}}{\nu} \tag{3.6}$$

where U_f is the local friction velocity and d_{50} is the mean size of the bed sediment. This definition is not practical in the present case as the friction velocity is still unknown underneath the scour protection and can again be replaced by the approach velocity:

$$Re = \frac{U_\infty d_{50}}{\nu} \tag{3.7}$$

Fig. 3.11 shows the critical mobility number as defined in eq. 3.5 as function of the Reynolds number as defined in eq. 3.7. The results are obtained under the conditions described in sec. 3.2 and 3.3. The test conditions and results are given in Table 3.2. The results seem to fall into two groups (separated by the dashed line indicated in Fig. 3.11): A large group with relatively low critical mobility number and with results from all the setups (1) $D_p = 0.55$ m and stone type 1 filter layer; (2) $D_p = 1.0$ m and stone type 3 filter layer and (3) $D_p = 0.55$ m and stone type 4 filter layer (for stone types see Table 3.1). The second group, which has higher critical mobility numbers, consists only of tests done with the third setup ($D_p = 0.55$ m and stone type 4 filter layer). The reason for this is found to be the increased pore size. The plan-view area of the particles for all the experiments varied from around 0.2 to 6 mm^2, while the pores plan-view area was approximately 100, 500 and 1800 mm^2 for the three setups. This means that the particles covered a relatively much smaller area of the pore in the case of larger filter stones. This will of course reduce the possibility of the particle being exposed to high bed shear stresses, if there are large variations in the bed shear stresses within a single pore. Such large variations within a single pore was actually observed in several pores during the experiments with the third setup: While relatively large sand grains were raised by a vortex in one part

of the pore, finer grains were not moving at all in other parts of the pore. Close inspection of fig. 3.11 shows an example of this: Two tests were made in the same pore (pore 2) and with approximately the same Reynolds number (500), but the critical mobility numbers for the two tests are very different: $\Omega_c \approx 1$ and $\Omega_c \approx 7$. This difference can only be explained by variations of the bed shear stresses within the pore and therefore different exposure of the particles because of different initial positions within the pore. The large scatter seen in fig. 3.11 is therefore a consequence of the variations of the bed shear stress within the pores.

Although there is a large scatter, Fig. 3.11 can be used to find the required filter stone size given the pile size, approach current velocity, size and specific weight of the sediment.

The results of the tests can also be used to estimate the critical bed shear stress underneath the scour protection in front of the pile: As the relative density and the size of the particles are known the bed shear stress can be determined in an iterative manner using a Shield diagram. In the present case the results were fitted to the trend line given in (Sumer and Fredsøe, 2002, p 10). Using this data it is possible to establish a relation between the critical approach velocity, U_∞ and the critical friction velocity, U_{fc}, underneath the scour protection upstream of the pile. This relation can be plotted (Fig. 3.12) as the Shields parameter as function of the Reynolds number (eq. 3.7), where the Shields number is defined as:

$$\theta = \frac{U_f^2}{g(s-1)d} \tag{3.8}$$

Fig. 3.11 can be used to determine the size of the filter stones to ensure no sediment motion underneath the scour protection, for example for design purposes. Fig. 3.12 can be used to find the bed shear stress under a scour protection, but it is mainly useful for validation of numerical models, as will be shown later.

3.5.3 Sediment bed experiments

Fig. 3.13 shows the sinking of scour protections with one layer of cover stones and a filter layer. Test conditions are given in Table 3.3. The data is divided in two main groups based on the critical mobility number, Ω_c (eq. 3.5). The critical mobility number is found to be approximately 6 from Fig. 3.11 for $Re = 77$, the Reynolds number for the tests indicated in Fig. 3.13. In the case of a mobility number larger than the critical the sinking is the same as expected for a scour protection without filter layer. In the other cases the sinking is either significantly lower than the expected for one cover layer without filter or just in general very low. The latter is the case for the point

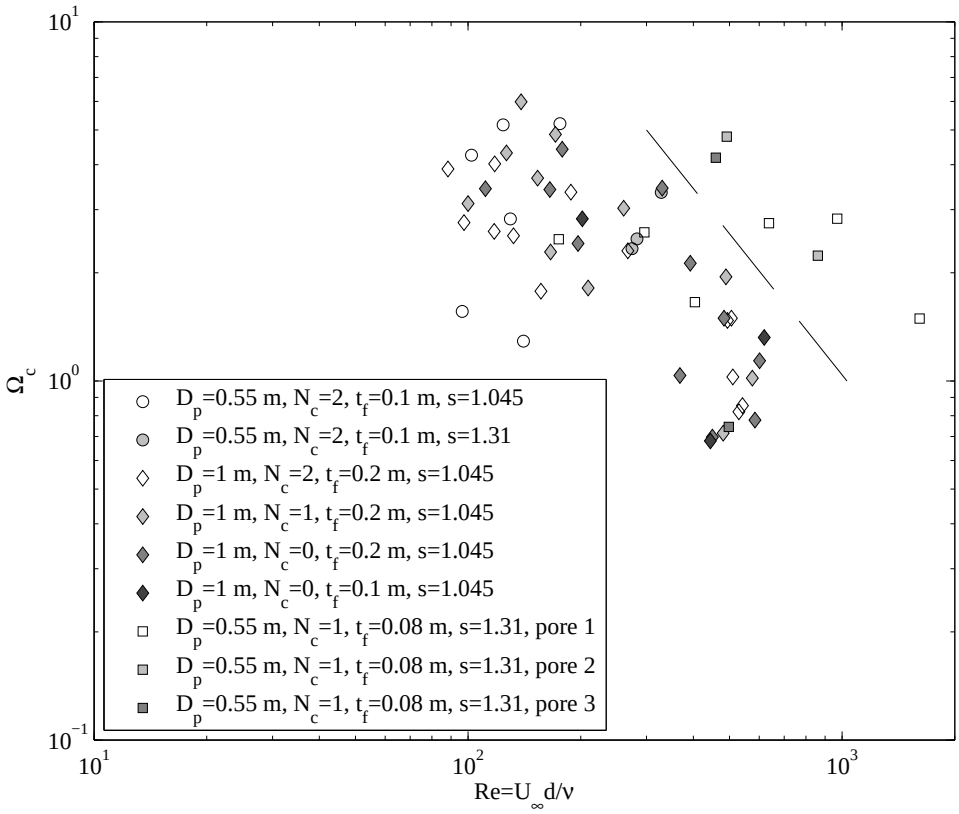

Figure 3.11: *Critical mobility number as defined in Eq. 3.5 as function of the Reynolds number (eq. 3.7). The dashed line separates the general group including results from all setups and the group which only includes results from the setup with coarse filter layer stones ($D_f = 4.3$ cm)*

at $D_p/D_c = 2$ and a sinking of $e_{max}/D_c \approx 0.5$ a reason for the relatively large sinking in this case might be that the mobility number was close to the critical: $\Omega = 5.9$. This was, however, also the case for one of the points at $D_p/D_c \approx 4.5$. Furthermore, it should be noted that the experiments for the critical bed shear stresses were conducted in one single point relative to the pile. This point was used because it is within an area with high bed shear stresses, but not necessarily the highest bed shear stresses found around the pile.

As seen in Fig. 3.13, there is an influence of the thickness of the filter layer. A filter layer around 1 to 2 layers of stones is significantly less effective compared to a thicker filter layer, in this case 2 to 3 layers of filter stones. The

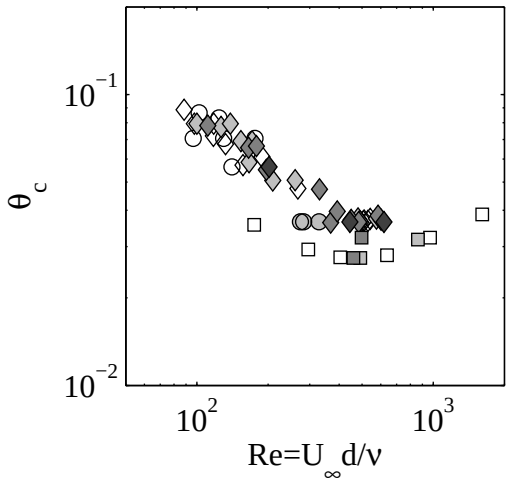

Figure 3.12: *Critical Shields parameter as function of the Reynolds number (eq. 3.7). The symbols are the same as used in fig. 3.11*

reason for this is that the water in the top layers of the filter is interacting with the water above the filter layer, which leads to increased flow velocities and turbulence in this region compared to deeper in the filter layer, see figs. 3.9 and 3.10. For a filter layers with a mobility below the critical and a thickness larger than at least three layers sinking is expected to be smaller than $0.1D_c$. In addition to the results shown in Fig. 3.13 a single test with two layers of cover stones was carried out for a mobility number $\Omega = 9.1$, $D_p/D_c = 2.5$ and $N_f = 1.3$. The result of the test was a relative sinking of $e_{max}/D_c = 0.6$. This is within the reported range for two cover layers without filter layer in Nielsen *et al.* (2011).

Sinking will take place if the critical mobility number is exceeded and the equilibrium sinking seems to be the same as for a scour protection without a filter layer. The latter corresponds to the reported results for scour around a pile, where the equilibrium scour depth is independent of the Shields parameter, in the live bed situation, see e.g. Sumer and Fredsøe (2002).

3.6 Results of the numerical models

3.6.1 Velocities in a scour protection of one layer of stones

Two different setups were used in the case of one layer of stones around a pile: Spheres in a regular pattern and a porous medium. Nielsen *et al.*

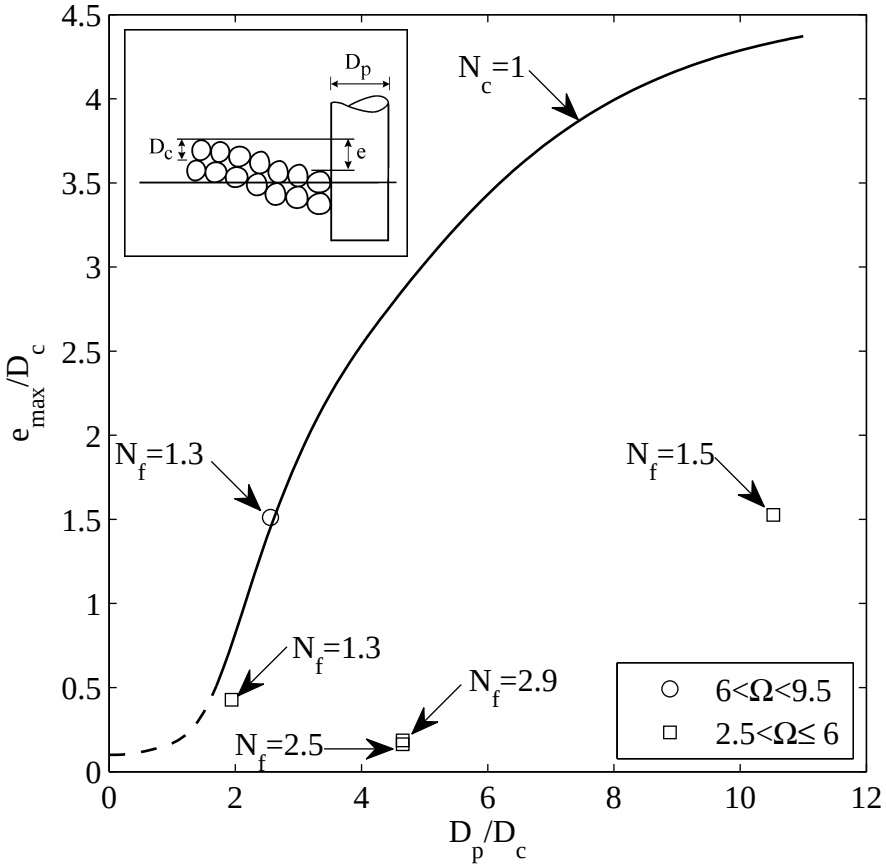

Figure 3.13: *Sinking of scour protections with one layer of cover stones and filter layer. The curve is the expected sinking in case of one cover layer and no filter layer adapted from Nielsen* et al. *(2011). The number of filter layers is defined as* $N_f = t_f/D_f$.

(2011) presented a schematic figure showing the flow through a scour protection around a mono pile, the results of the numerical simulations verifies this picture. Fig. 3.14 shows selected streamlines in the scour protection. It is clear that one of the streamlines is entering the scour protection just upstream of the pile, is following the horseshoe vortex inside the scour protection and is transported far out to the side where it goes out of the scour protection and continues downstream. Other streamlines are just deflected by the pile. In two cases these streamlines are entering the scour protection at the side of the pile and leaving again just downstream of the pile, this can

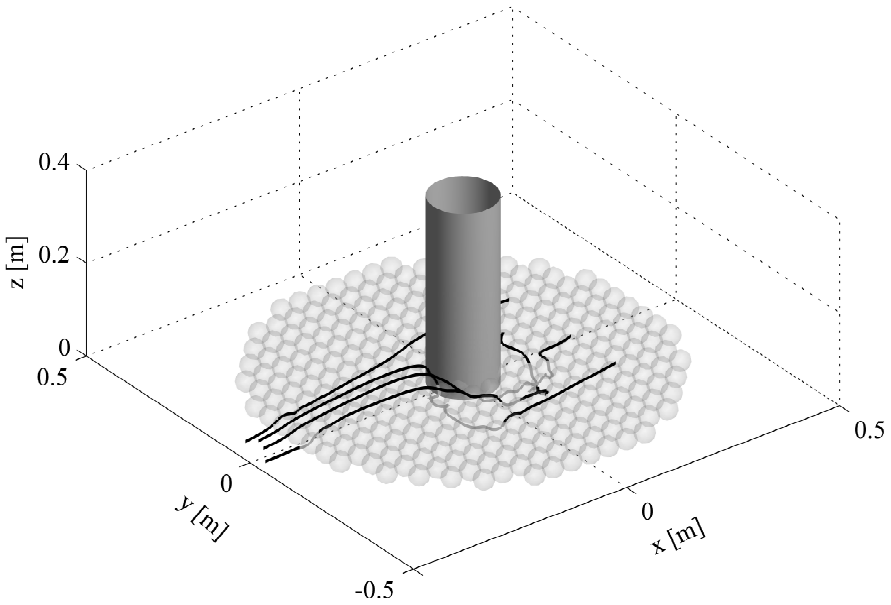

Figure 3.14: *Selected streamlines around the pile in case of one layer of stones. The scour protection is modelled as spheres. The streamlines are grey when in the lower part of the scour protection. The approach flow is in the positive x-direction.*

explain that the largest sinking was often observed at the sides of the pile, while there was almost always deposition of sediment downstream of the pile (Nielsen *et al.*, 2011).

Fig. 3.15 shows the velocities upstream of the mono pile in case of a one layer thick scour protection around the pile, where the scour protection is modelled by spheres. Panel (a) is the velocities measured in the physical model test (Nielsen *et al.* (2011)) and panel (b) is the velocities calculated in the numerical model. The velocities outside the scour protection is almost identical between the physical model test and the numerical model test. There are small differences in the velocities inside and near the scour protection, however, the differences are small. The flow directions for each velocity profile are the same for the physical and the numerical model except in the scour protection at $x = -7.7$ cm. Also the magnitude of the velocity is almost the same for both models. The reason for the change in the flow direction at $x = -7.7$ cm might be the regular placement of the spheres which are cut by the pile, creating large area with full contact between the pile and the part of the sphere outside the pile. The largest difference is found at the interface between the free flow and the scour protection, but

this is probably mainly because the scour protection in the numerical model is slightly thicker in (4.3 cm) than the scour protection in the physical model test (3.5 cm). This difference is due to the fact that the numerical model was made with spheres with a diameter of 4.3 cm, while the physical model was made with irregular crushed stones, with a mean size of 4.3 cm and mean height, in case of one layer, of 3.5 cm (stone no. 4, Table 3.1).

The velocities in the pores varied depending on the distance to the spheres creating the actual pore. The velocities presented in Fig. 3.15 are found 2 cm off the centre line of the mono pile in the cross-flow direction. The distance to the centre of the mono pile in the streamwise direction is kept the same as the measurements in the physical model test. It is found that these locations are comparable to the locations measured in the physical model test, although slightly higher and lower velocities can be found within the pores where the velocity profiles are found, the profiles shown in Fig. 3.15 are found to be representative for velocity in the pores.

The turbulent kinetic energy was found for both the physical and the numerical models in the case of spheres. The results are shown in Fig. 3.16. The turbulent kinetic energy is in general lower in the case of the numerical model compared to the measured values from the physical model. The overall trend is the same for both, with the highest values at the top of the scour protection. Both models give a low turbulent kinetic energy above the scour protection, while the numerical model under predicts the turbulent kinetic energy in the scour protection.

The velocities inside the scour protection in the case of one layer of stones, were also calculated using a porous medium to simulate the scour protection, see Fig. 3.17. The velocity calculated in the porous medium is divided by the porosity of the stones used in the physical model test to obtain the actual pore velocity. The porosity of the stones used in this study is approximately 0.5. As in the case of scour protection modelled as spheres (3.15) panel (a) is the velocities measured in the physical model test (Nielsen *et al.* (2011)) and panel (b) is the velocities calculated in the numerical model. As for the numerical model with spheres the flow outside the scour protection is modelled correctly compare with the measured values in the physical model. Also the velocities inside the scour protection are comparable to the measured values, although they are more uniform in the vertical direction. This is most likely because the porous medium are homogeneous, while the actual stones and spheres are inhomogeneous.

3.6.2 Velocities in a scour protection of four layers of stones

Nielsen *et al.* (2011) showed that a secondary horseshoe vortex will develop under the primary horseshoe vortex in a relatively thick scour protection

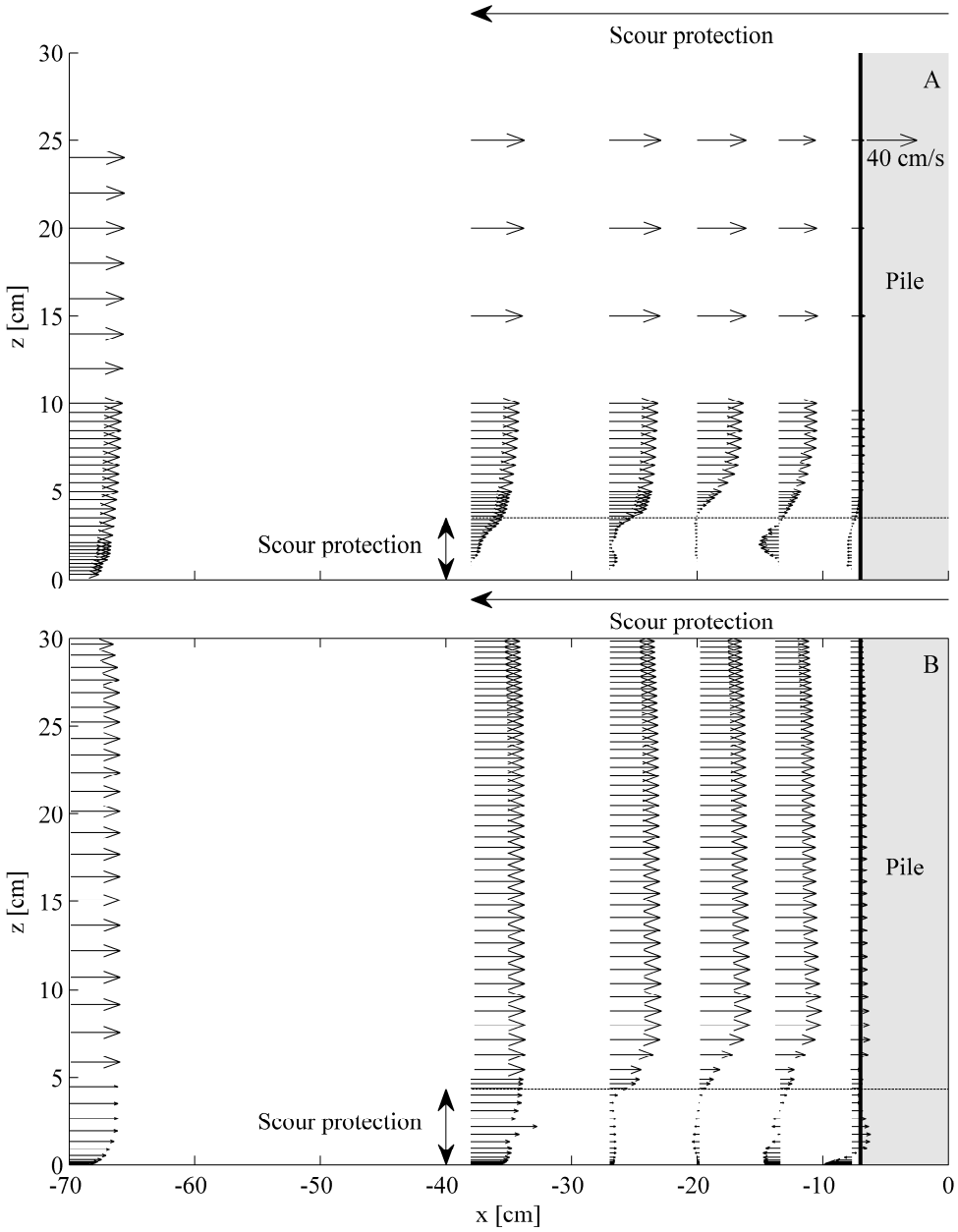

Figure 3.15: *Velocities upstream of a mono pile with a one stone layer thick scour protection. Panel (a) is the velocities measured in a physical model test (Nielsen* et al. *(2011)). Panel (b) is the result of the numerical model, where the scour protection is model by spheres.*

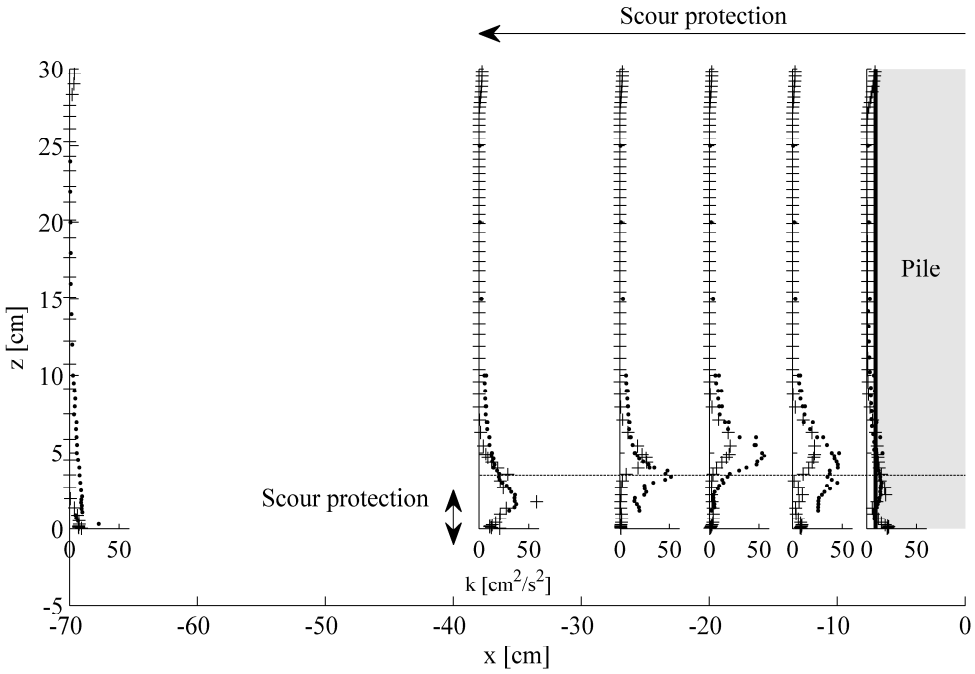

Figure 3.16: *Turbulent kinetic energy upstream of a mono pile with a one stone layer thick scour protection.* • *is measured in a physical model (Nielsen* et al. *(2011)).* + *is the result of the numerical model, where the scour protection is model by spheres.*

($D_p/t_{SP} < 1$). Fig. 3.18 shows the velocities in case of a scour protection of four layers of stones upstream of a mono pile in the case of (1) physical model test; (2) a hybrid model; and (3) a fully porous model. Both the hybrid and the porous medium model capture the overall flow in the scour protection. The hybrid model is significantly closer to the results of the physical model test in the upper part of the scour protection (The porous medium and the upper layer of spheres). The velocities are on the other hand highly overestimated in the lower layer of spheres. The velocity in the lower layer of spheres are also overestimated in the case of the porous medium model, but not as much. On the other hand, the velocity in the lower two third of the scour protection is overestimated while it is underestimated in the upper third of the scour protection, in the case of the porous medium model. The primary reason for this is that the location of the two horseshoe vortices is different in the fully porous model compared with the hybrid and physical models. The results of the physical model test showed that the primary (upper) vortex is located in the upper approximately 5 cm of

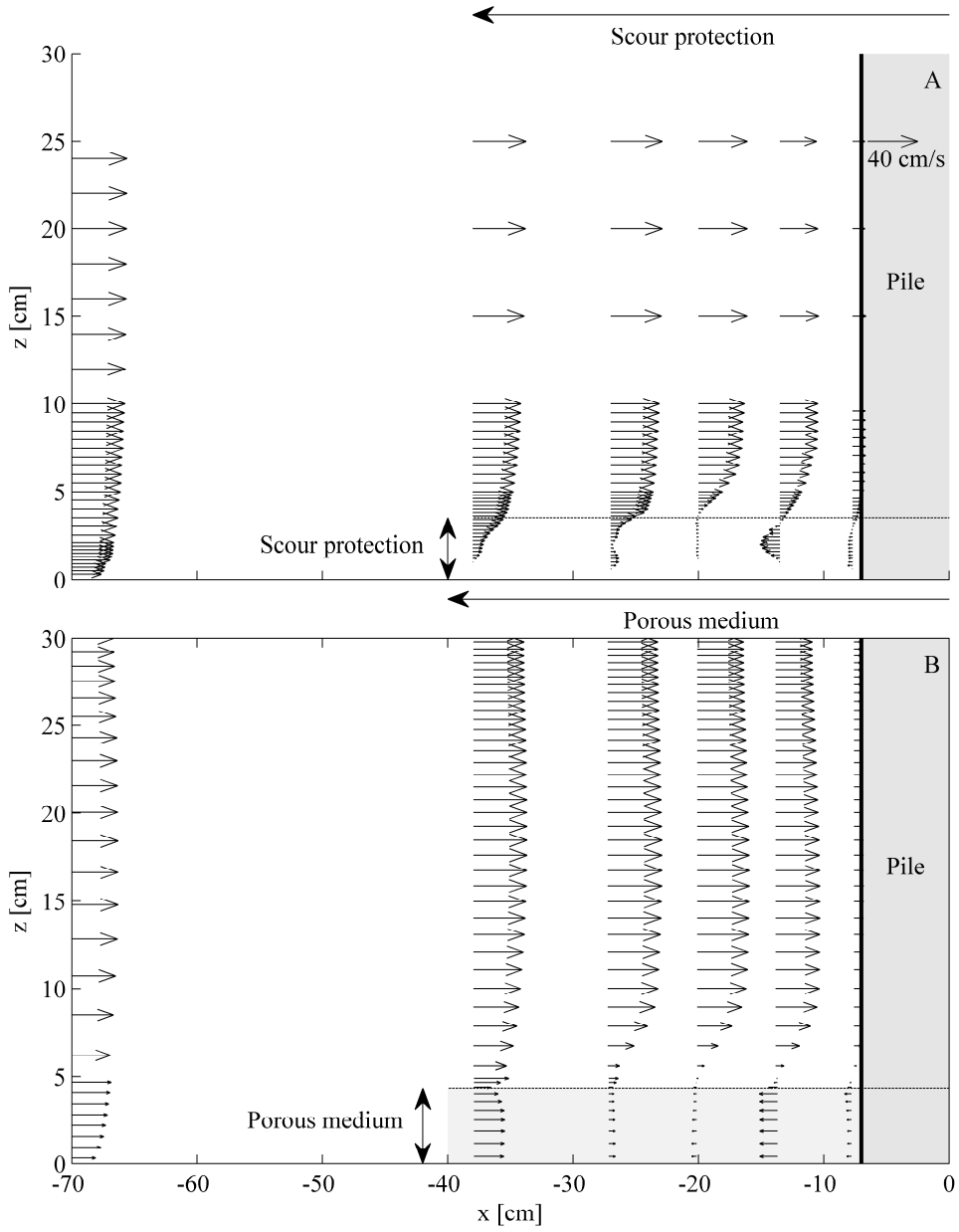

Figure 3.17: *Velocities upstream of a mono pile with a one stone layer thick scour protection. Panel (a) is the velocities measured in a physical model test (Nielsen* et al. *(2011)). Panel (b) is the result of the numerical model, where the scour protection is model by a porous medium.*

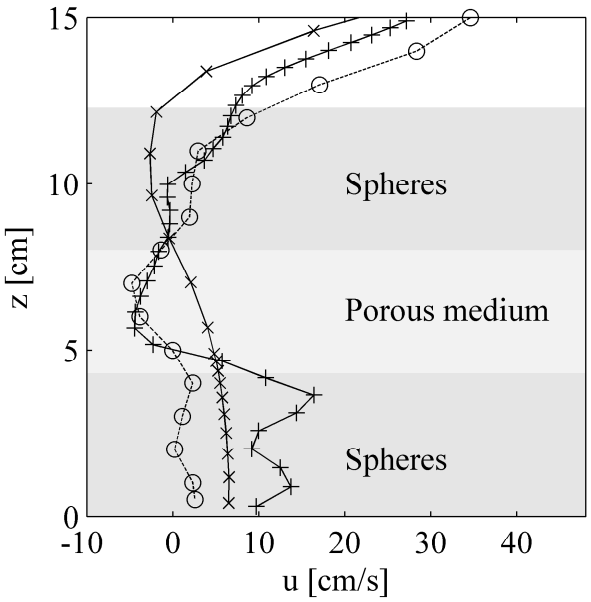

Figure 3.18: *Velocities upstream of a mono pile with a four stone layer thick scour protection. Points marked with ∘ are measurements from physical model tests (Nielsen* et al. *(2011)), points marked with + are results from the hybrid model and points marked with × are results calculated by the fully porous medium model. The grey bands indicate the distribution of the spheres and the porous medium in the hybrid model.*

the scour protection, while the secondary (lower) vortex is located in the lowermost approximately 7 cm. This is also the case for the hybrid model. In the case of the porous medium model the primary vortex is only located in the upper 2 cm of the scour protection while the secondary vortex is around 10 cm high. This is because the theoretical bed for the flow outside the scour protection is below the top of the spheres.

Fig. 3.19 shows the turbulent kinetic energy in case of a scour protection of four layers of stones upstream of a mono pile in the case of physical model test and a hybrid model. The result of the fully porous medium model is left out as the turbulent kinetic energy is not calculated inside the porous medium. The position of the profile is the same as in Fig. 3.18. As in the case of one layer of stones (Fig. 3.16) the calculated turbulent kinetic energy is significantly lower than the measured. In the case of the hybrid model, the turbulent kinetic energy is by definition zero in the porous medium and this reduced the turbulence near the porous medium.

Nielsen *et al.* (2011) reported the flow in between the stones in a four layer scour protection upstream of a half pile mounted on a transparent vertical

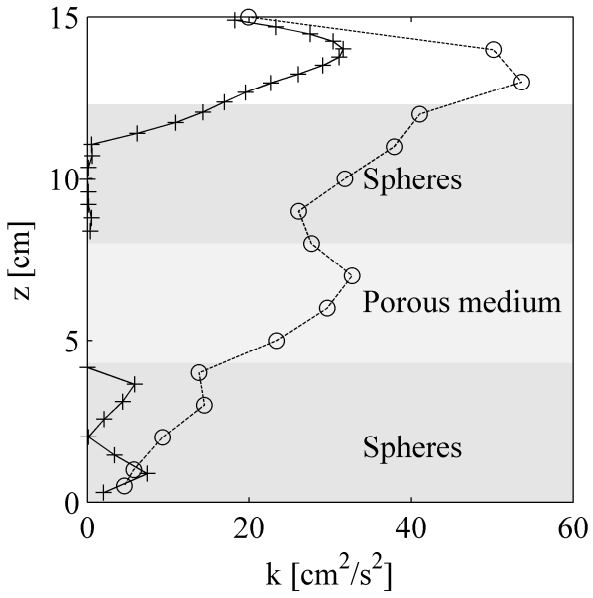

Figure 3.19: *Turbulent kinetic energy upstream of a mono pile with a four stone layer thick scour protection. Points marked with ∘ are measurements from physical model tests (Nielsen* et al. *(2011)) and points marked with + are results from the hybrid model. The grey bands indicate the distribution of the spheres and the porous medium in the hybrid model.*

surface piercing wall oriented in the streamwise direction. The flow is shown in Fig. 3.20 together with the similar plot of the result of the hybrid model. Although the flow are different due the different arrangements of the stones and the use of porous medium the two horseshoe vortices can still be seen in both the physical and numerical results.

3.6.3 Bed shear stresses under a scour protection with filter layer

In the case of the hybrid model, the bed shear stress is found from the strain rate calculated by FLOW-3D. In this case the vertical resolution was kept fine enough to ensure that at least one cell was within $y^+ < 10$ and for the most part $y^+ < 5$, where Reynolds stresses are neglectable (Grass, 1971). This method could not be used for the porous media as the vertical velocity profile is undeveloped in the porous media. To get a reasonable estimate of the bed shear stress an analogy with pipe flow was made: The flow in between the stones in the scour protection can be seen as flows in pipes. The size of the pores or the "pipe" is approximately the same as the size of

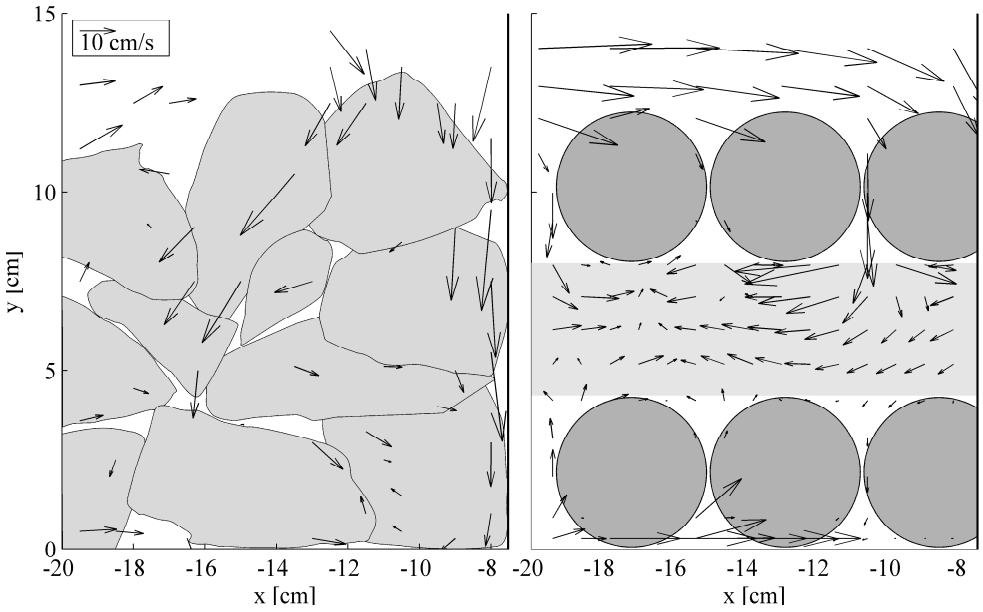

Figure 3.20: *Flow inside a four layer scour protection. The left panel is the flow upstream of a half pile mounted on a vertical wall oriented in the streamwise direction (Nielsen* et al. *(2011)). The right panel is the similar flow calculated by the hybrid model. The spheres and the porous medium in the hybrid model is shown.*

the filter stones so the friction velocity can be estimated as:

$$U_f = f\frac{1}{\sqrt{8}}\frac{V}{2.0\log\left(\frac{VD_f}{\nu}\frac{\sqrt{8}U_f}{V} - 0.8\right)} \tag{3.9}$$

where $f \approx 4.5$ is a correction factor for the flow through the scour protection, V is the average horizontal pore velocity, ν is the kinematic viscosity. The factor f is found be approximately 4.5 both in case of model 6 and 7.

Fig. 3.21 shows the results of the numerical models (model 5 to 8) together with the results of the physical model tests (Fig. 3.12). The figure shows that the models give reasonable results. The results of the numerical models (model 5 to 7) are given as an interval corresponding to the friction velocities found in an area of 2 times 2 cm, 40 cm upstream of the pile centre, with a 5 cm offset to the side. This is the same location as in the physical experiments. The Shields parameter is calculated for the same particle size and specific density (see Table 3.2, experiments 3 and 52) as in the physical experiments.

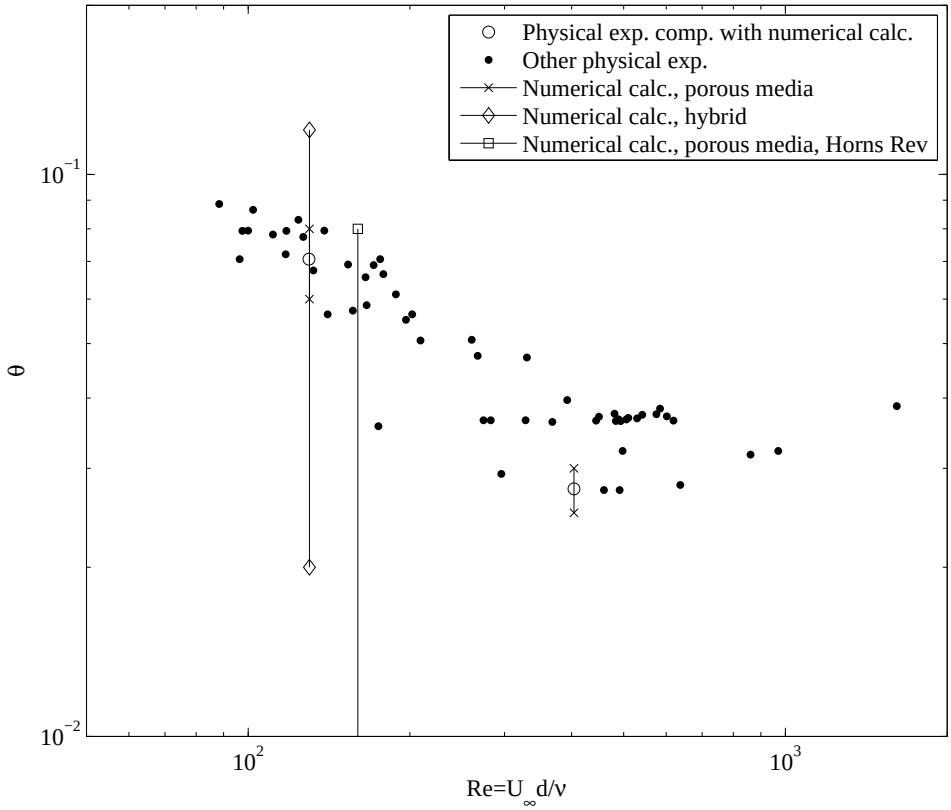

Figure 3.21: *The results of model 5 to 8 plotted together with the results of the physical experiments (Fig. 3.12).*

3.6.4 Bed shear stresses under the scour protection at Horns Rev

The result of the calculation for a full scale Horns Rev I Wind Farm foundation are shown in Fig. 3.22. The interval of the Shields parameter is shown in Fig 3.21 (vertical bars) as well. From the latter figure it is seen that the lower limit of the critical Shields parameter is around 0.05. This value is exceeded up to approximately 1 m away from the pile surface at the upstream edge of the pile. This corresponds very well with the observations at Horns Rev where the sinking took place 1 to 2 m from the pile surface (Hansen *et al.*, 2007).

Nielsen *et al.* (2011) concluded that the magnitude of the sinking of the scour protections at Horns Rev I Wind Farm could be explained by the current, if the bed was mobile underneath the scour protection. However,

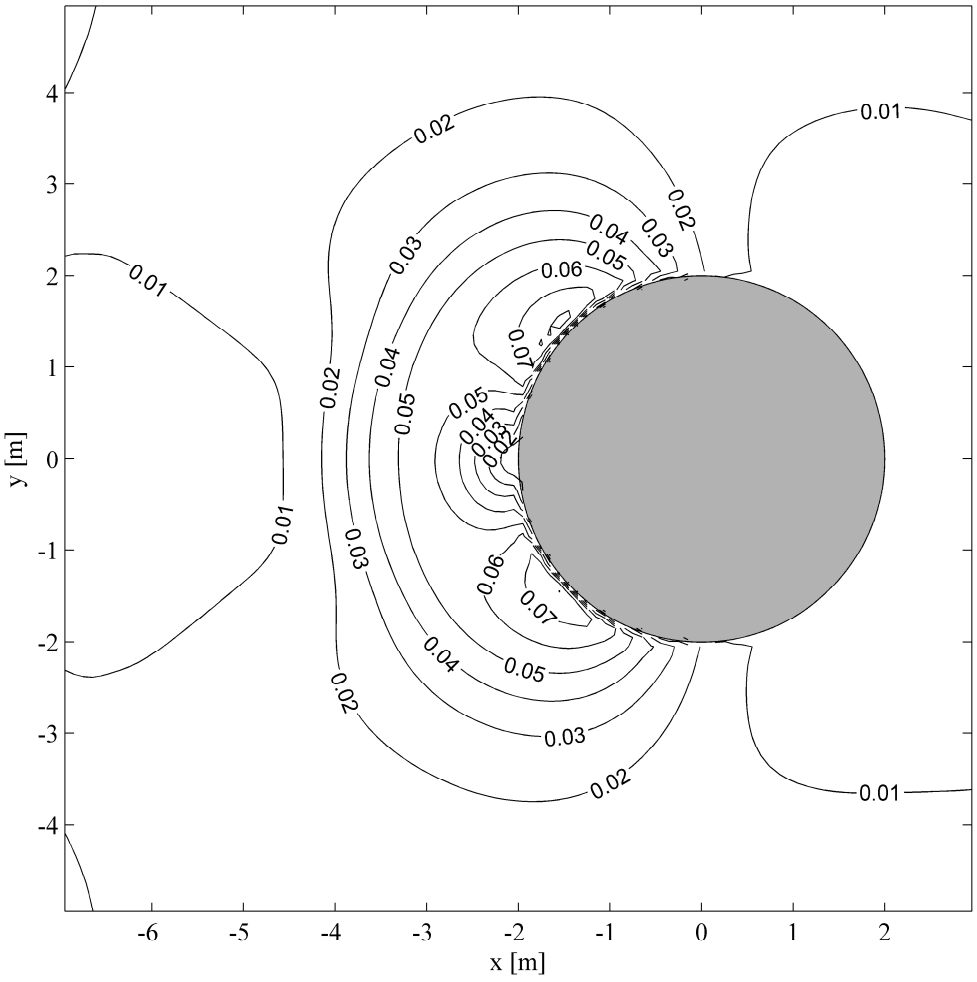

Figure 3.22: *The Shields parameter underneath the scour protection around the foundation for wind turbine 44 in Horns Rev I Wind Farm with an approach velocity of 0.8 m/s. The base sediment is assumed to consist of 0.2 mm sand with a specific density of 2.65.*

Nielsen *et al.* (2011) was unable to conclude whether the base sediment under the scour protections at Horns Rev 1 Wind Farm was mobile or not. The physical and numerical experiments presented here show that the sediment will be mobile under extreme current conditions. As the flow in the scour protection is caused by the pressure gradients it is likely that sediment motion will take place under less extreme conditions when the effect of wave action is considered. It should be noted that the gradation of the filter stones at Horns Rev is higher than the gradation used in the physical experiments and the numerical calculations, however, this will not change the porosity

significantly and the flow resistance in the filter layer significantly.

Chiew (1995); Chiew and Lim (2000) reported results of physical model tests with scour protection of bridge piers in current. The main focus was the stability or integrity of the scour protection itself not the sediment underneath. Chiew and Lim (2000) divided the damage to the scour protection into two categories: embedment and total disintegration. Embedment was the mildest category of damage and was partly caused by the processes described in Nielsen *et al.* (2011) and the present paper as sinking of the scour protection. Chiew and Lim (2000) only distinguished between embedmentsinking and total disintegration. Nielsen *et al.* (2011) and the present study can be applied in cases where even sinking of the scour protection is unacceptable and in cases where sinking is accepted, it can be used to estimate the anticipated sinking of the scour protection.

3.7 Conclusion

1. Physical model tests have shown that there is a relation between the approach velocity and the stability of the sediment underneath a scour protection around a mono pile.

2. Design guidelines to determine the necessary filter stone size to prevent sinking is given for a scour protection around a mono pile, given the approach velocity, pile diameter and sediment properties.

3. Physical experiments using sediment bed have shown that the sinking of the scour protection is reduced if the mobility number underneath the scour protection is below the critical, while a thin filter layer of coarser stones made no difference compared to similar scour protections without filter layers.

4. Using the present code, FLOW-3D, the flow and bed shear stresses in the scour protection around a mono pile can be modelled.

5. The numerical tests showed that the best results are obtained by simulating the scour protection by spheres, but this method is too computationally heavy for most full scale problems. Hybrid models using a combination of spheres and porous media is useful for larger and more complex model where only smaller areas are of interest.

6. Hybrid models are found to capture the overall flow in the scour protections and it can be used to determine the bed shear stresses underneath the scour protection.

7. Porous media are found to capture the overall flow in the scour protections. It can be used to determine the bed shear stresses underneath the scour protection, although the porous media model needs calibration.

3.8 Acknowledgement

This research was carried out as part of the Statkraft Ocean Energy Research Program, sponsored by Statkraft (www.statkraft.no). The study was partially supported by the Danish Council for Strategic Research (DSF)/Energy and Environment under the programme Seabed Wind Farm Interaction (http://sbwi.dhigroup.com, sagsnr. 2104-07-0010) and DHI (www.dhigroup.com). Part of the sediment bed experiments was conducted by François Roignant under supervision of the authors. Xiaofeng Liu also wants to thank the startup funding provided by the University of Texas at San Antonio, USA.

Chapter 4

Experimental Study on the Scour around a Mono Pile in Breaking Waves

This chapter is submitted to Journal of Waterway, Port, Coastal and Ocean Engineering:
Nielsen, A.W., Sumer, B.M., Ebbe, S.S. and Fredsøe, J.: "Experimental Study on the Scour around a Mono Pile in Breaking Waves"

Published article: A revised version of this chapter was accepted for publication on the 28th of February 2012. The reference is: Nielsen, A.W., Sumer, B.M., Ebbe, S.S. and Fredsøe, J. (2012). Experimental Study on the Scour around a Mono Pile in Breaking Waves. *Journal of Waterway, Port, Coastal and Ocean Engineering* (doi: 10.1061/(ASCE)WW.1943-5460.0000148).

Abstract

The scour process around mono piles caused by breaking waves is studied using physical model tests. The waves were breaking on a flat sand section after shoaling on a mildly sloping ramp.

It is found that the scour depth around a mono pile in breaking waves in some cases differ significantly from the scour depth in the case of non-breaking waves. The different is largest in the case of large piles.

Keywords: Scour; Pile foundation; Breaking waves; Wind power; Bars.

4.1 Introduction

During the last decade more and more wind farms, consisting of tens or hundreds of wind turbines, have been erected offshore. Many of these offshore wind farms are located in shallow waters and exposed to strong currents, waves and breaking waves. These effects cause scour around the foundations of the wind turbines, which are, for the most part, mono piles.

Scour around mono piles have been studied extensively over the last decades. Most of the available results are compiled in Breusers and Raudkivi (1991); Hoffmanns and Verheij (1997); Whitehouse (1998); Melville and Coleman (2000) and Sumer and Fredsøe (2002). This work has in recent years made it possible to develop numerical models for long-term prediction of the development of scour holes around mono piles (Nielsen and Hansen, 2007; Raaijmakers and Rudolph, 2008; Harris *et al.*, 2010).

Scour around the foundation of offshore structure may reduce the stability of the structure, e.g. mono pile for an offshore wind turbine and change for instance the natural frequency of the dynamic response of an offshore wind turbine in an unfavorable manner.

Scour induced by breaking waves has not been studied nearly as much. Carreiras *et al.* (2000) tested the scour around a pile in breaking waves on a 1:20 slope. Carreiras *et al.* (2000) concluded that: "When the pile is located at the breaking point or onshore of it, global large scale bed changes, namely the formation of the bar, are superposed to the local scour processes." They did not present any compensation for the global large bed changes. Furthermore no guidelines were given in Carreiras *et al.* (2000) on how to determine scour around piles in breaking waves. Bijker and de Bruyn (1988) presented results of scour around a pile in combined breaking waves and current. They concluded that combined current and breaking waves increased the scour compared to both the current-alone case and wave-alone cases. The latter authors did not present the results of breaking-waves alone.

The purpose of the present study is to investigate in a systematic manner scour around unprotected mono piles exposed to breaking waves. The study shows that the scour can increase significantly under breaking waves compared with that experienced in case of non-breaking waves. This is apparently especially true for larger piles.

4.2 Experimental Setup

The experiments were conducted in a 28 m long (excluding in- and outlet sections), 4 m wide and 1 m deep flume, see Fig. 4.1. A 0.35 m thick and 10 m long sand section was placed across the entire width of the flume, beginning approximately 9.5 m from the wave paddle. In front of the sand

section a 3 m long slope was constructed. The slope (1:8.6) was made of a core of concrete blocks covered by at least one layer of stones ($d_{50} = 4.3$ cm).

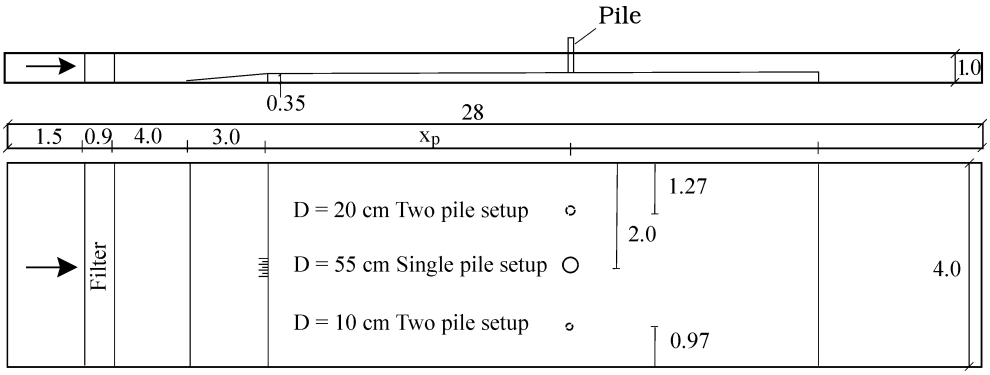

Figure 4.1: *Sketch of the flume and setup. Single pipe setup: Only with 55 cm pile. Two pile setup: Only with 10 cm and 20 cm piles, and 55 cm pile was removed. Measures in meters.*

Piles with three different diameters were tested: $D = 10$ cm, 20 cm and 55 cm. The piles were sealed at the bottom. The first two piles with $D = 10$ cm and 20 cm were tested concurrently, in order to save time. They were placed at the same distance from the wave maker, and the distance between the piles was 1.75 m, which was large enough to ensure no interference. The 55 cm pile, on the other hand, was tested alone.

The scour development was monitored by a camera inside the pile. The camera was pointing in the offshore direction as this turned out to be the location with the largest scour. The 10 cm and 20 cm piles were transparent plastic piles, and the scour was measured via the camera using horizontal grooves engraved onto the outer surface of the piles for every 5 mm. The 55 cm pile, on the other hand, was a semitransparent plastic pipe, and therefore the previously described technique proved inconvenient. Instead, four rulers were placed inside the pile, one offshore, one onshore and two at each side of the pile.

Around the piles measuring vertical pins (3.0 mm diameter) were placed in order to determine the width and shape of the scour hole. Near the pile the pins were placed 5 cm apart, and further away from the pile the pin spacing was increased. The sand bed was initially leveled off, and flat in all experiments.

Contrary to scour experiments in current, waves and combined waves and current, the scour in breaking waves develops with a "background" bar-

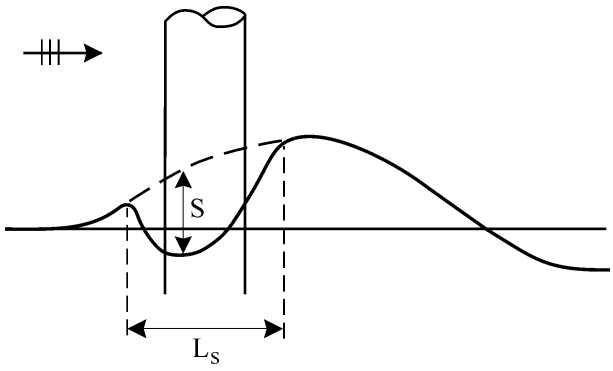

Figure 4.2: *Definition of scour and bed elevation.*

trough system. The change in bed level due to this bar-trough system was not a part of the scour process. To find the actual scour, each experiment was run twice: (1) undisturbed case (without the pile) and (2) disturbed case (with the pile). The difference in the bed level between the two cases was defined as the actual scour, see Fig. 4.2. In the undisturbed case the bed level at the pile location was measured using measuring pins, one at the offshore location of the pile surface, one at the onshore location and two pins at each side, in addition to the pins placed further away from the pile for all experiments. The general change in the bed level was monitored from outside: The bed level at the location of interest was video recorded from outside through the transparent glass wall.

The water surface elevation was measured by traditional wave gauges. Two wave gauges were located offshore: One just after the wave filter and one at the toe of the slope. Two other wave gauges were located at the sand section: One at the top of the slope and one at the breaking point.

Parallel to the sediment bed experiments a number of flow visualizations were conducted in another flume. This flume was 14 m long (from the wave maker to the wave absorber), 60 cm wide and 80 cm deep. A horizontal, rigid false bottom, 16 cm above the base bottom was installed 9.0 m from the wave maker and was continued to the wave absorber. A 1.5 m long slope (1:9.4) connected the false bottom and the base bottom. A pile with a diameter of 10 cm was placed 1.5 m onshore of the top of the slope. Flow visualizations were made with light plastic particles and by tracing small air bubbles. Different distances between breaking point and pile were tested by varying the wave height and period. The water depth was kept constant at 31 cm to the base bottom.

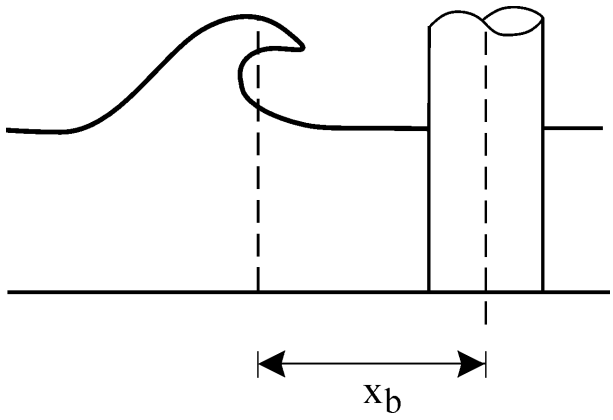

Figure 4.3: *Definition of the distance from wave breaking to the pile center.*

4.3 Test Conditions

Throughout the sediment bed experiments the water depth was kept constant at 65 cm at the wave paddle, corresponding to an initial water depth of 30 cm at the test section. The sand remained the same for all the tests: $d_{50} = 0.18$ mm. The following input parameters were varied: The diameter of the pile, D, the wave height at breaking H_b, the wave period, T, and the distance from the breaking point to the center of the pile, x_b, see definition in Fig. 4.3. The point of breaking was changing slightly during the experiment because of the changing bathymetry this leads to an uncertainty of the breaking point of approximately ± 0.2 m. The test conditions are listed in Table 4.1. Together with the test conditions the most important results are listed in Table 4.1: The scour depth, S, the maximum width of the scour hole, L_s, the time scale of the scour process, T_s and actual bed elevation with and without pile at the point of maximum scour.

Table 4.1: *Test conditions and the most important results of the tests. For definition of scour see Fig. 4.2.* $\eta_{b,u}$ *is the undisturbed equilibrium bed level at the point of maximum scour and* η_b *is the equilibrium bed elevation at the same location with the pile. Both are relative to the initial bed level.* $\eta_b > 0$ *for scour.*

Test	D [cm]	H_b [cm]	T [s]	S_{max} [cm]	$\eta_{b,u}$ [cm]	η_b [cm]	x_b [m]	L_s [cm]	Distance from top of slope to pile [m]	T_s [min]
1	10	24.0	2.9	0.9	5.0	4.1	0.0	15.0	2.5	1.8
2	20	24.0	2.9	2.0	4.0	2.0	0.0	22.5	2.5	2.3
3	10	30.0	2.9	4.1	0.0	-4.1	1.5	14.0	2.5	0.9
4	20	30.0	2.9	2.4	-1.0	-3.4	1.5	22.5	2.5	2.3
5	10	32.0	2.9	4.1	-2.5/-3.0	-6.6/-7.1	2.2	23.5	2.5	2.0
6	20	32.0	2.9	4.3	-3.5	-7.8	2.2	30.0	2.5	2.1
7	10	25.0	4.0	0.6	2.0	1.4	1.0	11.0	3.5	2.8
8	20	25.0	4.0	1.8	-0.3	-1.5	1.0	17.0	3.5	-
9	10	27.0	4.0	3.5	-2.5	-6.0	1.5	15.0	2.5	2.4
10	20	27.0	4.0	4.6	-3.0	-7.6	1.5	30.0	2.5	6.8
11	10	27.0	4.0	3.2	4.0	0.8	2.5	15.0	3.5	0.9
12	20	27.0	4.0	9.2	7.5	-1.7	2.5	38.0	3.5	22.0
13	10	30.0	4.0	6.2	-5.5	-11.7	2.3	20.0	2.5	4.0
14	20	30.0	4.0	7.0	-3.0	-10.0	2.3	30.0	2.5	5.0
15	55	28.0	3.5	2.1	4.0	1.9	1.7	-	2.5	3.8
16	55	28.0	3.5	10.5	10.0	-0.5	2.7	50.0	3.5	9.9
17	55	25.0	3.5	4.0	6.5	2.5	2.1	50.0	2.5	2.9
18	55	25.0	3.5	15.6	16.8	1.2	3.1	70.0	3.5	7.0
19	55	27.0	3.5	6.0	5.5/4.0	-0.5/-2.0	2.5	-	2.5	4.2
20	55	27.0	3.5	13.3	19.0	5.7	3.5	60.0	3.5	9.3
21	55	27.0	3.5	4.5	4.2	-0.3	4.5	-	4.5	-
22	55	27.0	3.5	4.3	6.5	2.2	5.5	-	5.5	3.1
23	10	27.0	3.5	3.5	6.0	2.5	3.5	17.0	3.5	-
24	20	27.0	3.5	7.7	10.0	2.3	3.5	35.0	3.5	7.5
25	10	27.0	3.5	2.7	2.3	-0.4	4.5	-	4.5	-

The time scale for the scour process in breaking waves is somewhat more complex than the time scale for scour caused by current and non-breaking waves, since, in the present case, more than one process take place concurrently, namely the scour process and the process of general morphological development of the bed (the bar-and-trough system). The experiments showed that the scour process is much faster than the development of the general morphological features. This makes it possible to estimate the time scale on the basis of the initial scour and the initial equilibrium, which occur before a substantial amount of change occurs in the general bed morphology. The definition of the time scale in the case of a location at a bar or in a trough is given in Fig. 4.4.

4.4 Results

The scour depth around a mono pile in breaking waves is a function of several parameters. Given that there is live-bed regime in the region of breaking, the most important parameters determining the scour depth are: Pile diameter, D, wave height at breaking, H_b, distance from the pile to the breaking point, x_b, and the wave length, L_b. The water depth is also important, and is included indirectly in the breaking wave height as H_b is controled by the water depth. On dimensional grounds, the scour depth can be written in the following non-dimensional form:

$$\frac{S}{D} = f\left(\frac{H_b}{D}, \frac{x_b}{L_b}\right) \tag{4.1}$$

Here, the wave height of the breaking wave is normalized by the pile diameter, H_b/D, and this parameter can be viewed as a "degenerated" Keulegan-Carpenter number, the key parameter controlling scour in the case of non-breaking waves (e.g. Sumer and Fredsøe (2002)). On the other hand, the distance from the breaking point, (see Fig. 4.3), determines the bed shear stress (both the mean and the turbulence), see e.g. Sumer *et al.* (2011). The distance from the breaking point to the pile is normalized with the wave length at the point of breaking, calculated from linear wave theory.

There are two effects that will have different strength in different regions of the breaking: (1) Mechanism associated with the formation of the bar-trough system; and (2) That due to scour as a result of the pile presence. In the case of the general morphological development it is controlled by the breaking wave, see Fig. 4.5: The level of the bed shear stresses is relatively low at the breaking point (stage 2, Fig. 4.5) as no turbulence has yet been generated by the breaker at this point. From the breaking point the bed shear stresses will increase as the turbulence generated by the wave breaking

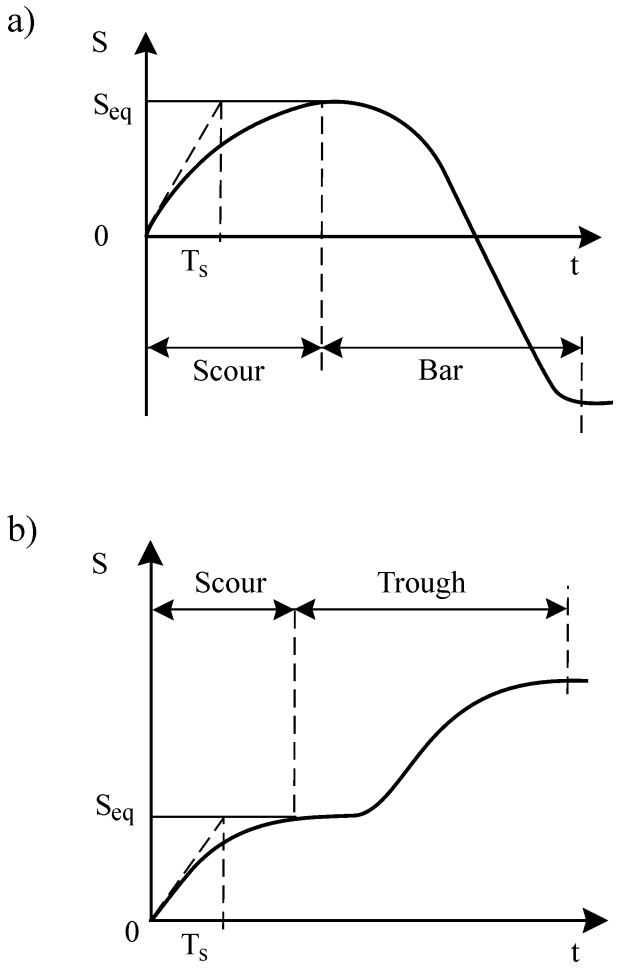

Figure 4.4: *Definition of the time-scale in case of a) location on a bar and b) location off a bar. "Scour", "Bar" and "Trough" indicates whether development of scour, bar or trough is dominating.*

will reach the bottom (stages 5 to 7, Fig. 4.5). When the wave has lost most of its energy it will stop breaking and the bed shear stresses will start to decrease again. Large amounts of sediment will be mobilized at the point where the breaking induced turbulence reaches the bottom. The mobilized sediment will be transported offshore by the cross shore flow where it will be deposited as a bar. The generation of the trough (erosion) and the bar (deposition) will cause the breaking to move offshore followed by the trough and bar until an equilibrium with the water level at the top of the bar and the wave height is reached. Nadaoka *et al.* (1988) observed a similar mobilization of the sediment under a breaking wave. These effects are removed from the

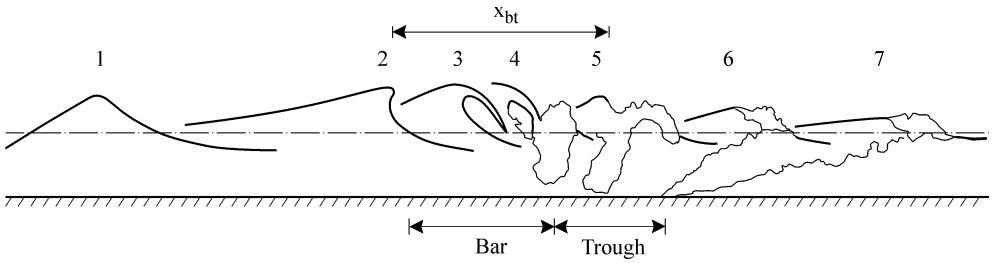

Figure 4.5: *The sequence of breaking for a plunging breaker. Small numbers denote different stages of the breaking process. Adapted from Svendsen (2006).*

results in the present case, by subtracting an undisturbed bathymetry from the disturbed bathymetry (with pile).

The actual scour is caused by the presence of the pile. Detailed studies of the flow around the pile have shown that the most important reason for the generation of the scour is the downflow of highly turbulent water along the offshore side of the pile: When the bore of the breaking wave hits the pile a portion of the highly turbulent water in the bore will be forced down towards the bottom. The amount of turbulent energy that will reach the bottom will mainly depend on the distance from the bore to the bottom.

When the pile is located offshore of the bar crest (stages 2 and 3, Fig. 4.5) the breaking wave or the bore of the breaking wave are still concentrated near the surface, so the distance from the bore to the bottom is relatively large and only (if any) a limited amount of turbulence will reach the bottom. This will cause a relatively smaller scour. When the pile is placed at the onshore half of the bar the turbulence has still not reached the bottom, but the distance has decreased significantly and a significant amount of turbulence will be diverted down to the bottom by the pile, causing large scour (stage 4, Fig. 4.5). The trough is the area where most of the breaking induced turbulence reaches the bottom (stage 5, Fig. 4.5). Therefore this stage is, again, associated with relatively large scour depths, although the actual scour experiments indicate that the measured scour is somewhat smaller than that corresponds to stage 4. Further onshore (stages 6 and 7) most of the wave energy is dissipated by the wave breaking and the turbulence undergoes decay as the breaking wave travels onshore, leading to relatively smaller scour around the pile.

The description above corresponds to the results of the tests shown in Fig. 4.6. It is seen that the maximum scour, $S = 0.65D$, is located at $x_{bt} = 0.35L_b$ or at the middle of the bar and that the scour is decreasing on- and offshore of this point. The distance, x_{bt}, from the breaking point to the bar is around $0.2L_b$ to $0.5L_b$. The maximum scour was located approximately

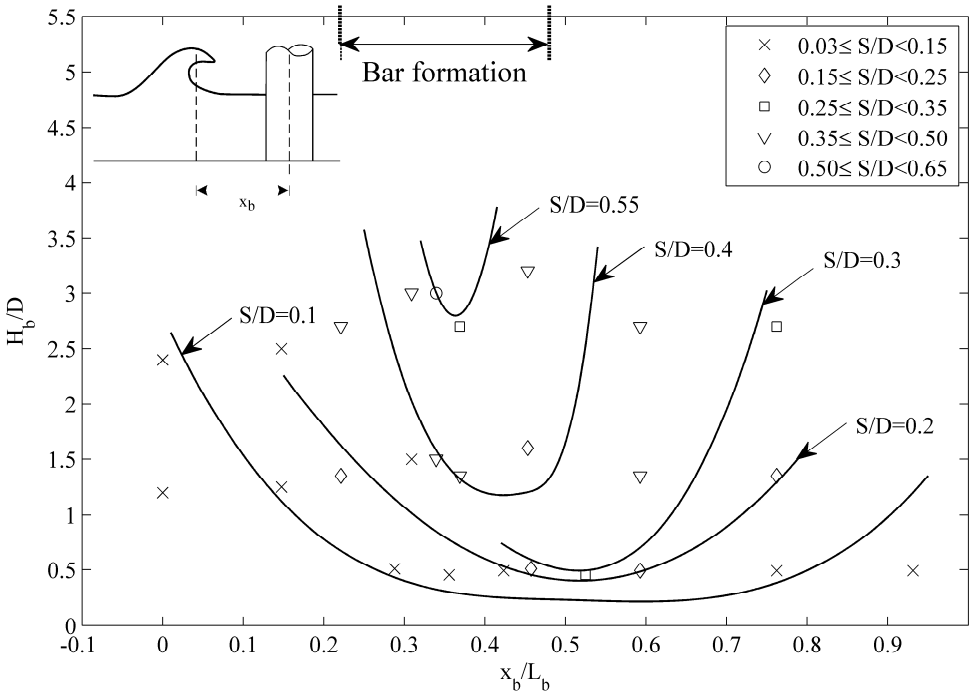

Figure 4.6: *The normalized scour depth for a pile in breaking waves.*

$0.35L_b$ to $0.4L_b$ from the breaking point.

The observed location of the bar corresponds to the results reported by Deigaard *et al.* (1991). Deigaard *et al.* (1991) measured the bed shear stress under a breaking wave on a flat mildly sloping bed (1:30) and reported the highest bed shear stresses approximately 0.35 to $0.45L$ from the breaking point. In other words the maximum scour at a bar is just offshore of the point where the breaking induced turbulence reaches the bottom.

It has been discussed whether wave run-up on the mono pile caused by the breaking wave (see e.g. Mase *et al.* (2001); De Vos *et al.* (2007); Myrhaug and Holmedal (2010)) could have an influence on the scour, either by flows caused directly by the impact of the breaking wave or by the water directed downwards after the wave run-up. Flows generated directly by the impact of the breaking wave have not been observed, while the downward directed water was observed penetrating into the water column and in case of the flow visualizations. This downward directed water carried air bubbles down to approximately 5 cm above the bottom. However, it has not been possible to relate sediment transport to this mechanism. The mechanism is strongest at the early stages of breaking (stage 2 and 3, Fig. 4.5) and disappears more or less in the later stages, this corresponds with observations that the largest

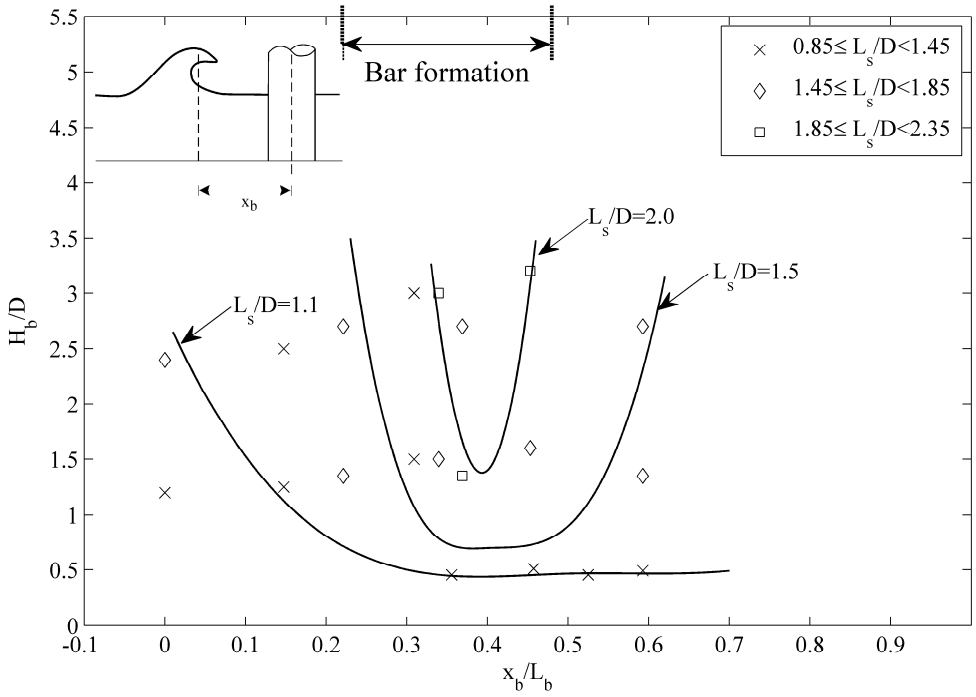

Figure 4.7: *Overall extension of the scour hole around a pile in breaking waves.*

wave run-up is just around the breaking point.

The scour induced by breaking waves can also be compared to the scour caused by non-breaking waves, see e.g. Sumer and Fredsøe (2002). The Keulegan-Carpenter number, $KC = U_m T/D$ (U_m is the maximum undisturbed orbital motion at the bed), is in the present experiments kept in the interval from approximately 5 to 35 (calculated using linear wave theory at the point of breaking). This will in the case of non-breaking waves causes a scour of approximately $0.01D$ to $0.7D$ for $KC = 5$ and $KC = 35$, respectively. In the case of breaking waves the scour was found to be between 0 and $0.3D$ for $KC = 5$ and between 0 and $0.6D$ in the case of $KC = 35$. This means that for small KC-numbers (like O(5)) there is a risk of significant larger scour in the case breaking waves compared to non-breaking waves. For larger KC-numbers the maximum scour will be almost the same in case of breaking and non-breaking waves.

The overall extension of the scour hole is shown in Fig. 4.7. The figure shows a similar overall picture to Fig. 4.6, with the largest scour holes in the case of breaking around $0.4L_b$ offshore of the pile.

The time-scale of the scour process is shown in Fig. 4.8. The dimensionless time-scale, T^*, is defined as in the case of current and non-breaking

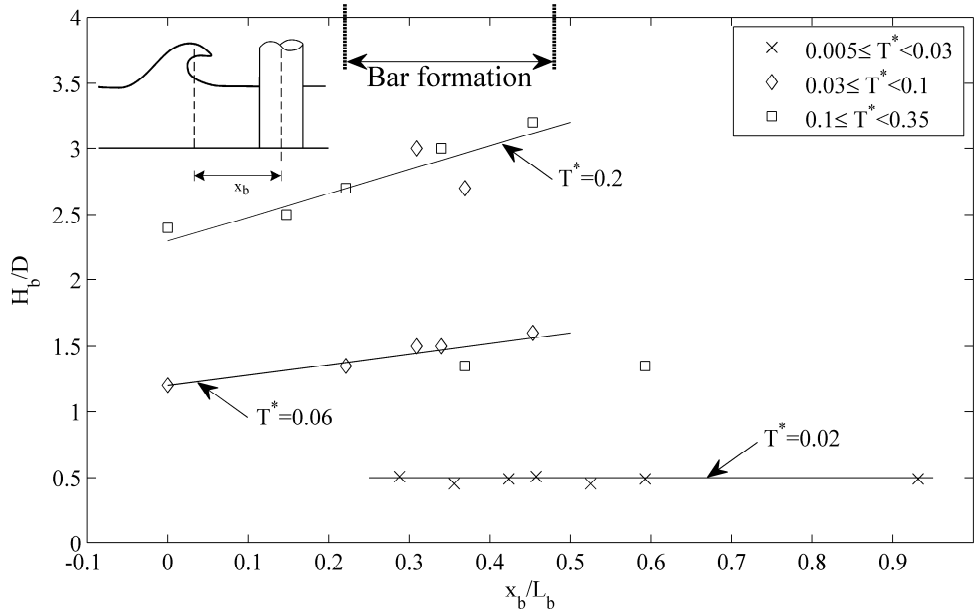

Figure 4.8: *Time-scale of the scour process in breaking waves. Valid for* $\zeta = 1.3$ *to 4.2*

waves, see e.g. Sumer and Fredsøe (2002):

$$T^* = \frac{\sqrt{g(s-1)d_{50}^3}}{D^2} T_s \tag{4.2}$$

where g is the acceleration due to gravity, s is the specific weight of the sediment, d_{50} is the sediment size, D is the pile diameter and T_s is the time scale as defined in e.g. Sumer and Fredsøe (2002).

In the case of current and non-breaking waves induced scour, the time-scale is a function of the normalized bed shear stress; the Shields parameter, see e.g. Sumer and Fredsøe (2002). Involving the latter quantity in the present work is impractical for breaking waves as there is no well established method to calculate the bed shear stresses under breaking waves. For this reason the mobility number introduced in Nielsen *et al.* (2012):

$$\zeta = \frac{(H_b/T)^2}{s(s-1)d_{50}} \tag{4.3}$$

is adopted in the present study. The mobility number, defined in Eq. 4.3, represents the balance between the agitating forces and the resisting forces. The most important agitating forces are upwards pressure gradients and drag forces on the sediment grain, while the most important resisting forces

are gravity and friction between the grains. Sumer *et al.* (2001) used the bed friction velocity, U_f , as a characteristic velocity near the bed (steady current), and Dixen *et al.* (2008) used the maximum value of the wave-induced velocity at the top of the armor stones, U_m. These have lead to the classic Shields parameter in the case of steady currents, and a "gross" Shields parameter in the case of waves, both presumably characterizing the mobility of the sediment. The above quantities, U_f and U_m are impractical to use in the present case as they are difficult to determine in breaking waves. For this reason, the mobility number in the present case is defined as in Eq. 4.3, using the wave height and the wave period. The advantage of using this definition of the mobility number is that the input parameters will be known at the design state of most projects.

The present experiments have been conducted in an interval from 1.3 to 4.2 of the mobility number. That range of ζ is rather narrow (in Nielsen *et al.* (2012) the tested range was approximately 10^{-4} to 2), plotting the time scale data cannot indicate a correlation between the time scale and the mobility number. Nielsen *et al.* (2012) showed a clear correlation between the onset of suction of sediments from between armor stones under breaking waves and the mobility number (Eq. 4.3). This indicates that the parameter is governing for the sediment transport under breaking waves.

4.5 Numerical Example

A foundation of an offshore wind turbine is made of a mono pile with a diameter of 4 m. It is placed in 7.0 m water depth on a mildly sloping bottom: 1:100 in the offshore direction. No measurements or simulations are available at the location, but the offshore conditions are known to be $H_s = 5.6$ m and $T_p = 10.5$ s. Assuming the bottom contours are parallel to the wave crests the local wave height can be calculated as:

$$H = H_0 \sqrt{\frac{\coth kh}{(1 + \frac{2kh}{\sinh 2kh})}} \tag{4.4}$$

where H_0 is the deep water wave height, k is local wave number and h is the local water depth. Assuming that the wave will break at $H_b/h = 0.8$, the distance from breaking to the pile can be in an iterative manner. This gives $x_b = 36$ m offshore of the pile, $L_b = 85$ m, $H_b = 5.9$ m, $x_b/L_b = 0.42$ and $H_b/D = 1.5$. From Fig. 4.6 it is found to give a scour depth $S/D \approx 0.4$ or a scour of 1.6 m.

The time-scale of the scour can be found in Fig. 4.8 to approximately 12 to 13 hours assuming a sand size of 0.2 mm and $s = 2.65$. This is for a mobility number, ζ, just below 100 or two orders of magnitude higher than

for the physical model tests. Although there was no influence on the time scale in the case of the narrow range in the experiments there might be an influence when the mobility number is increased that much. If the time scale is influenced by the mobility number it is assumed that the time scale will decrease for increasing mobility number.

4.6 Conclusions

It is found that breaking waves will generate scour relative to the developed system of bars and trough in the surf zone. The scour was for all cases smaller than the maximum scour expected for current alone, but in the case of larger piles the scour was one order of magnitude larger than the scour of non-breaking waves. For more slender piles the scour was approximately the same for breaking and non-breaking waves.

Acknowledgment

This research was carried out as part of the Statkraft Ocean Energy Research Program, sponsored by Statkraft (www.statkraft.no). The study was partially supported by the Danish Council for Strategic Research (DSF)/Energy and Environment under the program Seabed Wind Farm Interaction (http://sbwi.dhigroup.com, sagsnr. 2104-07-0010) and DHI (www.dhigroup.com).

Chapter 5

Experiments on Removal of Sediment from between Armor Blocks. Part 3: Breaking Waves

This chapter is submitted to ASCE Journal of Hydraulic Engineering:
Nielsen, A.W., Sumer, B.M., and Fredsøe, J.: "Experiments on Removal of Sediment from between Armor Blocks. Part 3: Breaking Waves"

Note: The experiments made on the 1:30 slope were conducted as a part of Anders Wedel Nielsen's master's thesis, see Nielsen (2004). The results have been interpreted for this paper.

Published article: A revised version of this chapter was accepted publication on the 16$^{\text{th}}$ of March 2012. The reference is: Nielsen, A.W., Sumer, B.M., and Fredsøe, J. (2012). Suction Removal of Sediment from between Armor Blocks. Part 3: Breaking Waves. *ASCE Journal of Hydraulic Engineering*, **138**, 803-811 (doi: 10.1061/(ASCE)HY.1943-7900.0000592).

Caution: The wave height in this chapter is not well defined and this may lead to confusion. This is corrected in the published journal article refered above. The correction has influenced several important parameters used in the study. This includes data in tables, coefficients used in equations as well as the numbers found in Figs. 5.5 to 5.8. For this reason only data from the journal article should be used. However, the overall descriptions given in this chapter and the journal article remain the same.

Abstract

When a sediment beach covered by stones or an armor layer is exposed to breaking waves, the turbulence generated by the breaking waves can cause mobilization and removal of the sediment underneath the stones. In two earlier studies by the DTU-group the suction of sediments from between armor blocks has dealt with the case of steady current and non-breaking waves. The present study is an extension of these studies and the results will be presented in a similar way. The critical conditions for removal of sediment are determined. It is found that the onset of suction is governed by three parameters: (1) the sediment mobility (based on the sediment size, wave height and wave period), (2) the ratio between the sediment size and the stone size, d/D, and (3) surf similarity parameter, $\xi = \tan(\beta_0)/(H/L_0)^{0.5}$. The variation of the critical mobility number for removal of sediment as function of d/D and ξ is determined for the range $0.001 < d/D \leq 1.0$ and $0.15 < \xi < 6.00$. The experiments were made on 1:2, 1:14 and 1:30 slopes. Spilling, plunging and surging breakers were used in the experiments. Both one and two layers of armor stones and rectangular blocks were studied.

Keywords: Scour, Beaches, Breakwaters, Breaking waves, Armor units

5.1 Introduction

Stone dumping is one of the most widely used methods for scour protection. This is used for natural beaches near structures as well as for armor layers at breakwaters. These types of stone protection are invariably exposed to breaking waves. When exposed to breaking waves, the sand underneath the protection layer may be agitated by the turbulence generated by the breaking process.

Overall stability of hydraulic structures like piles, bridge piers, breakwaters, seawalls and groins have been studied extensively during the last decades, e.g. stability of breakwaters, seawalls and groins, see for example the detailed account in Oumeraci (1994); stability of the armor layers on breakwaters, around piles exposed to current and waves etc. (e.g. Raudkivi and Ettema (1985); Melville *et al.* (2008)). Scour is one of the critical failure modes of such structures, and has been studied by various authors, Hughes and Kamphius (1996); Fredsøe and Sumer (1997); Hughes and Schwichtenberg (1998); Ming and Chiew (2000); Sumer *et al.* (2005) among others. Detailed reviews of the subject can be found in the books by Whitehouse (1998) and Sumer and Fredsøe (2002). Detailed design guidelines can also be found in Morang (2003). Although much effort has been put in the study of the above mentioned issues, no detailed study of the interaction between

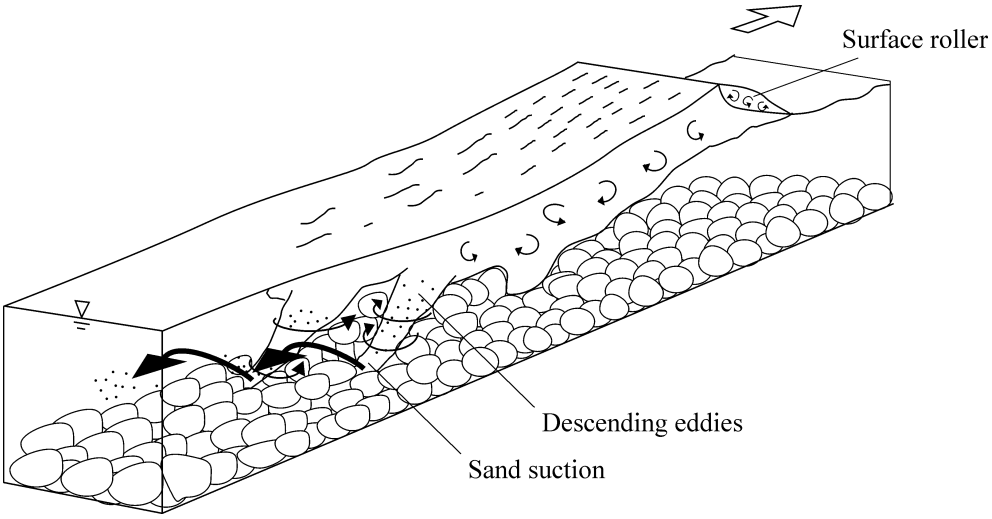

Figure 5.1: *Removal of sediment from between armor blocks by a pair of oblique descending eddies. Adapted from Nadaoka* et al. *(1989).*

the base sediment underneath the protection work and the breaking waves is yet available.

When the waves break, high levels of turbulence will be generated at the water surface. Depending on the type of wave breaking, portions of the highly turbulent water may reach the bottom and cause high bed shear stresses and excess turbulence. Experiments show that this highly turbulent water can penetrate into the stone cover and mobilize the sediment that will eventually be sucked (or winnowed) out between the stones or armor blocks (Fig. 5.1). If larger amounts of sand are removed the stones will start sinking and finally the scour protection may fail. The scour protection needs to be designed in such a way that the sinking is limited to an acceptable level. Sumer *et al.* (2001) were the first to study the suction removal of the sediment from between armor stones and they focused on the process in steady currents. In a follow-up study, Dixen *et al.* (2008) extended this to the wave case, where the waves were non-breaking. The present study is essentially a continuation of the previous two investigations, with the special focus on the suction removal of sediment under breaking waves (spilling, plunging and surging breakers). The different types of wave breaking is essentially obtained by using different bed slopes (1:2, 1:14 and 1:30) as well as wave periods and heights. Further, different configurations of the protection material are analyzed: one and two layers of stone protection, as well as rectangular blocks, placed in regular and staggered patterns.

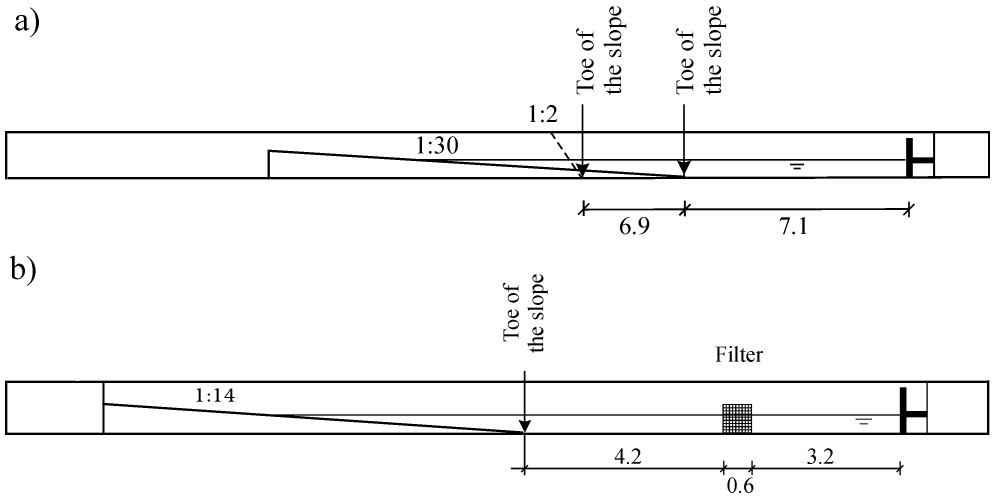

Figure 5.2: *Sketch of flume 1 (a) and flume 2 (b). Measures in meters.*

5.2 Experimental Facility

5.2.1 Flume and the test setup

The experiments were carried out in two different flumes, designated as Flume 1 and Flume 2 (Fig. 5.2). Flume 1 was 0.6 m wide and 0.8 m deep and 34 m long while Flume 2 was 4.0 m wide and 1.0 m deep and 34 m long. Both wave flumes were equipped with piston type wave makers controlled by DHI Wave Synthesizer with AWACS version 2.15 (Active Waves Absorption Control System).

In Flume 1, two different bed slopes with inclinations of 1:2 and 1:30 were installed and in Flume 2, a 1:14 bed slope was installed.

The 1:2 slope was made of a plywood plate supported by a rigid structure of steel beams. It was sealed at the side walls of the flume, so that the sloping bottom was impermeable. The entire slope was covered by stones from the toe to above the swash zone. To ensure the stability of the armor stones on the smooth plywood plate the stones were glued to the plate. The water depth at the wave maker was kept constant at 40.0 cm for the different tests. This gave a water depth at the test site from around 13 cm to 16 cm (Still Water Level, SWL). A few tests were made in holes between the stones above SWL. These holes were placed at 4.5 and 6.3 cm above SWL.

The 1:14 slope was made on a loose bed, consisting of fine sand (d_{50} = 0.2 mm). This study compliments the fixed bed experiments in studying what happens over larger exposed area. The slope spanned over the entire width of the flume but only a 0.6 m wide part of the flume was covered

by armor stones. This layer covered an area from 1 to 2 m offshore off the breaking point to above the swash zone. The water depth at the wave maker was kept in the range from 34 cm to 44 cm for the different tests. This gave a typical water depth at the test sites in the range from around 5 cm to 17 cm SWL. For some of the tests the sand at the test section was replaced by a box with sediments with different properties. A series of tests using rectangular concrete blocks was carried out on this slope as well. The blocks were 9x9 cm in plan-view extension and 8 cm high. The blocks were placed in an area 5 blocks wide and 24 blocks long. The area had approximately the same size as the area covered by the armor stones. The blocks were tested in a regular arranged pattern and in a staggered pattern, see inserts in Fig. 5.8.

The 1:30 slope was made of concrete slabs supported by a rigid plywood structure. The concrete slabs were sealed together and also at the side walls so that the sloping bed was impermeable. The entire slopping part of the bed was covered by the armor stones from the toe to above the swash zone. The water depth at the wave maker was kept in the range from 35.0 cm to 42.5 cm for the different tests. This gave a typical water depth at the test sites in the range from around 5.5 cm to 16.5 cm SWL.

Four different types of stones were used: Crushed stones with a mean diameter of $D = 2.5$ cm and $D = 4.0$ cm and natural round stones with mean diameter $D = 8.5$ cm and $D = 10.0$ cm. The stones were placed in one or two layers in a densely packed manner. The diameter of the stones was obtained from a random sample of 30 stones. Samples of the stones are shown in Fig. 5.3.

5.2.2 Sediment and Single Particle Experiments

The sediment-size-to-stone-size ratio, d/D, is one of the parameters controlling the suction of the sediment, see Sumer *et al.* (2001) and Dixen *et al.* (2008). Small values of d/D are relevant for stones placed on sand beds, while larger values of d/D is relevant for stone layers placed on bedding material. In the case of small values of d/D a sediment bed was used to determine the onset of suction, while for large values of d/D the experiments were made using single particles as described in Dixen *et al.* (2008). The sediment bed experiments were carried out on the 1:14 and 1:30 slopes, while the single particle experiments were carried out on the 1:2 and 1:30 slopes.

Fine sediments ($0.2 < d_{50} < 3.8$ mm, Table 5.3) were used for the solid wall test at the 1:14 and 1:30 slopes. For the loose sediment bed (slope 1:14) the sediment layer had a large thickness of at least 15.0 cm (in the cases where a sandbox was placed at the test section). The sand box was 56.0 cm long, 36.5 wide and 15.0 cm deep. In the 1:30 slope case a thin layer

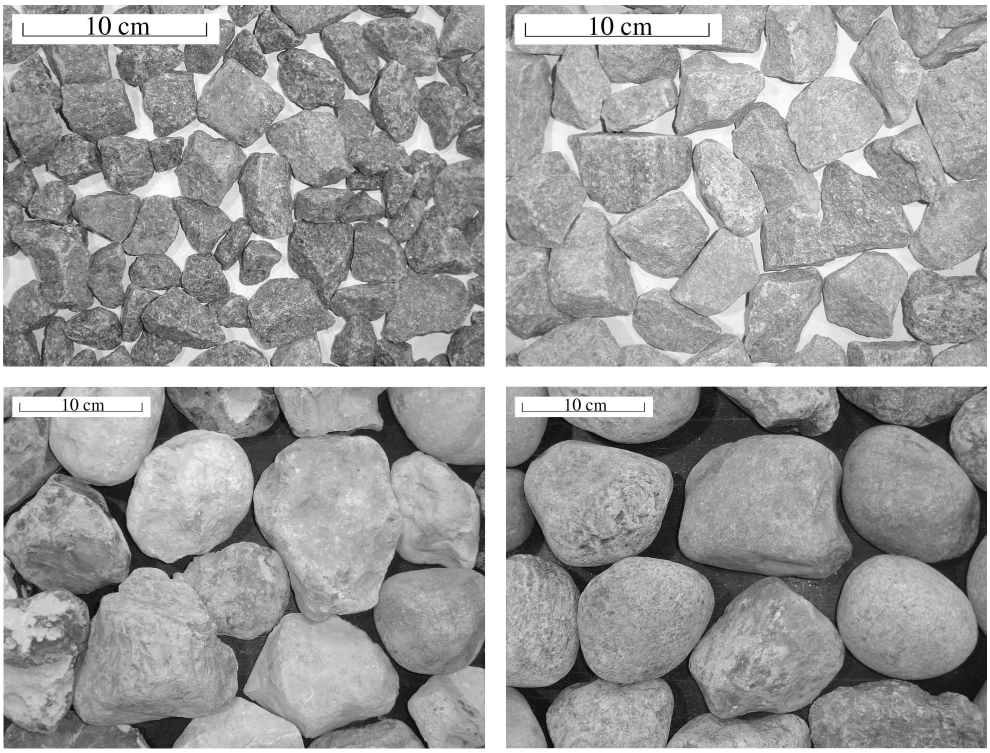

Figure 5.3: *Stones used for the experiments. Upper left corner: Crushed stones* $D = 2.5$ *cm. Upper right corner: Crushed stones* $D = 4.0$ *cm. Lower left corner: Natural stones* $D = 8.5$ *cm. Lower right corner: Natural stones* $D = 10.0$ *cm.*

of sediment, around 3 mm thick for the fine sediment or 2 to 3 diameters thick for the larger material, was placed on the sloping bed in a small area of interest, and the critical conditions for suction was studied by varying the wave height and period.

The single particles used at the 1:2 and 1:30 slopes were made of plastic and wood and were in spherical shape ($4.0 \leq d \leq 70.0$ mm, Table 5.1 and 5.3). The specific gravity of the particles was adjusted by injecting small pieces of metal into the particle. The hole through which the metal pieces were inserted was covered by wax. The single particles were used for values of d/D down to 0.26.

5.2.3 Procedure for onset of suction tests

Two different procedures were used to determine the onset-of-suction. For the single particle experiments the specific gravity of the particles was de-

creased in small increments until suction occurred. The wave height and period were kept constant during a single particle experiment. For the sediment experiments the specific gravity could for practical reasons not be changed and the wave height was increased instead until suction occurred.

The definition of suction is adopted from the previous studies (Dixen *et al.*, 2008): "The following 'strict' definition of the onset of suction was adopted in the above procedure. The onset of suction is defined as the occurrence of entrainment of grains/single particle into the main body of the water (the water body above the top of the cover stones/blocks). In the case of the sediment bed, the entrainment of even a single grain was sufficient to assume that suction occurred." In the present study the sediment/single particle was considered not to be entrained, if it returned to the original hole during the same wave period as it was entrained from the hole.

The necessary test duration of the experiment was determined in the same way as in Sumer *et al.* (2001) and Dixen *et al.* (2008). A spherical plastic particle with a diameter 10.4 mm and specific gravity 1.05 was used. The particle was placed in 4 different holes between the stones and the duration from the release and suction of the particle was recorded for different wave heights. The wave period was kept constant at 3.0 s. The test was repeated 10 times for each hole and wave height. The result of the test showed that a test duration of 70 wave periods was sufficient.

5.3 Test Conditions

The tests have been divided into six groups: (1) Tests with 1:2 slope with one layer of armor stones; (2) Those with 1:14 slope with one layer of armor stones; (3) Those with 1:30 slope with one layer of armor stones; (4) Those with 1:14 slope with two layers of armor stones; and (5) Those with 1:14 slope with regular blocks placed in one layer; and (6) The same as (5) but with a staggered layout of the blocks. 297 tests have been carried out in total, with 15 tests (group 1), 72 tests (group 2), 162 tests (group 3), 20 tests (group 4), 12 tests (group 5) and 6 tests (group 6). This is a large amount of data and for this reason only the ranges of the test conditions are given in this article.

Table 5.1 to 5.4 shows ranges of the test conditions for group 1 to 4. In the tables the quantities H and T are the wave height and the wave period, respectively, D is the size of the armor stones, d is the sediment size (d_{50}) or single particle, s is the specific gravity of the sediment or single particle, ξ is the surf similarity parameter (or Irribarren number) defined by (see e.g. Fredsøe and Deigaard (1992)):

$$\xi = \frac{\tan(\beta_0)}{\sqrt{H/L_0}} \tag{5.1}$$

where β_0 is the slope of the beach, H is the wave height and L_0 is the deep water wave length. and ζ is the mobility number defined by:

$$\zeta = \frac{(H/T)^2}{g(s-1)d_{50}} \tag{5.2}$$

Table 5.1: *Test conditions and results in terms of surf similarity parameter, ξ, and mobility number, ζ in the case of a 1:2 slope and one layer of stones. The data are given in ranges.*

D [cm]	d [mm]	s	d/D	H [cm]	T [s]	ξ	ζ
$4.0 - 10.0$	$16.0 - 43.4$	$1.19 - 1.63$	$3.74 \cdot 10^{-1} - 5.00 \cdot 10^{-1}$	$10.7 - 11.1$	3.0	$5.62 - 5.73$	$1.20 \cdot 10^{-2} - 1.84 \cdot 10^{-2}$
4.0	$25.0 - 28.0$	$1.35 - 1.41$	$6.25 \cdot 10^{-1} - 7.00 \cdot 10^{-1}$	$10.7 - 10.9$	3.0	$5.68 - 5.72$	$1.28 \cdot 10^{-2} - 1.37 \cdot 10^{-2}$
$4.0 - 10.0$	$20.0 - 49.9$	$1.10 - 1.79$	$2.20 \cdot 10^{-1} - 5.00 \cdot 10^{-1}$	$10.0 - 10.6$	3.0	$5.76 - 5.92$	$7.53 \cdot 10^{-3} - 2.48 \cdot 10^{-3}$
$4.0 - 10.0$	$25.0 - 70.0$	$1.13 - 1.84$	$6.25 \cdot 10^{-1} - 9.38 \cdot 10^{-1}$	$10.2 - 10.6$	3.0	$5.75 - 5.87$	$4.72 \cdot 10^{-3} - 1.52 \cdot 10^{-2}$

Table 5.2: *Test conditions and results in terms of surf similarity parameter, ξ, and mobility number, ζ in the case of a 1:14 slope and one layer of stones. The data are given in ranges.*

D [cm]	d [mm]	s	d/D	H [cm]	T [s]	ξ	ζ
8.5	1.4	2.65	$1.65 \cdot 10^{-2}$	$7.9 - 12.2$	$1.1 - 1.3$	$0.33 - 0.38$	$2.27 \cdot 10^{-1} - 4.21 \cdot 10^{-1}$
$4.0 - 8.5$	$1.4 - 3.8$	$1.39 - 2.65$	$3.50 \cdot 10^{-2} - 4.47 \cdot 10^{-2}$	$3.8 - 7.5$	$1.0 - 1.1$	$0.39 - 0.49$	$1.02 \cdot 10^{-1} - 2.06 \cdot 10^{-1}$
4	3	2.65	$7.50 \cdot 10^{-2}$	$6.9 - 7.6$	1.3	$0.45 - 0.46$	$6.29 \cdot 10^{-2} - 7.09 \cdot 10^{-2}$
2.5	3	2.65	$1.20 \cdot 10^{-1}$	$6.5 - 6.5$	1.3	0.47	$5.59 \cdot 10^{-2}$
4	1.4	2.65	$3.50 \cdot 10^{-2}$	4.1	1.1	0.52	$6.01 \cdot 10^{-2}$
2.5	1.4	2.65	$5.60 \cdot 10^{-2}$	$3.2 - 4.9$	$1.1 - 1.3$	0.54 - 0.56	$4.20 \cdot 10^{-2} - 6.87 \cdot 10^{-2}$
2.5	3	2.65	$1.20 \cdot 10^{-1}$	$6.9 - 7.2$	$1.4 - 1.5$	$0.51 - 0.54$	$4.79 \cdot 10^{-2}$
8.5	1.4	2.65	$1.65 \cdot 10^{-2}$	4.5	3	1.35	$1.01 \cdot 10^{-2}$
8.5	3	2.65	$3.53 \cdot 10^{-2}$	$5.5 - 8.2$	3	$1.01 - 1.23$	$6.93 \cdot 10^{-3} - 1.55 \cdot 10^{-2}$
$2.5 - 4.0$	$1.4 - 3.0$	2.65	$5.60 \cdot 10^{-2} - 7.50 \cdot 10^{-2}$	$3.9 - 8.8$	$3.0 - 3.4$	$1.10 - 1.46$	$7.52 \cdot 10^{-3} - 1.37 \cdot 10^{-2}$
2.5	3	2.65	$1.20 \cdot 10^{-1}$	$5.5 - 5.7$	$3.3 - 3.5$	$1.36 - 1.39$	$5.66 \cdot 10^{-3}$
8.5	1.4	2.65	$1.65 \cdot 10^{-2}$	$2.9 - 7.2$	$3.0 - 5.0$	$1.68 - 1.90$	$4.24 \cdot 10^{-3} - 9.09 \cdot 10^{-3}$
$4.0 - 8.5$	$1.4 - 3.0$	2.65	$3.50 \cdot 10^{-2}$	$2.8 - 9.7$	$3.0 - 5.0$	$1.52 - 1.73$	$3.82 \cdot 10^{-3} - 7.72 \cdot 10^{-3}$
$2.5 - 4.0$	$1.4 - 3.0$	2.65	$5.60 \cdot 10^{-2} - 7.50 \cdot 10^{-2}$	$3.1 - 8.0$	$3.0 - 5.2$	$1.63 - 1.83$	$4.20 \cdot 10^{-3} - 5.25 \cdot 10^{-3}$
8.5	1.4	2.65	$1.65 \cdot 10^{-2}$	5.2	5	2.1	$4.81 \cdot 10^{-3}$
4	1.4	2.65	$3.50 \cdot 10^{-2}$	4.1	5.1	2.42	$2.87 \cdot 10^{-3}$
2.5	1.4	2.65	$5.60 \cdot 10^{-2}$	4.4	$4.9 - 5.1$	$2.26 - 2.35$	$3.23 \cdot 10^{-3} - 3.49 \cdot 10^{-3}$
4	1.4	2.6	$3.50 \cdot 10^{-2}$	3.9	5.3	2.54	$2.50 \cdot 10^{-3}$
2.5	1.4	2.65	$5.60 \cdot 10^{-2}$	3.7	5.3	2.65	$2.15 \cdot 10^{-3}$
2.5	3	2.65	$1.20 \cdot 10^{-1}$	$3.6 - 3.7$	$5.3 - 5.4$	$2.63 - 2.73$	$9.28 \cdot 10^{-4} - 1.02 \cdot 10^{-3}$

Table 5.3: *Test conditions and results in terms of surf similarity parameter, ξ, and mobility number, ζ in the case of a 1:30 slope and one layer of stones. The data are given in ranges.*

D [cm]	d [mm]	s	d/D	H [cm]	T [s]	ξ	ζ
10	0.2	2.65	$1.70 \cdot 10^{-3}$	$11.9 - 12.6$	1.6	0.19	$1.99 - 2.25$
10	0.4	2.65	$4.00 \cdot 10^{-3}$	$10.3 - 11.8$	1.6	$0.19 - 0.21$	$6.34 \cdot 10^{-1} - 8.40 \cdot 10^{-1}$
4	0.7	2.79	$1.86 \cdot 10^{-2}$	$10.9 - 14.4$	1.6	$0.18 - 0.20$	$3.52 \cdot 10^{-1} - 6.24 \cdot 10^{-1}$
10	3.8	1.39	$3.80 \cdot 10^{-2}$	$12.8 - 14.4$	1.6	$0.18 - 0.19$	$4.40 \cdot 10^{-1} - 5.57 \cdot 10^{-1}$
4	3	1.98	$7.50 \cdot 10^{-2}$	$17.6 - 18.6$	3	$0.29 - 0.30$	$1.20 \cdot 10^{-1} - 1.33 \cdot 10^{-1}$
$4.0 - 10.0$	$10.4 - 37.4$	$1.01 - 1.35$	$2.60 \cdot 10^{-1} - 3.75 \cdot 10^{-1}$	$10.7 - 13.8$	1.6	$0.18 - 0.20$	$1.63 \cdot 10^{-1} - 2.15$
4	24.5	$1.11 - 1.17$	$6.13 \cdot 10^{-1}$	11.9	1.6	0.19	$1.36 \cdot 10^{-1} - 2.09 \cdot 10^{-1}$
4	37.4	$1.09 - 1.18$	$9.35 \cdot 10^{-1}$	$13.2 - 13.4$	1.6	0.18	$1.06 \cdot 10^{-1} - 2.07 \cdot 10^{-1}$
10	0.4	2.65	$4.00 \cdot 10^{-3}$	$8.6 - 11.8$	3	$0.36 - 0.43$	$1.27 \cdot 10^{-1} - 2.39 \cdot 10^{-1}$
10	0.7	2.65	$7.20 \cdot 10^{-3}$	$11.8 - 14.1$	3	$0.33 - 0.36$	$1.33 \cdot 10^{-1} - 1.88 \cdot 10^{-1}$
4	0.7	2.79	$1.86 \cdot 10^{-2}$	$7.0 - 11.4$	3	$0.37 - 0.47$	$4.17 \cdot 10^{-2} - 1.10 \cdot 10^{-1}$
10	3.8	1.39	$3.80 \cdot 10^{-2}$	$10.0 - 12.4$	3	$0.35 - 0.40$	$7.57 \cdot 10^{-2} - 1.18 \cdot 10^{-1}$
4	3	1.98	$7.50 \cdot 10^{-2}$	$13.7 - 15.4$	3	$0.32 - 0.34$	$7.18 \cdot 10^{-2} - 9.14 \cdot 10^{-2}$
10	15	1.08	$1.50 \cdot 10^{-1}$	$11.0 - 13.5$	3	$0.34 - 0.38$	$1.09 \cdot 10^{-1} - 1.64 \cdot 10^{-1}$
$4.0 - 10.0$	$10.4 - 37.4$	$1.02 - 1.47$	$2.60 \cdot 10^{-1} - 3.75 \cdot 10^{-1}$	$11.8 - 14.1$	$2.8 - 3.0$	$0.33 - 0.36$	$3.46 \cdot 10^{-2} - 3.35 \cdot 10^{-1}$
4	24.5	$1.11 - 1.13$	$6.13 \cdot 10^{-1}$	$11.9 - 13.4$	3	$0.34 - 0.36$	$5.56 \cdot 10^{-2} - 7.52 \cdot 10^{-2}$
4	37.4	$1.10 - 1.19$	$9.35 \cdot 10^{-1}$	14	3	0.33	$3.09 \cdot 10^{-2} - 6.00 \cdot 10^{-2}$
10	0.7	2.65	$7.20 \cdot 10^{-3}$	$12.1 - 12.8$	4.5	$0.52 - 0.54$	$6.20 \cdot 10^{-2} - 6.89 \cdot 10^{-2}$
10	1	2.65	$1.03 \cdot 10^{-2}$	$12.0 - 12.9$	4.5	$0.52 - 0.54$	$4.30 \cdot 10^{-2} - 4.89 \cdot 10^{-2}$
4	0.7	2.79	$1.86 \cdot 10^{-2}$	$7.8 - 11.0$	4.5	$0.57 - 0.67$	$2.30 \cdot 10^{-2} - 4.57 \cdot 10^{-2}$
4	3	1.98	$7.50 \cdot 10^{-2}$	$9.8 - 11.9$	4.5	$0.54 - 0.60$	$1.63 \cdot 10^{-2} - 2.42 \cdot 10^{-2}$
10	15	1.08	$1.50 \cdot 10^{-1}$	$7.5 - 9.8$	4.5	$0.60 - 0.68$	$2.25 \cdot 10^{-2} - 3.80 \cdot 10^{-2}$
$4.0 - 10.0$	$10.4 - 37.4$	$1.02 - 1.90$	$2.60 \cdot 10^{-1} - 3.75 \cdot 10^{-1}$	$9.9 - 12.8$	$4.1 - 4.5$	$0.52 - 0.60$	$5.61 \cdot 10^{-3} - 1.26 \cdot 10^{-1}$
4	24.5	$1.13 - 1.27$	$6.13 \cdot 10^{-1}$	$11.3 - 11.9$	4.5	$0.54 - 0.56$	$9.54 \cdot 10^{-3} - 2.07 \cdot 10^{-2}$
4	37.4	$1.19 - 1.42$	$9.35 \cdot 10^{-1}$	$12.4 - 12.5$	4.5	0.53	$4.97 \cdot 10^{-3} - 1.09 \cdot 10^{-2}$

Table 5.4: *Test conditions and results in terms of surf similarity parameter, ξ, and mobility number, ζ in the case of a 1:14 slope and two layers of stones. The data are given in ranges.*

D [cm]	d [mm]	s	d/D	H [cm]	T [s]	ξ	ζ
4	1.4	2.65	$3.50 \cdot 10^{-2}$	14	1.1	0.28	$7.14 \cdot 10^{-1}$
4	1.4	2.65	$3.50 \cdot 10^{-2}$	$10.1 - 11.2$	1.1	$0.32 - 0.33$	$3.72 \cdot 10^{-1} - 4.56 \cdot 10^{-1}$
7.5	3.8	1.39	$5.07 \cdot 10^{-2}$	6.6	1.3	0.48	$1.80 \cdot 10^{-1}$
7.5	1.4	2.65	$1.87 \cdot 10^{-2}$	16.1	3	0.72	$1.27 \cdot 10^{-1}$
7.5	3.8	1.39	$5.07 \cdot 10^{-2}$	$3.9 - 5.3$	$1.1 - 1.2$	$0.50 - 0.54$	$8.43 \cdot 10^{-2} - 1.33 \cdot 10^{-1}$
7.5	1.4	2.65	$1.87 \cdot 10^{-2}$	$12.8 - 14.7$	3	$0.75 - 0.81$	$8.04 \cdot 10^{-2} - 1.06 \cdot 10^{-1}$
4	1.4	2.65	$3.50 \cdot 10^{-2}$	$7.5 - 7.6$	$3.3 - 3.5$	$1.15 - 1.23$	$2.01 \cdot 10^{-2} - 2.35 \cdot 10^{-2}$
7.5	3.8	1.39	$5.07 \cdot 10^{-2}$	$4.0 - 4.7$	$2.5 - 2.7$	$1.11 - 1.27$	$1.58 \cdot 10^{-2} - 2.45 \cdot 10^{-2}$
7.5	1.4	2.65	$1.87 \cdot 10^{-2}$	$6.8 - 7.8$	$5.1 - 5.2$	$1.77 - 1.88$	$7.87 \cdot 10^{-3} - 1.02 \cdot 10^{-2}$
4	1.4	2.65	$3.50 \cdot 10^{-2}$	$4.3 - 5.8$	$5.4 - 5.6$	$2.23 - 2.49$	$2.86 \cdot 10^{-3} - 4.80 \cdot 10^{-3}$
4	1.4	2.65	$3.50 \cdot 10^{-2}$	4.4	5.5	2.5	$2.84 \cdot 10^{-3}$

Tables 5.5 and 5.6 show the ranges of the test conditions for group 5. In the tables, G is the gap between the blocks (see the inset in Fig. 5.8 for the definition sketch), "pattern" refers to the way the blocks were placed relative to each other. In these experiments the base sediment was unchanged with $d_{50} = 0.2$ mm and $s = 2.65$. The rectangular blocks were 9 times 9 cm in the plane and 8 cm high.

Table 5.5: *Test conditions and results in terms of surf similarity parameter, ξ, and mobility number, ζ in the case of a 1:14 slope and rectangular blocks in one layer. The data are given in ranges.*

G [mm]	G/D	H [cm]	T [s]	ξ	ζ
10	0.13	$3.1 - 3.6$	$1.2 - 1.3$	0.66	$2.02 \cdot 10^{-1} - 2.34 \cdot 10^{-1}$
20	0.25	3.1	1.1	0.61	$2.38 \cdot 10^{-1}$
26	0.33	$2.6 - 3.0$	$1.1 - 1.2$	$0.66 - 0.68$	$1.69 \cdot 10^{-1} - 1.98 \cdot 10^{-1}$
35	0.44	2.6	1	0.59	$2.16 \cdot 10^{-1}$
20	0.25	2.6	1.2	0.72	$1.44 \cdot 10^{-1}$
26	0.33	2.6	$1.3 - 1.4$	$0.77 - 0.83$	$1.09 \cdot 10^{-1} - 1.26 \cdot 10^{-1}$
35	0.44	$2.6 - 2.7$	$1.2 - 1.5$	$0.72 - 0.87$	$1.04 \cdot 10^{-1} 1.42 \cdot 10^{-1}$

Table 5.6: *Test conditions and results in terms of surf similarity parameter, ξ, and mobility number, ζ in the case of a 1:14 slope and rectangular blocks with staged layout in one layer. The data are given in ranges.*

G [mm]	G/D	H [cm]	T [s]	ξ	ζ
10	0.13	$3.8 - 3.9$	$1.2 - 1.3$	$0.59 - 0.64$	$2.63 \cdot 10^{-1} - 3.19 \cdot 10^{-1}$
26	0.33	$3.1 - 3.4$	$1.1 - 1.2$	$0.57 - 0.65$	$2.11 \cdot 10^{-1} - 3.01 \cdot 10^{-1}$
10	0.13	3.9	1.5	0.73	$2.04 \cdot 10^{-1}$
26	0.33	3.3	1.4	0.74	$1.69 \cdot 10^{-1}$

5.4 Governing Parameters

On dimensional grounds, the critical condition corresponding to the onset of suction removal of sediment is described by the following three parameters: (1) the mobility number, ζ; (2) the surf similarity parameter, ξ; and (3) the sediment-size-to-stone-size ratio. Each parameter is now considered individually.

5.4.1 Mobility number

The mobility number, defined in Eq. 5.2, represents the balance between the agitating forces and the resisting forces. The most important agitating forces are upwards pressure gradients and drag forces on the sediment grain, while the most important resisting forces are gravity and friction between the grains. Sumer *et al.* (2001) used the bed friction velocity, U_f , as a characteristic velocity near the bed (steady current), and Dixen *et al.* (2008) used the maximum value of the wave-induced velocity at the top of the armor stones, U_m. These have led to the classic Shields parameter in the case of steady currents, and a "gross" Shields parameter in the case of waves, both presumably characterizing the mobility of the sediment. The above quantities, U_f and U_m are impractical to use in the present case as they are difficult to determine in breaking waves. For this reason, the mobility number in the present case is defined as in Eq. 5.2, using the wave height and the wave period. The advantage of using this definition of the mobility number is that the input parameters will be known at the design state of most projects.

5.4.2 Breaking parameter

One of the most common breaking parameters is the surf similarity parameter, defined in Eq. 5.1. The surf similarity parameter describes the breaker type, with the following boundaries (approximately):

Spilling breaker:			ξ	$<$	0.5
Plunging breaker:	0.5	$<$	ξ	$<$	3.3
Surging breaker:	3.3	$<$	ξ		

The spilling and plunging breakers are very similar in the way they break although the intensity of the turbulence in the case of a plunging breaker is much higher than in the case of a spilling breaker. The results show that the spilling and plunging breakers are so similar that they can be placed in the same group.

The suction occurs due to the generation of turbulence from the wave breaking. Actually this process can be divided into two stages: Firstly the penetration of the near surface water like that from plunging breaker, see Fig. 5.4, which eventually may hit the bottom and cause suction. In the next stage, diffusion of turbulence from the broken wave comes into action: Turbulence from the migrating bore will spread downwards and cause suction. Of the two stages, it is observed that the second stage is far the most important: No suction takes place in the first stage, while suction becomes violent in the second stage, especially due to the descending eddies, see also Nadaoka *et al.* (1989). This corresponds to the observations by Deigaard *et al.* (1991) and Cox and Kobayashi (2000). They observed highly increased (up to 10

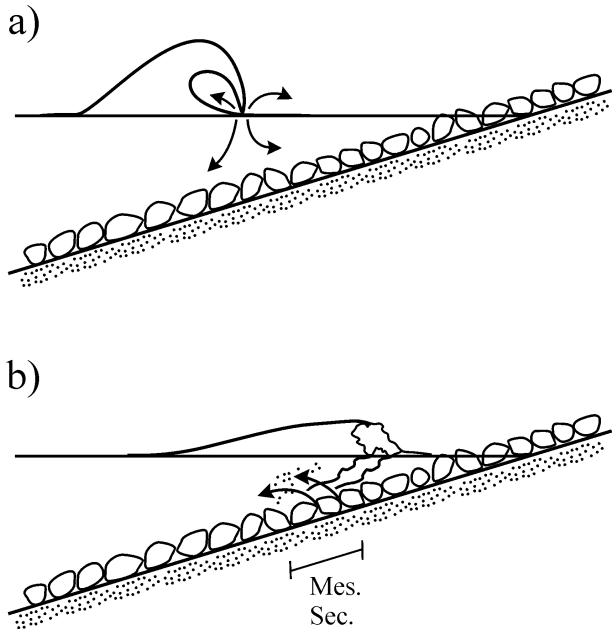

Figure 5.4: *Main location of removal of sediment from between armor blocks in breaking waves.*

times higher) bed shear stresses or levels of turbulence near the bed onshore of the breaking point compared to the levels at the breaking point.

The surging breaker is very different from the two others. In the case of a surging breaker most of the turbulence is generated during the down-rush, while almost no breaking takes place during the incoming wave crest, this result in a significant lower level of turbulence and suction. It should be remembered that the present study focus on suction in the breaking zone and not in the down-rush, as sketched in Fig. 5.4. The velocities in the down-rush can be high and it is likely that it can move base sediment even though the sediment is stable in the breaking zone.

The higher the surf similarity parameter is, the more vulnerable the sediment will be to suction, for a given type of breaker. If the slope is increased the sediment will become more exposed, due to the smaller stabilizing gravity force.

5.4.3 Sediment-size-to-stone-size ratio

A third parameter is the ratio between the size of the sediment and that of the armor stones, d/D. This parameter represents the effect of the penetration (down to the sediment bed) of the previously mentioned agitating forces.

The smaller the value of this parameter, the less susceptible the sediment will be to removal. This is because the agitating forces may not be able to penetrate to such depths in the hole.

5.5 Critical Conditions for Suction in Breaking Waves

The data regarding onset of suction is divided into four groups corresponding to Table 5.1 to 5.6. The data are grouped according to the surf similarity parameter and plotted in Figs. 5.5 to 5.8.

Fig. 5.5 shows the critical conditions for the onset of suction in the case of spilling and plunging breakers and one layer of armor stones. Each curve in the figure divides the $(\zeta, d/D)$-plane into two regions: (1) Region below the curve corresponding to No Suction; and (2) Region above the curve corresponding to Suction. It is clearly seen that the data from both the 1:14 slope and the 1:30 slope coincide.

Fig. 5.5 indicates that there exist three distinct suction regimes: (1) Small d/D regime ($d/D \lessapprox 0.1$); (2) Large d/D regime ($0.3 \lessapprox d/D \lessapprox 1$); and (3) Transition ($0.1 \lessapprox d/D \lessapprox 0.3$). The reason for the existence of two different regimes is, that the mechanism of suction changes: For large values of d/D the particle will more or less fill out the entire hole, leave no or limited space for the turbulence in the outer flow to penetrate into the hole and mobilize the sediment. At the same time, the large particle will be more exposed to the outer flow because the distance from the top of the particle to the top of the surrounding stones are small. This situation corresponds to damage of the protection layer itself by removal of the smallest stones.

In the case of small values of d/D the turbulence is able to penetrate into the hole. Video recordings have shown that especially the oblique descending eddies, described by Nadaoka *et al.* (1989), play an important role in the process of mobilization of fine sediment: When an oblique descending eddy passes over the hole the eddy will agitate the water in the hole causing a significant mobilization and eventually suction of the bed sediment, like a tornado transport debris.

Two empirical relations have been established to estimate the critical mobility number for small and large values of d/D, respectively. In both cases the equation are of the form:

$$\zeta = b(\xi) \left(\frac{d}{D} \right)^a \tag{5.3}$$

where a is a constant equal to -0.55 and -2.1 for small values of d/D ($d/D =$ 0.001 to 0.1) and large values of d/D ($d/D = 0.3$ to 1.0), respectively. b is a function of the surf similarity parameter and can, in the case of small values

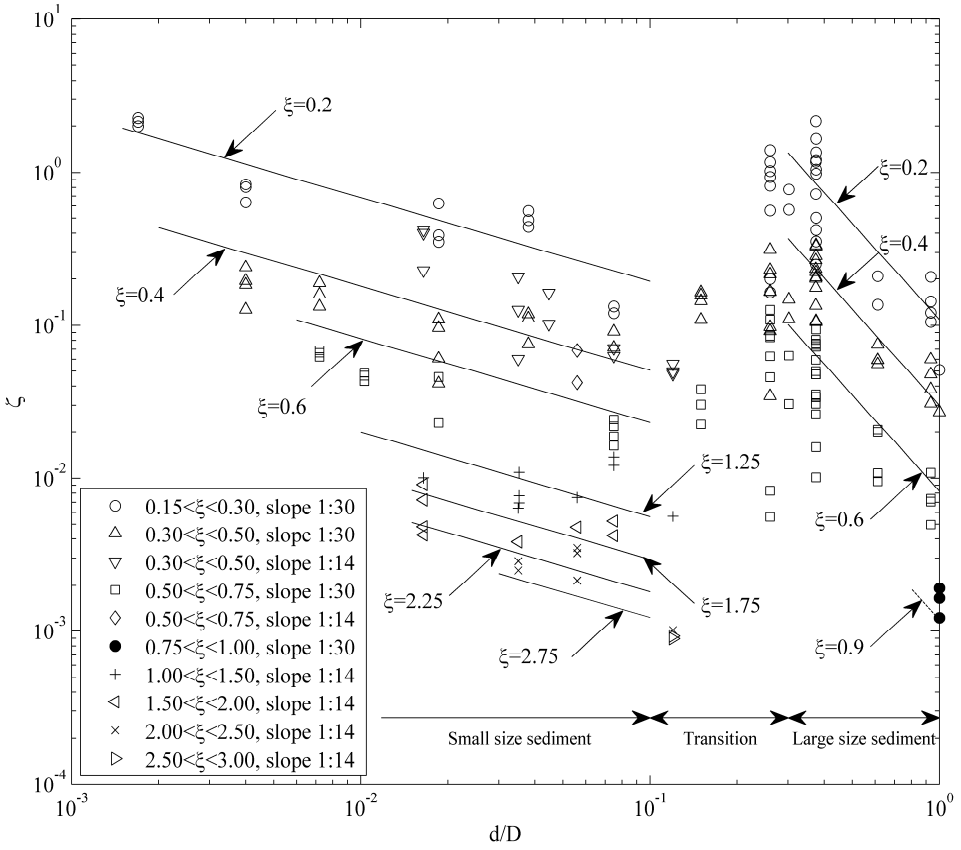

Figure 5.5: *Mobility number as function of d/D for different ranges of the surf similarity parameter in case of one layer of stones. The diagram is valid for spilling and plunging breakers over randomly placed stones. The trend lines are according to Eqs. 5.3, 5.4 and 5.5.*

of d/D, be determined as:

$$b(\xi) = \beta \xi^{\alpha} \tag{5.4}$$

where $\alpha = -1.93$ and $\beta = 0.0024$. In the case of large values of d/D:

$$b(\xi) = 10^{(\alpha\xi+\beta)} \tag{5.5}$$

where $\alpha = -2.8$ and $\beta = -0.40$.

Fig. 5.6 shows the critical conditions for onset of suction in the case of spilling and plunging breakers but with two layers of armor stones. The figure is based on the data presented in Table 5.4. Fig. 5.6 shows that the studied area ($0.015 < d/D < 0.055$) has the same tendency as in the case

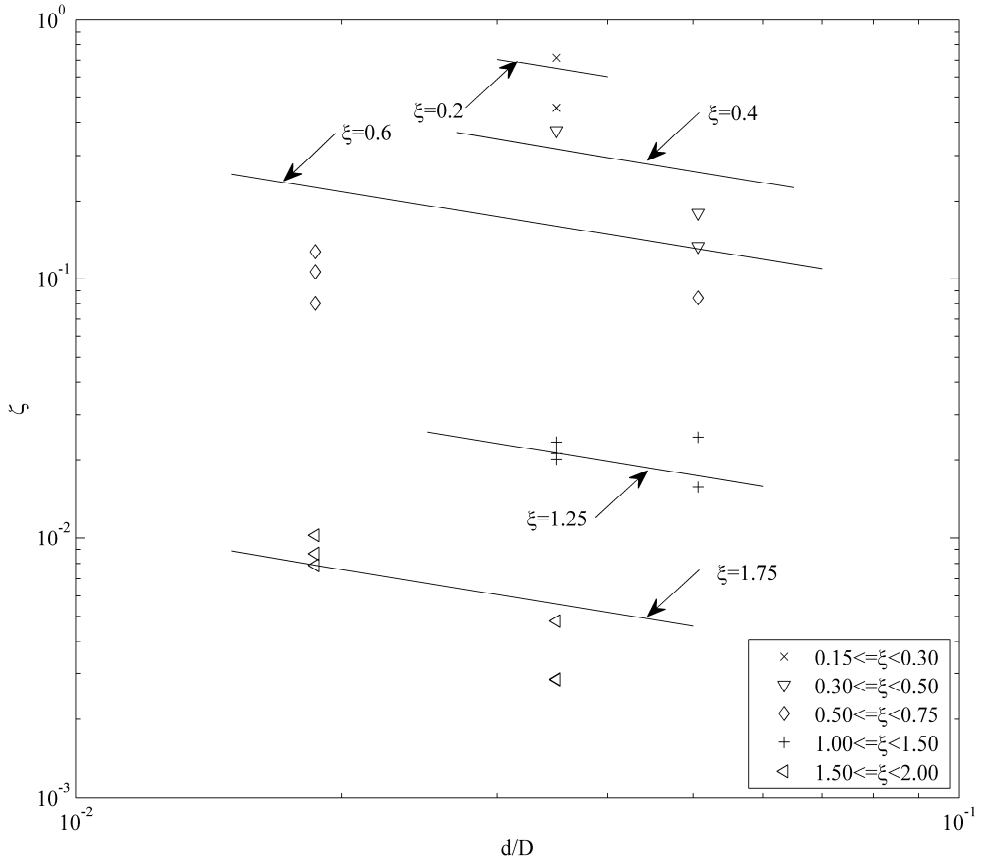

Figure 5.6: *Mobility number as function of d/D for different ranges of the surf similarity parameter in case of two layers of stones. The diagram is valid for spilling and plunging breakers and randomly placed stones. The trend lines are according to Eqs. 5.3 and 5.6.*

of one layer of stones, but the protection of the sediment is better compared to the one layer case. For low values of the surf similarity parameter up to approximately 1 the critical mobility number is around two times higher than in the case of one layer. For higher values of the surf similarity parameter the critical mobility number is almost the same. The reason for the small difference in the case of higher values of the surf similarity parameter is that the plunging breaker produces more turbulent energy there can penetrate into the protection layer.

As in the case of one layer of protection stones an empirical equation has been established to be able to determine the critical mobility number. The equation has the same form as Eq. 5.3. a is the same as in case of one layer of protection stones ($a = -0.55$) and b is given as:

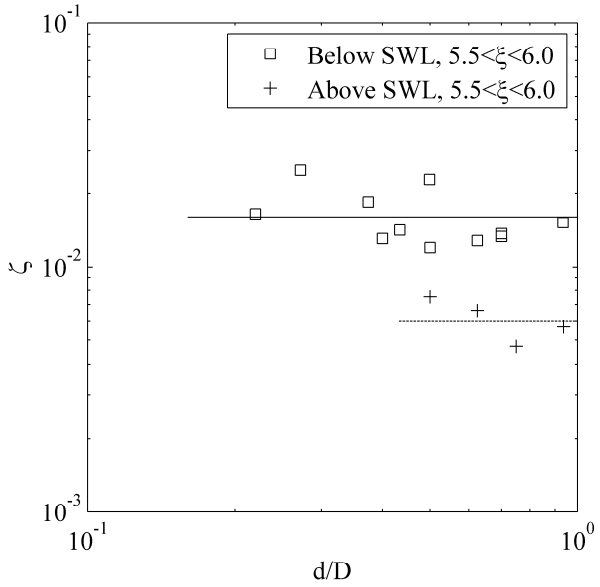

Figure 5.7: *Mobility number as function of d/D for a ranges of the surf similarity parameter ($5.5 < \xi < 6.0$) in case of one layer of stones. The diagram is valid for surging breakers and randomly placed stones.*

$$b(\xi) = 10^{(\alpha\xi^2+\beta\xi+\gamma)} \tag{5.6}$$

where $\alpha = 0.16$, $\beta = -1.6$ and $\gamma = -0.67$.

Fig. 5.7 shows the critical conditions for onset of suction in the case of surging breakers ($5.5 < \xi < 6.0$) and one layer of armor stones. All the tests in this case have been conducted on the 1:2 slope. Tests have been conducted at below still water level (SWL) at the location where the eddy caused by the surging breaker is formed. The other location is above SWL in the swash zone.

Fig. 5.7 shows a plot in a similar way as fig. 5.5, but for a very steep slope and one layer of stones. The very steep slope (1:2) causes a surging breaker. This is a relative weak breaker compared to especially the plunging breaker. For the studied surf similarity range (5.5 to 6.0) the critical mobility number is around 0.006 for particles placed in the swash zone above SWL and 0.016 below SWL. Both values are independent of d/D and the surf similarity parameter within the studied intervals. For the tested range of d/D, this corresponds to a surf similarity of 0.5 to 0.9 in the case of spilling/plunging breakers in the same range of relative sediment size. The test for high surf similarity parameters were all made for high values of d/D. Finer sediment

will probably be much more vulnerable to suction as the surging breaker generate a strong bottom parallel down-rush during the breaking process from the top of the swash zone to around still water level. Sediment small enough to pass in between the pores of the armor stones will most likely be mobilized by this down-rush.

Cubes: Some additional experiments were performed using a different shape of the armor blocks that the natural and crushed stones, namely cubes, which are often used for hydraulic works.

Fig. 5.8 shows the critical mobility number as function of the surf similarity parameter, ξ, and G/D, where G is the gap between the cubes and D is the height of the blocks, as indicated in the figure. The upper plot is valid for blocks placed in a regular pattern, while the lower plot is valid for staggered blocks. The curves fitted to the results in Fig. 5.8 are made under the assumption that the mobility number must go to infinity for the gap going to 0.

For all the results presented in Figs. 5.5 to 5.8 the critical mobility number increases with decreasing surf similarity parameter. If the wave height is increased the surf similarity parameter decreases, in this case the breaking process will tend to move more in to the spilling breaker regime. This means that the turbulence will be spread over a larger distance and a higher mobility number is needed to mobilize the sediment.

It can also be observed that there is a relatively large scatter in the results presented in Figs. 5.5 to 5.8. There can be many reasons for that: First of all the data are given in intervals which can explain some of the scatter. Another reason may be the effect of randomly placed and shaped stones used for the results presented in Figs. 5.5 to 5.7. The latter will result in randomly sized and orientated holes between the stones and these holes will provide different protection for the sediment. The magnitude of this effect can be estimated by comparing the scatter seen in Figs. 5.5 to 5.7 with the scatter seen in Fig. 5.8. While the ratio between the maximum and minimum mobility number can be as large as 3 for a given surf similarity parameter and d/D in the case of randomly placed stones, this ratio is less than 1.5 for the regularly arranged blocks.

5.6 Numerical Example

Consider a moderate sloping beach (1:20) exposed to erosion. A structure placed on the beach will be protected using a riprap layer. The beach is exposed to waves with a peak period, $T_p = 6.6$ s or an offshore wave length of: $L_0 = 68$ m. The significant offshore wave height is $H_0 = 1.2$ m. This gives a surf similarity parameter:

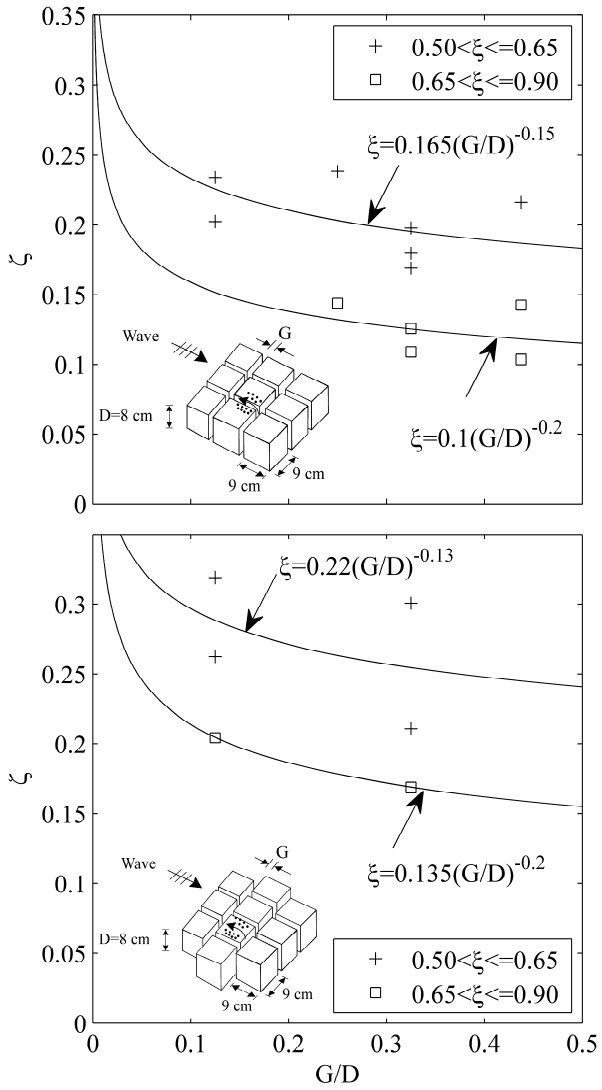

Figure 5.8: *Mobility number as function of the spacing between cubes in case of plunging breakers.*

$$\xi = \frac{\tan(\beta_0)}{\sqrt{H/L_0}} = 0.38 \tag{5.7}$$

The sediment size on the beach is $d_{50} = 25$ mm with a specific gravity of $s = 2.65$. The mobility number can then be calculated to:

$$\zeta = \frac{(H/T)^2}{g(s-1)d_{50}} = 0.08 \tag{5.8}$$

where $\alpha = 0.16$, $\beta = -1.6$ and $\gamma = -0.67$. Consider one layer of protection stones. For the latter Eqs. 5.3 and 5.4 apply (assuming that d/D will be small):

$$b(\xi) = \beta\xi^{\alpha} = 0.016 \tag{5.9}$$

Applying the values of $a = -0.5492$, b and ζ in Eq. 5.3 the required d/D can be found:

$$\frac{d}{D} = \sqrt[a]{\frac{\zeta}{b}} = 0.05 \tag{5.10}$$

This value of d/D is within the limits of small values of d/D as assumed previously. The required stone size is therefore around 0.5 m or larger.

5.7 Conclusion

- The onset of suction (of base sediment) from between armor blocks and stones was determined experimentally, for spilling, plunging and surging breakers.
- The critical condition at which the sediment is sucked from between the stones (the onset of suction) is governed by three parameters, namely, the mobility number ζ, the ratio of the sediment size and the stone size, d/D (or d_{50}/D) and the surf similarity parameter ξ.
- It was found that (1) the effect of a multilayer stone cover (Fig. 5.6); and (2) the effect of regular placed blocks (Fig. 5.8) are significant.

Acknowledgment

This research was carried out as part of the Statkraft Ocean Energy Research Program, sponsored by Statkraft (www.statkraft.no). The study was partially supported by the Danish Council for Strategic Research (DSF)/Energy and Environment under the program Seabed Wind Farm Interaction (http://sbwi.dhigroup.com, sagsnr. 2104-07-0010) and DHI (www.dhigroup.com). The physical model tests with stones on the 1:14 slope was conducted by Mr. P.C. Calsapeu. The physical model tests on the 1:2 slope was conducted by Mr. M. Dixen.

Chapter 6

Flow Velocities and Bed Shear Stresses in a Stone Cover under an Oscillatory Flow

This chapter has been published in Proceedings of the Fifth International Conference on Scour and Erosion, San Francisco, California, USA, November 2010:
Stevanato, F., Nielsen, A.W., Sumer, B.M., Fredsøe, J. (2010): "Flow Velocities and Bed Shear Stresses in a Stone Cover under an Oscillatory Flow", Proceedings of the Fifth International Conference on Scour and Erosion, ASCE, Vol. 1, p. 609-618.

Abstract

In order to get a better understanding of the interaction between the wave-induced, near-bed oscillatory flow, the stone cover and the sea bed, physical model tests were carried out. The tests were conducted in an oscillating water tunnel. The bottom of the tunnel was covered by one, two and three layers of stones. The flow velocities in the pores of the stones were measured using LDA (Laser Doppler Anemometer). In addition to the velocity measurements, the bed shear stresses were also measured using a hotfilm (Constant Temperature Anemometry).

It is found that the boundary layer of the outer flow penetrates quite a substantial amount of thickness into the stone cover, depending on the flow conditions above. Below this level the velocity remains constant. The level of turbulence in between the stones is found to be very high: 3 to 4 times higher than turbulence level over a ripple covered bed in steady current boundary layer without any externally generated turbulence. The bed shear

stress is found to be very low, more than ten times smaller than in the case of a smooth base bottom without stone cover.

6.1 Introduction

Stone covers have been used for scour protection of offshore structures for decades. This was also the case for many of the offshore wind farms erected during the last decade. These wind farms are located in shallow waters and some of them are exposed to high waves and strong currents. Under these extreme conditions the scour protection of the wind turbines suffered unacceptable damages. One of the reasons for these damages to the scour protection could be the heavy wave action.

The purpose of the present study is to gain a better understanding of the interaction between the wave-induced near-bed flow and a stone cover, with the focus on the flow through the pores of the stone cover layer. A significant amount of flow and turbulence was measured for all three cases, namely one, two, and three layers of stones, covered in the tests.

6.2 Setup

6.2.1 General Description

The experiments were conducted in an oscillatory water tunnel with a rectangular working section of 29 cm height and 39 cm width. The horizontal working section of the oscillator is 10 m. Both ends of the horizontal part of the oscillator are connected to a vertical riser. One of the risers is open, while the other is closed and connected to a pneumatic system. During the experiments the bottom of the working section was covered with crushed stones. One, two and three layers of stones were tested. A sketch of the setup is shown in Fig. 6.1.

The velocities were measured using a two component Laser Doppler Anemometer (LDA). The LDA system consisted of a 300mW argon-ion laser exciter, Dantec Dynamics LDA-04 System, Dantec Dynamics 55H21 Frequency tracker, Dantec Dynamics 55N11 Frequency shifter and a laser probe with focal length of 310 mm (in air). To record the direction of the flow a pressure cell was placed at the bottom of the open riser.

The velocity measurements were made through the transparent side wall of the tunnel. The velocities above the stone layer were measured at the center line of the tunnel to reduce the effects of secondary flows due to the rectangular cross section of the tunnel. It was not possible to measure at the center line in the pores of the stone layer as the stones between the LDA probe and the pores at the center line would block the laser beams. For this

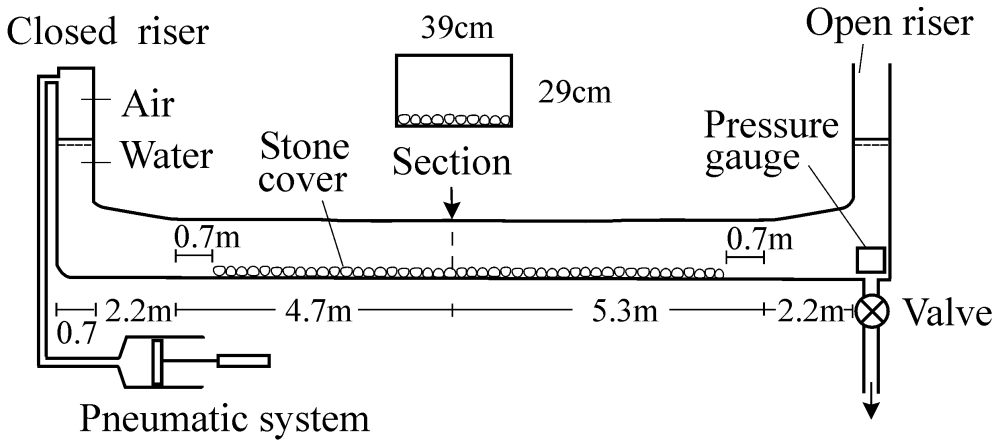

Figure 6.1: *Sketch of the oscillating water tunnel.*

reason the velocities in the pores between the stones were measured adjacent to the side wall. The sample frequency for the velocities and pressure measurements was 70 Hz, and 40 waves were recorded at each measuring point.

Three experiments have been conducted measuring the bed shear stress under three layers of stones. A one-component Dantec hot-film probe was used to measure the bed shear stress. It was mounted flush with the base bottom, and located 15.4 cm from the side wall, at the test section, and calibrated using a calibration channel. A detailed description of the measurement technique is given in Sumer *et al.* (1993a).

The stones had a mean height of $k = 36$ mm with a standard deviation of 9 mm. The height was measured by taking a random sample of 50 stones placed on the bottom of the tunnel, then the stone height was measured as the vertical distance from the bottom of the tunnel to the top of the stones.

6.2.2 Horizontal Position of the Velocity Measurements

The velocity measurements in the pores between the stones are affected by the horizontal position of the measurements. Nevertheless, measurements at the vertical line through the center of the pore would be a sensible option. However, due to the irregularities of the stones, the center of the pore is very hard to define. For this reason the "centroid" of the pore is defined, as in the following (Fig. 6.2):

1. The points of contact A and B between the horizontal projection of two adjacent stones and the side wall of the tunnel are identified.

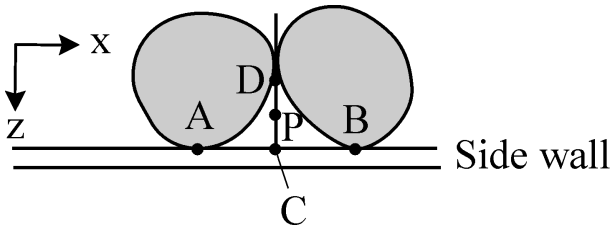

Figure 6.2: *Definition of the centroid, plan-view.*

2. The location of point C: The middle point between points A and B, is found.

3. The horizontal line through point C, perpendicular to the line between A and B, intersects the horizontal projection of the two stones at point D.

4. The centroid P is defined as the middle point between points C and D.

The velocity was measured across the vertical line passing through point P. Twenty different pores were measured.

6.3 Test Conditions

The maximum free stream velocity in the experiment was limited by the stability of the stones. The stones were stable for velocities smaller than approximately 1.1 m/s; free stream velocities larger than this would cause movements of the stones which were unacceptable for the experiment. To ensure stability for the stones a free stream velocity of approximately 1.0 m/s was used for the experiments (1.0 m/s for one layer of stones, 0.95 m/s for two layers of stones and 0.96 m/s for three layers of stones).

The wave period was governed by the natural frequency of the oscillation in the tunnel, as a wave period very different from the natural period of the tunnel would "contaminate" the velocity signal. The natural period of the flume was measured to be between 9.73 s and 10.02 s for no stones and 3 layers of stones, respectively. As the difference between the natural periods is small, the wave period was kept constant at $T = 9.73$ s for all the experiments.

6.4 Results

The velocities are phase and "pore" averaged; first the velocities are averaged over $N_w = 40$ wave periods:

$$\tilde{u}(y,\omega t) = \frac{1}{N_w}\sum_{n=1}^{N_w} u\left(y,\omega\left(t+(n-1)\,T\right)\right) \tag{6.1}$$

where u is the measured horizontal, streamwise velocity in position P (see Fig. 6.2) and elevation y (fixed), ω is the angular frequency of the oscillatory flow and t is the time. Then they are averaged over the $N_p = 20$ measured pores:

$$U(y,\omega t) = \frac{1}{N_p}\sum_{m=1}^{N_p} \tilde{u}(m,y,\omega t) \tag{6.2}$$

$\omega t = 0°$ is defined as the zero-up-crossing in the streamwise velocity in the field above the stones. The phase- and pore-averaged horizontal velocities for three layers of stones are shown in Fig. 6.3. The velocities are almost constant, for the particular phases, up to 6 to 7 cm above the base bottom then they increase towards the top of the stone cover. The region between y =6-7 cm and the top of the stones is influenced by the outer flow. The constant velocity layer is independent of the boundary, regardless of the number of stone layers. There will of course be a thin boundary layer at the base bottom.

There is a slight difference in the magnitude of the positive and the negative horizontal velocities. This is caused by the steady streaming induced by the convergent/divergent flow at the inlets from the risers, see Sumer *et al.* (1993b). This is also influencing the vertical velocities.

Due to the rectangular shape of the cross section of the tunnel, a secondary flow will appear in the cross section causing an upward-directed flow adjacent to the side wall. These secondary flows are directly linked to the streamwise flow; the larger the streamwise flow, the larger the secondary flows. As seen in Fig. 6.4 there is a general upward directed flow in the pores. However, this is larger for the phases from $\omega t = 0°$ to $\omega t = 90°$ than for the phases of $\omega t = 180°$ to $\omega t = 250°$. The reason is that the streamwise velocity is larger for the phases from $\omega t = 0°$ to $\omega t = 90°$ than from $\omega t = 180°$ to $\omega t = 250°$, as seen in Fig. 6.3.

The phase- and pore-averaged horizontal velocities for two layers of stones are shown in Fig. 6.5. As in the case of three layers of stones, the boundary layer flow over the stone cover in the outer flow penetrates into the stone cover over a depth of 4 cm below which the velocity remains constant, the constant velocity layer.

The phase- and pore-averaged horizontal velocities for one layer of stones are shown in Fig. 6.6. As in the cases of three and two layers of stones the outer boundary layer penetrates into the stone layer. In this case down to 1

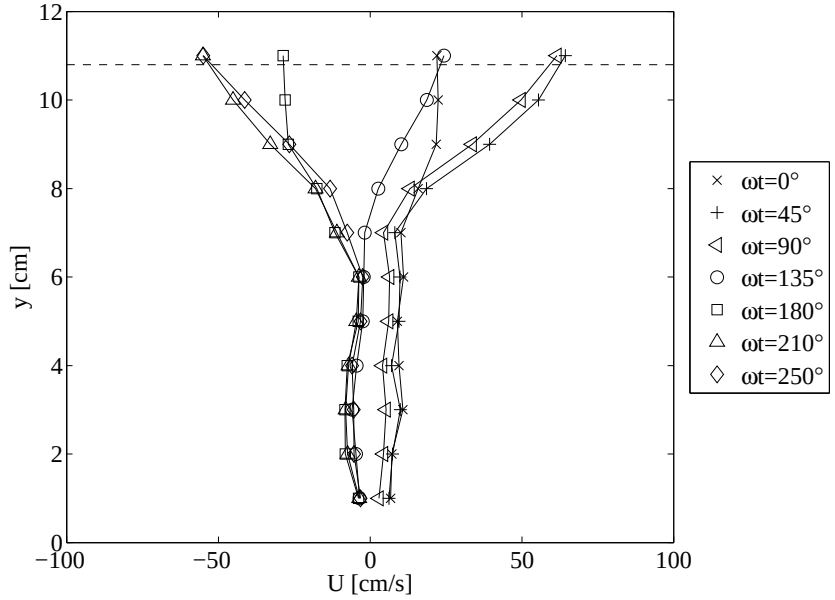

Figure 6.3: *The velocity profiles of horizontal phase- and pore-averaged velocities. Three layers of stones. Dashed line: The average height of the stones.*

cm above the base bottom. This shows that the constant velocity layer has become rather thin and it is expected, in the analogy with the two and three layer cases.

As seen from Figs. 6.3, 6.5 and 6.6, the horizontal velocities are significantly larger in the case of three layers of stones than in the case of one and two layers of stones. The level of turbulence is not influenced by this effect.

The phase- and pore-averaged horizontal turbulent velocities for three layers of stones are shown in Fig. 6.7. The turbulent velocity is defined as:

$$U_s(y,\omega t) = \frac{\sum_{i=0}^{N_P} \sqrt{[u'(i,y,\omega t)]^2}}{N_P} \tag{6.3}$$

where N_P is the number of pores, u' is the measured oscillatory component of the horizontal velocity and y is the vertical position. The turbulent velocities are very large over the entire stone cover. At the top of the stone cover they are between 7 and 12 cm/s decreasing to 2.5 to 4 cm/s 1 cm above the base bottom. The turbulent velocities are almost constant in the constant velocity layer.

The phase-average of the bed shear stresses under three layers of stones are shown in Fig. 6.8. The bed shear stresses were measured in three different

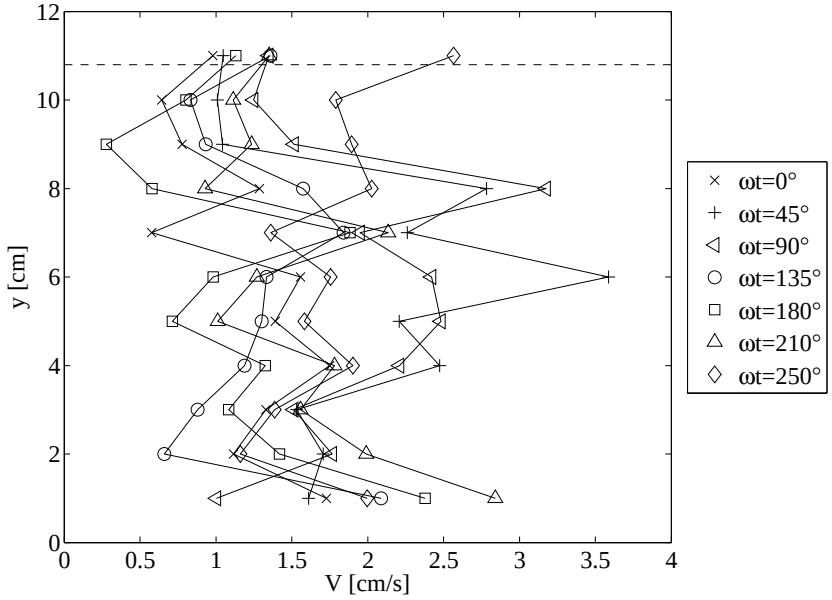

Figure 6.4: *The velocity profiles of vertical phase- pore-averaged mean velocities. Three layers of stones. Dashed line: The average height of the stone.*

layouts of the stones. The bed shear stresses measured in pore 1 and 2 were measured in the middle of the horizontal projection of a pore. In the case of pore 3 there was an offset in the streamwise direction. As seen in the figure the bed shear stress in pore 3 has a peak between 250° and 310° there is around 4 to 5 times higher than the bed shear stress measured in the two other pores. The reason for this can be the offset of the measuring position or the actual layout of the stones around the measuring point.

The bed shear stress is varying between 0.06 and 0.97 $\mathrm{cm}^2/\mathrm{s}^2$. This is a very low bed shear stress. For example Jensen *et al.* (1989) reported bed shear stresses up to around 10 $\mathrm{cm}^2/\mathrm{s}^2$ for an undisturbed oscillatory flow over a smooth bed with $U_{m0} = 0.45$ m/s. However, if the critical Shields number is reached for sediment under the stone protection a high rate of bed load is expected, due to the high level of turbulence. Sands with grain size of 0.05 to 0.1 mm will be unstable under the measured bed shear stress, assuming a critical Shields parameter of 0.03 and $s = 2.65$. Fig. 14 in Sumer *et al.* (2003) gives the dimensionless bed load discharge as function of the Shields parameter for different levels of turbulence near the bottom. The dimensionless bed load discharge in Sumer *et al.* (2003) is defined as:

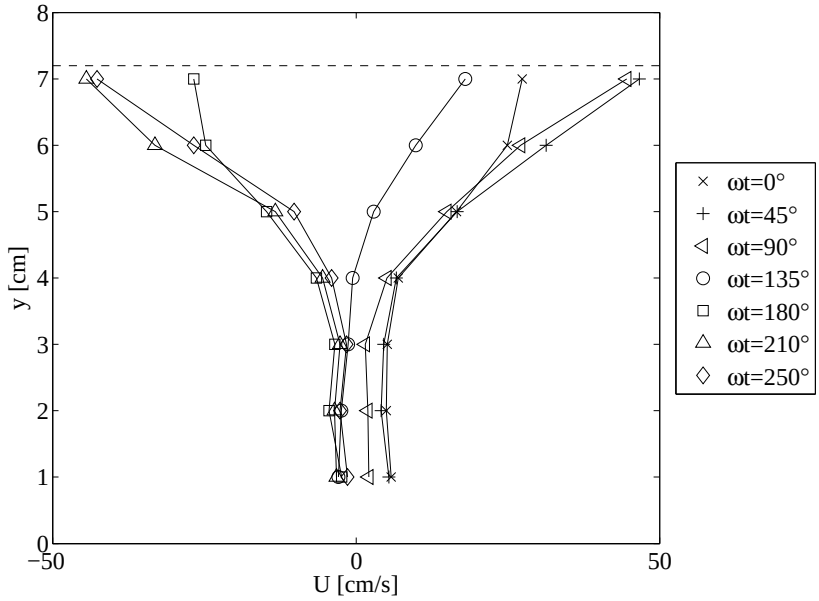

Figure 6.5: *The velocity profiles of horizontal phase- and pore-averaged mean velocities. Two layers of stones. Dashed line: The average height of the stones.*

$$\Phi_b = \frac{q}{\sqrt{g(s-1)d_{50}^3}} \tag{6.4}$$

where q is the discharge, g is the acceleration due to gravity, s is the specific gravity of the sediment and d_{50} is the mean size of the sediment. The dimensionless level of turbulence near the bottom is in the same publication defined as:

$$\left(\frac{\overline{u'^2}}{U_{fb}}\right)_0 \tag{6.5}$$

where U_{fb} is the friction velocity at the bottom, $U_{fb} = \sqrt{\tau_0/\rho}$.

A representative dimensionless peak level of turbulence will then be around 6 ($\omega t = 45°$, $U_s = 4$ cm/s and $\tau/\rho = 0.5$ cm^2/s^2), see Fig. 6.7 and Fig. 6.8. The highest values of the dimensionless turbulence level given in Sumer *et al.* (2003) are 2.5 to 2.75. Using this and assuming that the Shields parameter reach 0.06 will give a dimensionless bed load of around 0.03. This is a really high value for so small Shields numbers. A typical dimensionless turbulence level over a ripple covered bed in current without any

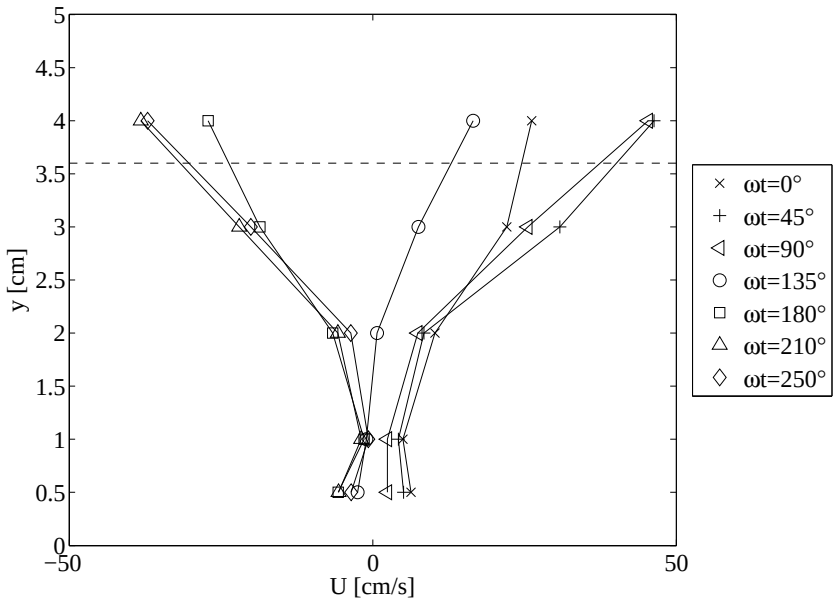

Figure 6.6: *The velocity profiles of horizontal phase- and pore-averaged mean velocities. One layer of stones. Dashed line: The average height of the stones.*

externally generated turbulence will be 1.7 and that will give a dimensionless bed load discharge around ten times smaller.

The zero-down-crossing phase for the three setups is shown in Fig. 6.9. There is a large change in the zero-crossing phase from the top of the stones to the base bottom of around 45°. This is expected as the flow velocities in the stone layer is relatively small compared to the free flow velocity and the flow resistance in the stones is large. This means that the momentum of the flow in the stone layer will be "dissipated" faster than the momentum in the free flow when the pressure gradient reverses.

6.5 Conclusion

The velocities and turbulence have been measured in the pores of a stone cover under an oscillatory flow. Cases with one, two and three layers of 4 cm large stones have been tested. In the case of three layers of stones the bed shear stress at the base bottom was also measured. It is found that the boundary layer of the outer flow penetrates into the stone cover over a depth of 4 cm. Below this level the velocity remains constant, the constant velocity

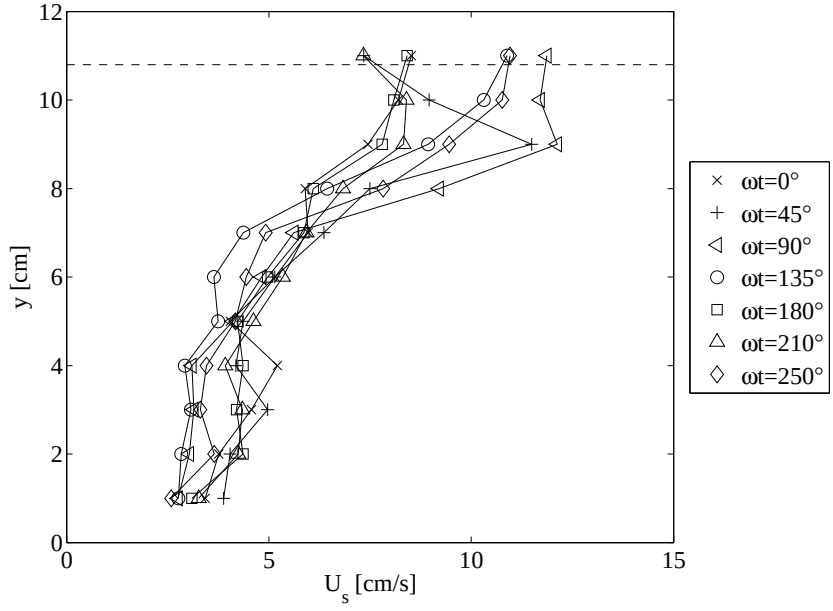

Figure 6.7: *The horizontal phase- and pore-averaged turbulent velocities for different phase values. Three layers of stones.*

layer. The level of turbulence in between the stones is found to be very high: 3 to 4 times higher than turbulence level over a ripple covered bed in steady current boundary layer without any externally generated turbulence. The bed shear stress is found to be very low, more than ten times smaller than in the case of a smooth base bottom without stone cover.

Acknowledgement

This research was carried out as part of the Statkraft Ocean Energy Research Program, sponsored by Statkraft (www.statkraft.no). The study was partially supported by the Danish Council for Strategic Research (DSF)/Energy and Environment under the program Seabed Wind Farm Interaction (http://sbwi.dhigroup.com, sagsnr. 2104-07-0010) and DHI (www.dhigroup.com). During his two years Master course, F. Stevanato was sponsored by "Universita' degli Studi di Padova" and the TIME network of Engineering Schools.

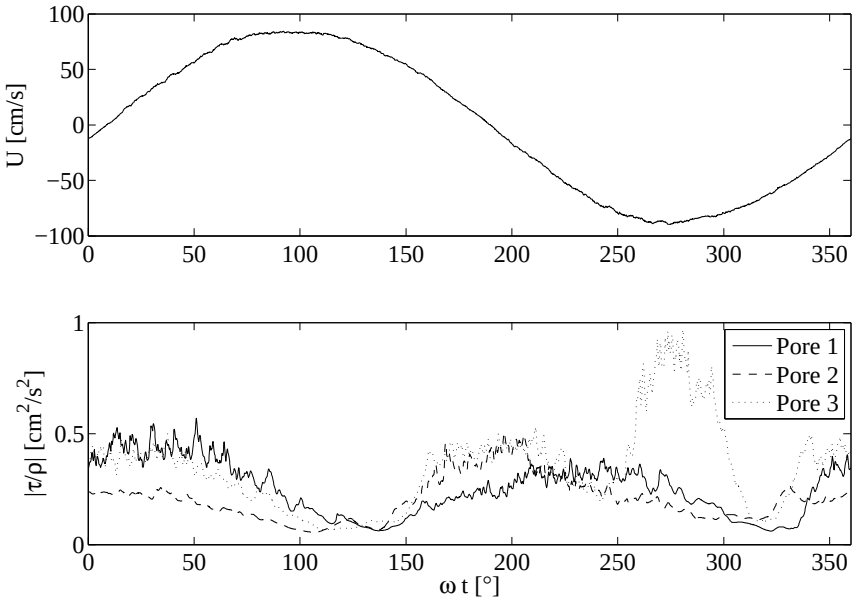

Figure 6.8: *Phase-average of the horizontal free stream velocity and the bed shear stress measured under three layers of stones. Bed shear stresses in three different pores are presented.*

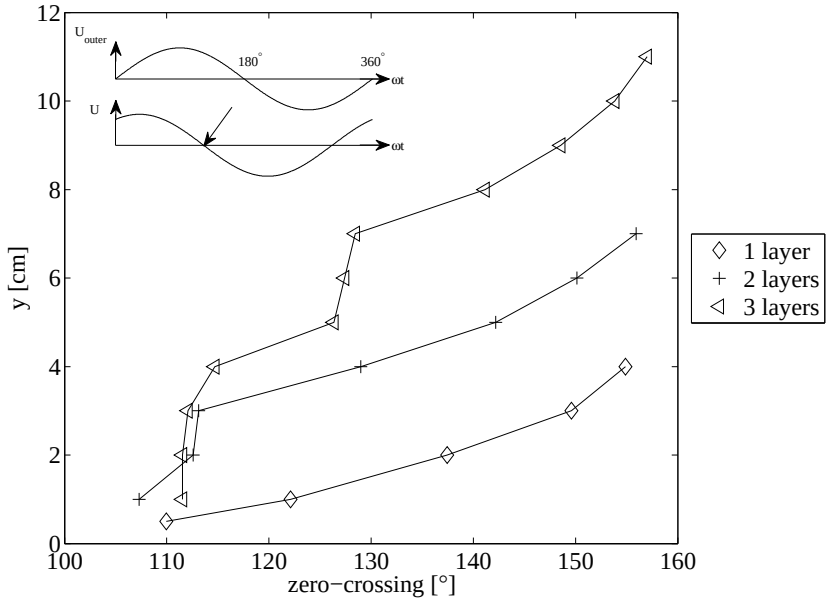

Figure 6.9: *Profiles for zero-down-crossing phase for one, two and three layers of stones.*

Chapter 7

Sinking of Armour Layer around a Cylinder exposed to Waves

7.1 Introduction

This thesis is related to offshore wind turbines which are exposed to both waves and current. The previous chapters describe the effect of current on the sinking of the scour protection around a pile (Chapters 2 and 3); The scour generated by breaking waves around an unprotected pile (Chapter 4); and the effects of breaking and non-breaking waves on scour protections without a structure (Chapters 5 and 6).

Dixen *et al.* (2008) reported the critical conditions for onset of suction from between armour stones under waves, but without a structure. They also reported the equilibrium sinking when critical conditions were exceeded, but as no structure was present in the experiments they did, the results cannot be applied directly in the present case. De Vos (2008) tested the stability of scour protections around mono piles in waves, but focused on the stability of the stones in the scour protection and most of the experiments were made with a geotextile between the scour protection and the sediment bed to prevent interaction. Some tests were conducted without the geotextile and showed no sinking, this was probably because of the small difference in size of the filter stones and the sediment in the bed.

In order to obtain basic knowledge about the magnitude of the sinking of scour protections around mono piles in non-breaking waves, physical model tests have been carried out in an attempt to obtain knowledge about the effect of waves on the sinking of scour protections around offshore wind turbine foundations.

This study addresses the live-bed situation where the flow is strong enough to penetrate the entire thickness of the scour protection and generate bed shear stresses at the base bottom high enough to cause sediment transport.

7.2 Experimental Setup

The experiments were conducted in two different flumes (1) a 28 m long (excluding in- and outlet sections), 4 m wide and 1 m deep flume and (2) a 28 m long (excluding in- and outlet sections), 0.6 m wide and 0.8 m deep flume.

In flume 1, a 0.35 m thick and 10 m long sand section was placed across the entire width of the flume, beginning approximately 9.5 m from the wave paddle. Offshore of the sand section a 3 m long slope was constructed. The slope (1:8.6) was made of a core of concrete blocks covered by at least one layer of stones ($d_{50} = 4.3$ cm). Two different piles were tested: $D_p = 11.0$ cm and 20.0 cm. The piles were sealed at the bottom. The tests were undertaken with the two piles present in order to save time. They were placed 4 m from the offshore edge of the sand section, and the distance between the piles was 1.75 m, which was large enough to ensure no interference (see also Chapter 2 and 3).

In flume 2, a 6 m long and 20 cm deep sand section was installed with the offshore edge 13.2 m from the wavemaker. 3 m long slopes (1:15) were installed on- and offshore of the sand section. The slopes were made of stones ($d_{50} = 4.3$ cm). The 4 cm pile was placed in the middle of the sand section.

The sinking of the stones was determined in the same way as in Chapters 2 and 3 by measuring the vertical displacement of the stones adjacent to the pile. To avoid disturbances due to the irregularities of the stones the sinking was measured with reference to the same point marked on the stone. In case of large rotations or if the stone was eventually covered by a thick layer of sand the measured sinking of that stone was disregarded. In the case where a disregarded stone was likely to be the stone with maximum sinking the entire test was abandoned. Based on the results of the tests it was found that the maximum sinking always occurred for the stones on the sides of the pile. Four or eight stones were used for measuring the sinking. The stones were placed adjacent to the pile evenly distributed around the pile.

Along with the sinking of the stone adjacent to the pile, the scouring and deposition of sand in the area around the pile was measured using measuring pins (3 mm in diameter) with scales in the form of coloured strips. The pins were placed in and around the scour protection.

The velocities were measured $D_p/2$ above the initial sediment bed at

the test section, using Laser Doppler Anometry (LDA). The relatively large distance from the initial bed was used to avoid disturbance by ripples and suspended sediment. Measurements have shown that the velocity profile was approximately constant up to at least $D_p/2$ and the measured velocities can be taken as the maximum orbital velocity at the bed.

7.3 Test Conditions

The varied test conditions are shown in Table 7.1. One sand size was used for the experiments, $d_{50} = 0.18$ mm. The overall extension of the scour protections, w_c, was 4.5 to 5.0 times the diameter of the piles. The experiments were carried out using irregular wave (JONSWAP-spectrum) to avoid bed undulations. In Table 7.1 D_p is the diameter of the pile, D_c is the mean size of the cover stones, N_c is the number of layers of stones, e_{max} is the maximum equilibrium sinking of the stones adjacent to the pile, H_s is the significant wave height at the measuring section, T_p is the peak wave period, U_m is the velocity amplitude at the measuring section calculated from $U_m = \sqrt{2}\sigma_U$ as defined in Sumer and Fredsøe (2001b) in which σ_U is the Root-Mean-Square (RMS) of U where U is the orbital velocity at the bed, L_p is the wave length at the measuring section, calculated using linear wave theory based on the peak period and h is the water depth again at the measuring section. It may be noted that U_m becomes identical to the maximum value of the orbital velocity at the bed for sinusoidal waves.

Table 7.1: *Test conditions and results.*

Test No.	D_p [cm]	D_c [cm]	N_c	e_{max} [cm]	H_s [cm]	T_p [s]	U_m [cm/s]	L_p [m]	h [cm]
1	4.0	1.9	1	0.4	7.1	4	15.0	7.8	40.0
2	4.0	1.9	1	0.2	9.4	2.5	16.8	4.7	40.0
3	11.0	4.3	1	1.1	13	1.5	20.6	2.3	30.0
4	20.0	4.3	1	1.7	13	1.5	19.8	2.3	30.0
5	11.0	1.9	1	1.7	13	1.5	20.6	2.3	30.0
6	20.0	1.9	1	1.7	13	1.5	19.8	2.3	30.0
7	11.0	4.3	1	1	8.3	5.0	16.9	8.5	30.0
8	20.0	4.3	1	1.1	8.3	5.0	17.1	8.5	30.0
9	11.0	1.9	1	1.5	8.3	5.0	16.9	8.5	30.0
10	20.0	1.9	1	0.7	8.3	5.0	17.1	8.5	30.0
11	11.0	1.9	2	0.6	8.3	5.0	16.9	8.5	30.0
12	20.0	10.3	1	4.1	8.3	5.0	17.1	8.5	30.0

7.4 Results

Fig. 7.1 shows the maximum sinking of the scour protection around a pile relative to the pile diameter versus the Keulegan-Carpenter number ($KC = U_m T_p/D_p$) for the tests, excluding test 12. The flow in the scour protection in test 12 was different from the flow in the other tests with the same KC-number as will be shown later.

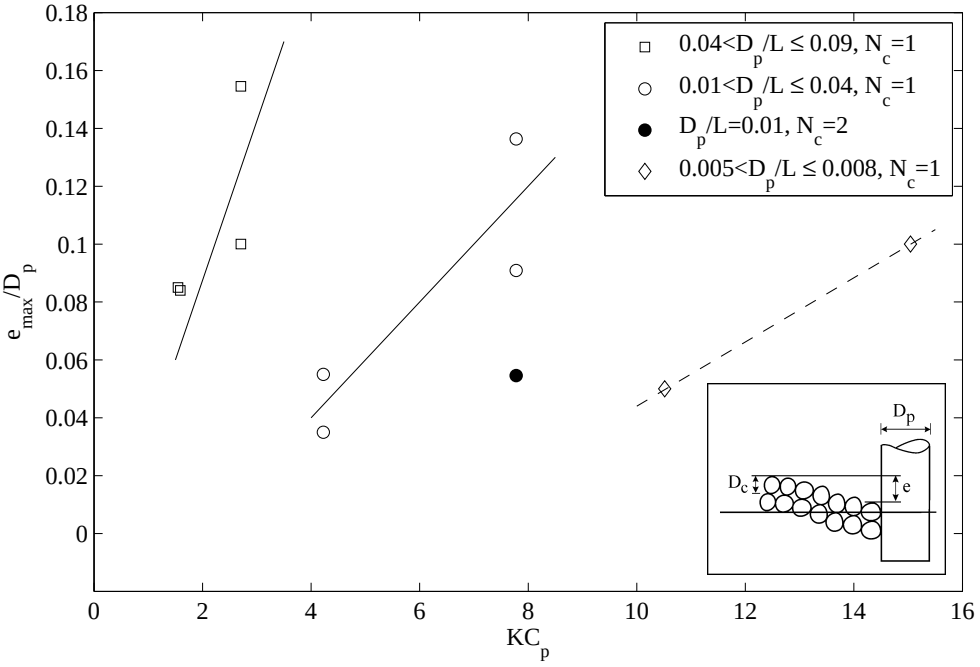

Figure 7.1: *Sinking of the stones adjacent to the pile when exposed to waves.*

As seen in Fig. 7.1 there is a trend that for a given interval of the diffraction coefficient D_p/L_p the relative sinking increases for increasing KC-number. For the tested range, $D_p/D_c = 2.1$ to 10.5 (excluding test 12) there is no significant influence of the stone size.

The magnitude of the relative sinking, e_{max}/D_p, for a given KC-number is comparable with the scour around unprotected piles reported by Sumer and Fredsøe (2001a) and around 5 to 10 times larger than the sinking reported by Dixen *et al.* (2008) for a stone cover under waves without a structure. It may be noted, however, for the very low KC-numbers a few tests even showed a two to three times larger sinking than the reported scour for unprotected piles. The sinking of the scour protection was for all the tested

cases much smaller than the sinking scour protection in current, see Chapter 2.

Physical experiments with sinking of scour protection around piles exposed to current (Chapters 2 and 3) have shown that the main mechanism of the sinking of the scour protection stones is the same that causes the scour around an unprotected pile namely the horseshoe vortex, while the vortices shedding, that also generates scour around an unprotected pile, is unable to mobilize the sediment underneath the scour protection to any significant degree. This will also be the case for scour protections around a pile in waves.

In the case of scour around an unprotected pile in waves there are four mechanisms causing the scour: Contraction of streamlines, horseshoe vortex, vortex shedding and steady streaming. Contraction of streamlines is important for most cases, but it is increasingly important for increasing pile size. Horseshoe vortex and vortex shedding are dominating for slender piles ($KC > 6$), while steady streaming is dominating in case of large piles ($KC < 2$ and D_p/L_p is larger than approximately 0.2), as the horseshoe vortex does not develop for KC-numbers smaller than 6, see Sumer *et al.* (1997) and it will not reach a significant size for $KC \lessapprox 20$, due to the relatively thin boundary layer at the bottom for smaller KC-numbers, see Sumer and Fredsøe (2001a). The mechanisms of scour around piles in waves are described in detail in e.g. Sumer and Fredsøe (2002).

Detailed studies of the mechanisms causing the sinking of the scour protection in waves has not been made, but based on the pattern of the sinking it is likely that a reverse flow taking place in the scour protection is an important mechanism in the sinking for KC-numbers larger than approximately 7. Figs. 7.2 to 7.4 show the scour protection offshore the pile at the equilibrium state of the sinking in case of KC-numbers 4.3, 7.7 and steady current ($KC \to \infty$). It is seen that in the case of small KC-numbers ($KC = 4.3$) there is deposition of sediment adjacent to the offshore side of the pile (Fig. 7.2), while in case of larger KC-numbers ($KC = 7.7$) there is no deposition and even sinking adjacent to the offshore side of the pile (Fig. 7.3). In this test the sediment bed was lowered as much as approximately 3 cm adjacent to the offshore side of the pile, this is twice the maximum sinking of the stones and 2 to 3 times the scour around an unprotected pile (Sumer and Fredsøe, 2001a). If Fig. 7.3 is compared with the current case (Fig. 7.4) it is seen that the cases are similar; sinking of the scour protection adjacent to the sides and offshore the pile and deposition in the scour protection further away from the pile, although the sinking in the wave case is smaller than in the current case. This indicates that a reverse flow has caused the sinking in the wave case in a similar way as the horseshoe vortex in the current case,

Figure 7.2: *The equilibrium state of test 10. The pile was 20.0 cm in diameter and the scour protection was one layer of 1.9 cm crushed stones. The KC-number was 4.3.*

For a reverse flow to take place the pressure gradient driving reverse flow must be strong enough to overcome the kinetic energy of the approach flow and the viscous forces. For the steady current case and for high KC-numbers this is possible because of the bottom boundary layer: The flow velocity and thereby the kinetic energy of the flow near the bed is low. This is not the case for small KC-numbers, where the boundary layer is very thin, but as seen in Chapter 6 the velocities of the water inside a stone cover under waves are very low. This means that it can easily be agitated by for example the adverse pressure gradient present when the wave crest passes the pile. This pressure gradient will drive the reverse flow through the stone cover, as the adverse pressure gradient drives the horseshoe vortex in the case of a steady current.

Fig. 7.5 shows the offshore side of the scour protection at the equilibrium of test 12. As seen the deposition of sediment adjacent to the offshore side of the pile is much smaller than in the, except for the cover stone size, equal

Figure 7.3: *The equilibrium state of test 9. The pile was 11.0 cm in diameter and the scour protection was one layer of 1.9 cm crushed stones. The KC-number was 7.7.*

Test 10 (Fig. 7.2). This indicates that the flow in the scour protection was different from the flow in tests 8 and 10 although the KC-number for the pile was the same. For example the ripples in the scour protection are highly disturbed in Fig. 7.5 while they are much less disturbed in Fig. 7.2. The changed flow may explain why the sinking in test 12 was extraordinarily large compared to the other results with the same KC-number.

7.5 Conclusion

Experiments with sinking of scour protection around a pile in waves have been carried out. The results have shown that the magnitude of the sinking of the scour protection ($e_{max}/D_p = 0.03$ to 0.21) is comparable to the scour expected for an unprotected pile in waves. The tested range of KC-numbers was KC_p 1.5 to 15. The relatively large sinking is caused by a reversed flow generated in the almost stagnant water in the pores of the stone cover. The sinking of the scour protection in the present wave cases has been found to

Figure 7.4: *The equilibrium state in case of steady current ($KC \rightarrow \infty$). The pile was 20.0 cm in diameter and the scour protection was one layer of 1.9 cm crushed stones.*

be much smaller than the sinking expected in the case of current.

Figure 7.5: *The equilibrium state of test 12. The pile was 20.0 cm in diameter and the scour protection was one layer of 10.3 cm round stones. The KC-number was 4.3.*

Bibliography

Abad, J. D., Rhoads, B. L., Güneralp, I., and García, M. H. (2008). Flow structure at different stages in a meander-bend with bendway weirs. *Journal of Hydraulic Engineering*, **134**(8), 1052–1063.

Baker, C. J. (1979). Laminar horseshoe vortex. *Journal of Fluid Mechanics*, **95**, 347–367.

Baker, C. J. (1985). The position of points of maximum and minimum shear stress upstream of cylinders mounted normal to flat plates. *Journal of Wind Engineering and Industrial Aerodynamics*, **18**(3), 263–274.

Bijker, E. and de Bruyn, C. (1988). Erosion around a pile due to current and breaking waves. 1368–1381, Reston, Viginia, USA. ASCE.

Breusers, H. N. C. and Raudkivi, A. J. (1991). *Scouring*. Balkema, Rotterdam. Hydraulic structures design manual : 2.

Burcharth, H. and Andersen, O. (1995). On the one-dimensional steady and unsteady porous flow equations. *Coastal Engineering*, **24**(3-4), 233–257.

Carreiras, J., Seabra-Santos, F., Larroudé, P., and Mory, M. (2000). Wave scour around piles. volume 276, 1860–1870, Reston, Viginia, USA. ASCE.

Chiew, Y. and Lim, F. (2000). Failure behavior of riprap layer at bridge piers under live-bed conditions. *Journal of Hydraulic Engineering*, **126**(1), 43–55.

Chiew, Y.-M. (1995). Mechanics of riprap failure at bridge piers. *Journal of Hydraulic Engineering*, **121**(9), 635–643.

Chiew, Y. M. (2002). Failure mechanism of riprap layer around bridge piers. In *Proceedings of the First International Conference on Scour of Foundations*, volume I, 70–92.

Cox, D. T. and Kobayashi, N. (2000). Identification of intense, intermittent coherent motions under shoaling and breaking waves (paper

2000jc900048). *Journal of Geophysical Research - Part C - Oceans*, **105**(6), 14223.

Dalton, C. (1982). A review of the fluid mechanics of ocean scour. *Ocean Engineering*, **9**(2), 159–170.

Dargahi, B. (1989). The turbulent flow field around a circular cylinder. *Experiments in Fluids*, **8**(1-2), 1–12.

De Vos, L. (2008). *Optimisation of scour protection design for monopiles and quantification of wave run-up - Engineering the influence of an offshore wind turbine on local conditions*. Ph.D. thesis, Dept. of Civil Engineering, University of Ghent.

De Vos, L., Frigaard, P., and De Rouck, J. (2007). Wave run-up on cylindrical and cone shaped foundations for offshore wind turbines. *Coastal Engineering*, **54**(1), 17–29.

Deigaard, R., Mikkelsen, M. B., and Fredsøe, J. (1991). Measurements of the bed shear stress in a surf zone. In *Progress Report 73*, 21–30. Institute for Hydrodynamics and Hydraulic Engineering, Technical University of Denmark, 2700 Kgs. Lyngby, Denmark.

Dixen, F. H., Sumer, B. M., and Fredsøe, J. (2008). Suction removal of sediment from between armour blocks. part 2. waves. *Journal of Hydraulic Engineering, ASCE*, **134**(10), 1405–1420.

Elselskabernes og Energistyrelsens Arbejdsgruppe for Havmøller (1997). Havmølle-handlingsplan for de danske farvande. Printed at SEAS, Slagterivej 25, 4690 Haslev, Denmark. In Danish.

Engelund, F. A. (1953). On the laminar and turbulent flows of ground water through homogeneous sand. Technical Report 3, Danish Academy of Technical Sciences.

Ferguson, R. I., Parsons, D. R., Lane, S. N., and Hardy, R. J. (2003). Flow in meander bends with recirculation at the inner bank. *Water Resources Research*, **39**(11), ESG21–ESG213.

Flow3D User Manual (2011). *Flow3D User Manual, v9.4.2*. Flow Science, Inc., Santa Fe, N.M.

Fredsøe, J. and Deigaard, R. (1992). *Mechanics of coastal sediment transport*, volume 3 of *Advanced series on ocean engineering*. World Scientific, London.

Fredsøe, J. and Sumer, B. (1997). Scour at the round head of a rubble-mound breakwater. *Coastal Engineering*, **29**(3-4), 231–262.

Graf, W. H. and Yulistiyanto, B. (1998). Experiments on flow around a cylinder; the velocity and vorticity fields. *Journal of Hydraulic Research/De Recherches Hydrauliques*, **36**(4), 637–653.

Grass (1971). Structural features of turbulent flow over smooth and rough boundaries. *Journal of Fluid Mechanics*, **50**, 233–255.

Hansen, E. A., Simonsen, H. J., Nielsen, A. W., Pedersen, J., and Høgedal, M. (2007). Scour protection around offshore wind turbine foundations, full-scale measurements. In *Scientific Proceedings of the European Wind Energy Conference 2007 (EWEC 2007)*, 132–138. http://www.ewec2007proceedings.info/index.php.

Harris, J. M., Whitehouse, R. J. S., and Benson, T. (2010). The time evolution of scour around offshore structures. *Proceedings of the Institution of Civil Engineers: Maritime Engineering*, **163**(1), 3–17.

Hirt, C. W. and Nichols, B. D. (1981). Volume of fluid (vof) method for the dynamics of free boundaries. *Journal of Computational Physics*, **39**(1), 201–225.

Hoffmanns, G. J. C. M. and Verheij, H. J. (1997). *Scour manual*. Balkema, Rotterdam.

Horns Rev Webpage (2011). Horns rev offshore wind farm, west of blåvandshuk. http://www.hornsrev.dk/Engelsk/default_ie.htm (30^{th} of July 2011).

Hughes, S. A. and Kamphius, J. W. (1996). Scour at coastal inlet structures. In *Proceedings of* 25^{th} *international conference on coastal engineering*, volume 2, 2258–2271, Reston, Viginia, USA. ASCE.

Hughes, S. A. and Schwichtenberg, B. R. (1998). Current-induced scour along a breakwater at ventura harbor, ca-experimental study. *Coastal Engineering*, **34**(1-2), 1–22.

Jensen, B. L., Sumer, B. M., and Fredsøe, J. (1989). Turbulent oscillatory boundary layers at high reynolds numbers. *Journal of Fluid Mechanics*, **206**, 265–297.

Kocaman, S., Seckin, G., and Erduran, K. S. (2010). 3d model for prediction of flow profiles around bridges. *Journal of Hydraulic Research*, **48**(4), 521–525.

Lai, J.-W., Hsu, T.-W., and Lan, Y.-J. (2010). Experimental and numerical studies on waves propagation over coarse grained sloping beach. In *Proceedings of the International Conference on Coastal Engineering 2010*, 1–15. http://journals.tdl.org/ICCE/index (20^{th} of July 2011).

Lane, S. N., Bradbrook, K. F., Richards, K. S., Biron, P. A., and Roy, A. G. (1999). The application of computational fluid dynamics to natural river channels: three-dimensional versus two-dimensional approaches. *Geomorphology*, **29**(1-2), 1–20.

Lauchlan, C. S. and Melville, B. W. (2001). Riprap protection at bridge piers. *Journal of Hydraulic Engineering*, **127**(5), 412–418.

Liu, X. and García, M. (2008). A 3d numerical model with free water surface and mesh deformation for local sediment scour. *Journal of Waterway, Port, Coastal, and Ocean Engineering*, **134**(4), 203–217.

Mase, H., Kosho, K., and Nagahashi, S. (2001). Wave runup of random waves on a small circular pier on sloping seabed. *Journal of Waterway, Port, Coastal and Ocean Engineering*, **127**(4), 192–199.

Melville, B., Parola, A. C., and Coleman, S. E. (2008). Bridge-scour prevention and contermeasures. In M. H. Garcia, editor, *Sedimentation Engineering - Processes, Measurements, Modelling, and Practice*. ASCE Manuals and reports on Engineering. No. 110.

Melville, B. W. and Coleman, S. E. (2000). *Bridge Scour*. Water Resources Publications, Highlands Ranch, Colerado, USA.

Ming, D. and Chiew, Y.-M. (2000). Shoreline changes behind detached breakwater. *Journal of Waterway, Port, Coastal and Ocean Engineering*, **126**(2), 63–70.

Morang, A. (2003). *Coastal engineering manual*. U.S. Army Corps of Engineers, Washington, DC.

Myrhaug, D. and Holmedal, L. E. (2010). Wave run-up on slender circular cylindrical foundations for offshore wind turbines in nonlinear random waves. *Coastal Engineering*, **57**(6), 567–574.

Nadaoka, K., Ueno, S., and Igarashi, T. (1988). Sediment suspension due to large scale eddies in the surf zone. *Twenty-First Coastal Engineering Conference*, 1646–1660.

Nadaoka, K., Hino, M., and Koyano, Y. (1989). Structure of the turbulent flow field under breaking waves in the surf zone. *Journal of Fluid Mechanics*, **204**, 359–387.

Nezu, I. and Nakagawa, H. (1993). *Turbulence in open-channel flows*. Balkema, Rotterdam. IAHR monograph series.

Nielsen, A. W. (2004). *Removal of Sediment from Between Armour Blocks in Breaking/Broken Waves*. Master's thesis, Dept. of Mechanical Engineering - Coastal and River Engineering, Technical University of Denmark.

Nielsen, A. W. (2007). Afsluttende rapport for erosionsbeskyttelse omkring havvindmøller. Technical report, DHI. Partly in Danish.

Nielsen, A. W. and Hansen, E. A. (2007). Time-varying wave and current-induced scour around offshore wind turbines. *Proceedings of the International Conference on Offshore Mechanics and Arctic Engineering - OMAE*, **5**, 399–408.

Nielsen, A. W. and Jacobsen, V. (2007). Wave run-up on a wind turbine foundation. In *Proceedings of the European Offshore Wind Conference 2007 (EOW 2007), Berlin, Germany*, PO.85 1 – PO.85 9.

Nielsen, A. W., Sumer, B. M., Fredsøe, J., and Christensen, E. D. (2010). Scour protection around offshore wind turbines. monopiles. In *Proceedings of the Fifth International Conference on Scour and Erosion 2010*, volume 1, 440–449.

Nielsen, A. W., Sumer, B. M., Fredsøe, J., and Christensen, E. D. (2011). Sinking of armour layer around a cylinder exposed to a current. *Proceedings of the Institution of Civil Engineers - Maritime Engineering*, **164**(Ma4), 159–172.

Nielsen, A. W., Sumer, B. M., and Fredsøe, J. (2012). Experiments on removal of sediment from between armor blocks. part 3: Breaking waves. *Journal of Hydraulic Engineering, ASCE*. In print.

Offshore Center Danmark (2011). Offshore wind farms. http://www.offshorecenter.dk/offshorewindfarms.asp (30^{th} of July 2011).

Oumeraci, H. (1994). Multi-disciplinary research experience in europe on vertical breakwaters. In *Proceedings of international workshop on wave barriers in deepwater*, 267–278, Yokosuka, Japan. Port and Harbour Research Institute.

Raaijmakers, T. and Rudolph, D. (2008). Time-dependent scour development under combined current and waves conditions - laboratory experiments with online monitoring technique. In *Proceedings of the Fourth International Conference on Scour and Erosion*, volume I, 152–161.

Raaijmakers, T. C., Rudolph, D., Bergen, M. R. J. v., and Lieshout, H. v. (2007). Offshore windpark egmond aan zee - performance of scour protection and edge scour development. In *Proceedings of the European Offshore Wind Conference 2007 (EOW 2007), Berlin, Germany*, 1–10.

Raudkivi, A. J. and Ettema, R. (1985). Scour at cylindrical bridge piers in armored beds. *Journal of Hydraulic Engineering*, **111**(4), 713–731.

Rodriguez, J. F., Bombardelli, F. A., García, M. H., Frothingham, K. M., Rhoads, B. L., and Abad, J. D. (2004). High-resolution numerical simulation of flow through a highly sinuous river reach. *Water Resources Management*, **18**(3), 177–199.

Rødsand Webpage (2011). Nysted offshore windfarm. http://www.dongenergy.com/Nysted/EN/Pages/index.aspx (30$^{\text{th}}$ of July 2011).

Roulund, A., Sumer, B. M., Fredsøe, J., and Michelsen, J. (2005). Numerical and experimental investigation of flow and scour around a circular pile. *Journal of Fluid Mechanics*, **534**, 351–401.

Sumer, B. and Fredsøe, J. (2001a). Wave scour around a large vertical circular cylinder. *Journal of Waterway, Port, Coastal and Ocean Engineering*, **127**(3), 125–134.

Sumer, B. M. and Fredsøe, J. (2001b). Scour around pile in combined waves and current. *Journal of Hydraulic Engineering*, **127**(5), 403–411.

Sumer, B. M. and Fredsøe, J. (2002). *The mechanics of scour in the marine environment*, volume 17 of *Advanced series on ocean engineering*. World Scientific, London.

Sumer, B. M., Christiansen, N., and Fredsøe, J. (1992). Time scale of scour around a vertical pile. In *Proceedings Second (1992) International Offshore and Polar Engineering Conference*, volume III, 308–315.

Sumer, B. M., Arnskov, M. M., Christiansen, N., and Jørgensen, F. E. (1993a). Two-component hot-film probe for measurements of wall shear stress. *Experiments in Fluids*, **15**(6), 380–384.

Sumer, B. M., Laursen, T. S., and Fredsøe, J. (1993b). Wave boundary layers in a convergent tunnel. *Coastal Engineering*, **20**(3-4), 317–342.

Sumer, B. M., Christiansen, N., and Fredsøe, J. (1997). The horseshoe vortex and vortex shedding around a vertical wall-mounted cylinder exposed to waves. *Journal of Fluid Mechanics*, **332**, 41–70.

Sumer, B. M., Cokgor, S., and Fredsøe, J. (2001). Suction removal of sediment from between armor blocks. *Journal of Hydraulic Engineering*, **127**(4), 293–306.

Sumer, B. M., Chua, L., Cheng, N. S., and Fredsøe, J. (2003). Influence of turbulence on bed load sediment transport. *Journal of Hydraulic Engineering ASCE*, **129**, 585–596.

Sumer, B. M., Fredsøe, J., Lamberti, A., Zanuttigh, B., Dixen, M., Gislason, K., and Di Penta, A. F. (2005). Local scour at roundhead and along the trunk of low crested structures. *Coastal Engineering*, **52**(10-11), 995–1025.

Sumer, B. M., Sen, M. B., Karagali, I., Ceren, B., Fredsøe, J., Sottile, M., Zilioli, L., and Fuhrman, D. R. (2011). Flow and sediment transport induced by a plunging solitary wave. *Journal of Geophysical Research-Oceans*, **116**, 1–15.

Svendsen, I. (2006). *Introduction to nearshore hydrodynamics*, volume 24 of *Advanced series on ocean engineering*. World Scientific, London.

Whitehouse, R. (1998). *Scour at marine structures*. Telford, London.

Whitehouse, R. J., Harris, J. M., Sutherland, J., and Rees, J. (2011). The nature of scour development and scour protection at offshore windfarm foundations. *Marine Pollution Bulletin*, **62**(1), 73–88.

Yakhot, V. and Orszag, S. A. (1986). Renormalization group analysis of turbulence. i. basic theory. *Journal of Scientific Computing*, **1**(1), 3–51.

Yakhot, V. and Smith, L. M. (1992). The renormalization group, the ϵ-expansion and derivation of turbulence models. *Journal of Scientific Computing*, **7**(1), 35–61.

Appendix A

Scour Protection around Offshore Wind Turbines. Monopiles

This chapter has been published in Proceedings of the Fifth International Conference on Scour and Erosion, San Francisco, California, USA, November 2010:
Nielsen, A.W., Sumer, B.M., Fredsøe, J. and Christensen, E.D.: "Scour Protection Around Offshore Wind Turbines. Monopiles", Proceedings of the Fifth International Conference on Scour and Erosion, ASCE, Vol. 1, p. 440-449.

Note: In the published version the vectors in the different velocity profiles in Fig. A.5 was not correctly scaled relative to each other, this is corrected in the present version.

Abstract

The flow processes in a scour protection around a mono-pile in steady current is described in relation to transport of sediment in the scour protection based on physical model tests. Transport of sediment in the scour protection may cause sinking of the scour protection. This may reduce the stability of the mono-pile and change for instance the natural frequency of the dynamic response of an offshore wind turbine in an unfavorable manner. The most important flow process with regard to transport of sediment and sinking of the scour protection is found to be the horseshoe vortex.

It is found that a larger pile diameter relative to the size of the protection stones will cause a larger sinking and that two layers of stones will decrease the sinking relative to one layer of stones with the same size.

A.1 Introduction

During the last decade more and more wind farms have been erected offshore. One of the first larger offshore wind farms is the Horns Rev I. The Horns Rev I is located in relatively shallow water (6.5 to 13 m water (MSL)) about 20 km off the Danish West Coast in the North Sea. This area is exposed to strong tidal currents and large waves from the North Sea. The wind turbines are founded on mono-piles with a scour protection made of a two-layer cover (quarry run from around 350 mm to 550 mm) and a 0.5 m thick filter layer (sea stones from around 30 mm to 200 mm) between the armor layer and the seabed. The wind farm was installed in the summer 2002. A control survey in 2005 showed that the scour protections adjacent to the mono-piles sank up to 1.5 m. This was unexpected and shortly after the survey in 2005 the holes were repaired by adding additional stones.

Scour around unprotected piles have been studied extensively over the last decades. Most of the available results are compiled in Breusers and Raudkivi (1991); Hoffmanns and Verheij (1997); Melville and Coleman (2000) (mostly river application), Whitehouse (1998) and Sumer and Fredsøe (2002) (mostly marine application). Scour protection of piles has not been studied nearly as much and the mechanism of failure of scour protections around a mono-pile has only been described briefly. In order to gain an understanding of the mechanisms that cause the sinking of the scour protection, an extensive program of physical model tests with steady current has been carried out in the present study, in an attempt to contribute to the knowledge obtained recently by Chiew and Lim (2000); Lauchlan and Melville (2001); Chiew (2002); De Vos (2008) among others. The model tests showed that the horseshoe vortex, the key element to cause scour around unprotected piles, see e.g. Dargahi (1989) and Roulund *et al.* (2005), is a key flow feature governing the sinking process.

A.2 Experimental Setup

The tests were conducted in two different current flumes. (1) A 2 m wide, 23 m long (excluding in- and outlet sections) and 0.5 m deep flume; and (2) a 4 m wide, 28 m long (excluding in- and outlet sections) and 1.0 m deep flume. The flumes were equipped with recirculation pumps providing mean current speeds of more than 60 cm/s in the actual setups. Two different setups were used for the tests in the 2 m wide flume: A fixed bottom setup used for flow visualizations and velocity profiles measurements, and a live-bed test setup with a 10 m long and 0.15 m deep sand section, see Fig. A.1. The ramps towards the sand section were made of smooth plywood plates. In the case of the 4 m wide flume only live-bed tests were conducted. The sand section

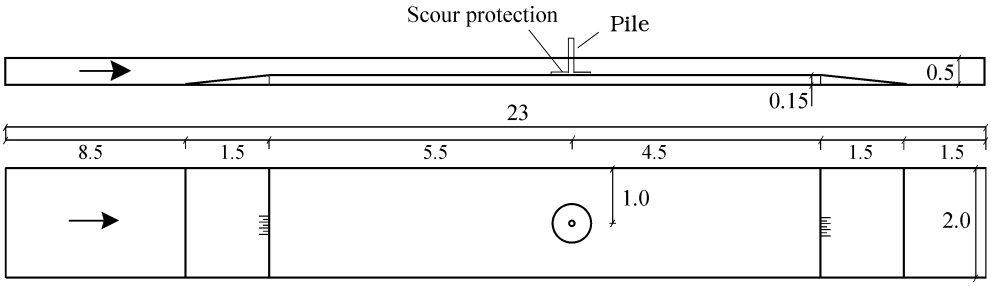

Figure A.1: *Setup for the 2 m wide flume.*

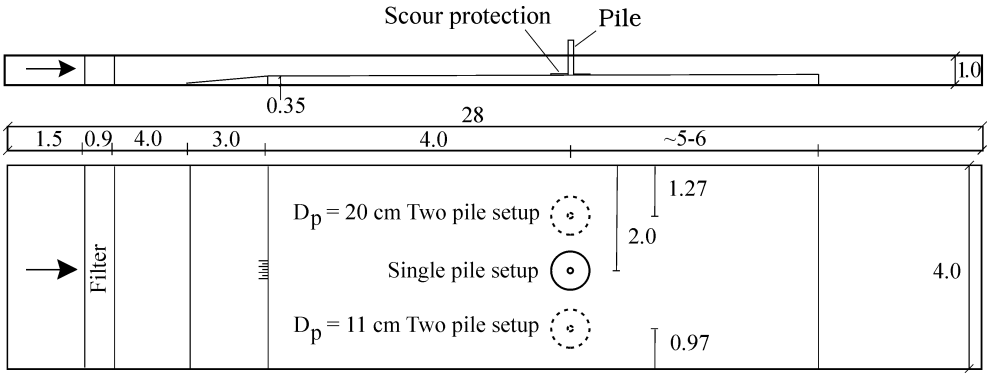

Figure A.2: *Setups for the 4 m wide flume.*

was around 10 m long and 0.35 m deep. The ramp from the actual bottom to the sand section was 3 m long with a core of concrete blocks covered with at least one layer of stones ($d_{50} = 4$ cm), see Fig. A.2. In some of the tests in the 4 m wide flume, two piles were tested at the same time, in order to save time. The piles were placed at the same distance from the inlet and the distance between the piles was 1.75 m, which was large enough to ensure no interference.

In the case of the fixed-bottom experiments an approximately 0.5 cm thick, 2.9 m long, white plastic plate, with 15 cm long tapered upstream edge, was placed on the base bottom over the entire width of the flume enabling a good contrast for the flow visualizations. For the velocity profile measurements (using Laser Doppler Anemometry, LDA) the plate was painted matte black to reduce reflections of the laser beams. The pile was placed 2.0 m downstream of the upstream edge of the plastic plate (approximately 15 m from the inlet section).

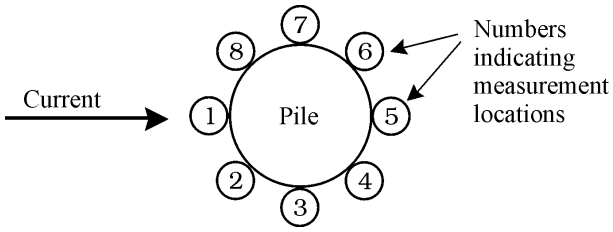

Figure A.3: *Position of the stones used for measuring the sinking of the scour protection.*

In all setups the bottom end of the piles were closed by an end plate to ensure that the bottom of the pile was completely sealed.

The flow velocity was measured in two different ways: A small propeller (3 cm in diameter) was used in the case of the live-bed tests and a submerged pen size LDA probe was used in the case of the fixed-bottom velocity profiles measurements. The pen-size LDA probe was a two component probe, approximately 1 cm in diameter and 15 cm long. It had a focal length of 80 mm (in water), a beam spacing of 8 mm and a beam diameter of 0.27 mm. The probe was placed vertically pointing downwards, when used to measure velocities in between the stones and placed horizontally when used outside the stones.

The sinking of the stones was determined by measuring the vertical displacement of the stones adjacent to the pile. To avoid disturbances due to the irregularities of the stones the sinking was measured with reference to the same point marked on the stone. In case of large rotations or if the stone was covered by other stones the measuring of the sinking of that stone was disregarded. In the case when a disregarded stone was likely to be the stone with maximum sinking the entire test was disregarded. Based on the results of the tests it was found that the maximum sinking always occurred for the stone upstream of the pile or on the sides of the pile (stone positions 1, 2, 3, 7 and 8 in Fig. A.3). The number of stones where the sinking was measured around the pile was between three and eight for each test. In the case of only three stones were measured, these were 1, 3 and 7.

Along with the sinking of the stone adjacent to the pile, the scouring and deposition of sand in the area around the pile was measured using measuring pins (3 mm in diameter) with scales in the form of colored strips. The pins were placed in and around the scour protection.

A.3 Test Conditions

One sand size was used for the experiments, $d_{50} = 0.18$ mm. The pile diameter, D_p, was changed in the interval 7.5 cm to 20.0 cm. The extent of the scour protection, w_{cover}, was kept in the interval of 20 to 90 cm giving a relative extension of the scour protection, w_{cover}/D_p, of 2.0 to 4.5, in which w_{cover} is the plan-view extension of the scour protection from upstream edge to downstream edge. The size of the cover stones, D_{cover}, was in the interval 1.9 cm to 10.3 cm (d_{50}) and applied in one to three layers. The water depth, h, was maintained at 29 cm to 30 cm and at 56 cm, giving a relative water depth, h/D_p, of 2.1 to 5.1. The velocity, $U_{D/2}$, at half the pile diameter above the bottom was kept within the interval 35 cm/s to 55 cm/s giving a Shield parameter from 0.10 to 0.23 in which θ is defined as:

$$\theta = \frac{U_f^2}{g(s-1)d_{50}}$$

where U_f, the friction velocity associated with the far field, is calculated using the Colebrook-White equation.

Three different materials were used for the scour protection: Round stones with a mean diameter (d_{50}) of $D_{cover} = 10.3$ cm with $d_{15} = 9.0$ cm and $d_{85} = 11.2$ cm, The stones were used in one layer with a mean thickness of 7.6 cm; crushed stones with mean diameter of $D_{cover} = 4.3$ cm with $d_{15} = 3.7$ cm and $d_{85} = 4.9$ cm and, the stones were used in one, two and three layers with a mean thickness of 3.2, 6.2 and 9.0 cm, respectively; crushed stones $D_{cover} = 1.9$ cm with $d_{15} = 1.6$ cm and $d_{85} = 2.8$ cm, the stones were used in one and two layers with a mean thickness of 1.8 and 3.3 cm, respectively.

A.4 Results

A.4.1 Fixed-Bed Results

The flow around/in the scour protection around the monopile has been investigated using flow visualization and velocity measurements (LDA). The flow visualizations were made by adding blue and green dye at the edge of the scour protection and in between the stones adjacent to the upstream side of the pile. Only one layer of 4 cm stones was used in order not to block the view of the flow near the base bottom and to keep the overall view relatively simple.

The flow visualizations showed that flow pattern around the monopile is very similar to the pattern around an unprotected monopile. The flow around an unprotected pile has been studied extensively and the results are

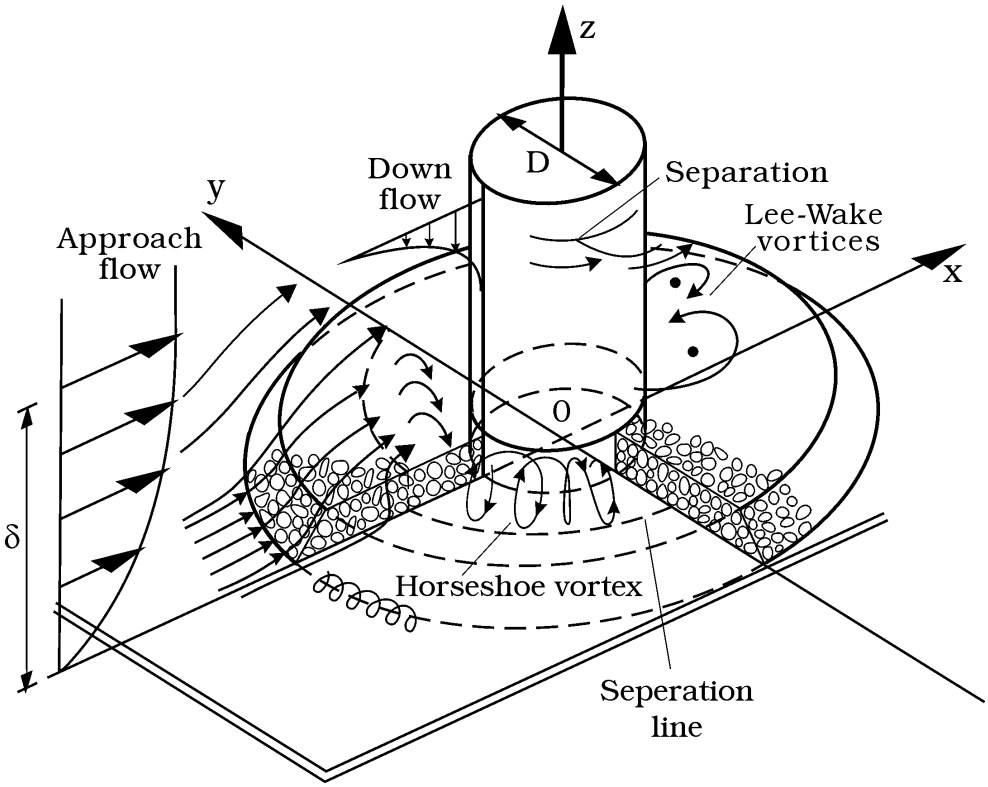

Figure A.4: *Sketch of the flow around a mono-pile with scour protection.*

compiled in for example Sumer and Fredsøe (2002). In relation to scour development the most important flow feature is the horseshoe vortex, see for example Baker (1979, 1985); Dalton (1982); Dargahi (1989) and Roulund *et al.* (2005).

The present flow visualization showed that the horseshoe vortex is still the main reason for the removal of sediment close to the upstream side of the pile, see Fig. A.4: When adding dye at the top of the stones adjacent to the upstream side of the pile, the dye was transported down into the stones and then upstream in between the stones. Around 10 to 15 cm from the upstream edge of the pile and 10 to 15 cm from the upstream edge of the scour protection these two, opposite directed flows met at a separation line. At the separation line they were forced upwards into the main flow and transported away.

By adding dye at the upstream edge of the scour protection two important flow patterns were observed: Small horseshoe vortices were generated in front of the protection stones (as sketched in Fig. A.4) while water was able to flow into the scour protection in the gaps between the stones.

Flow visualizations were made at different position at the side of the pile and downstream of the pile. These flow visualizations showed no important flow features in relation to the sinking of the scour protection. The flow at the side of the pile was dominated by the downstream part of the horseshoe vortex. A flow into the scour protection at the downstream edge of the scour protection was observed, but this flow was weak and it has not been possible to relate it to any important effect in relation to the sinking of the scour protection. The most important flow feature at the downstream side of the cylinder is the vortex shedding, see Fig. A.4. The live-bed tests showed that the vortex shedding was not causing any significant sinking, however.

Velocity profiles in between the stones have been measured from approximately 1.5 cm above the base bottom to the surface using LDA. The reason for the relatively large distance from the base bottom to the lowest measuring point was that the LDA probe needed to be vertical in order to measure in between the stones. This caused some heavy reflections from the base bottom which made it impossible to measure closer to the bottom with the available equipment.

The velocity profiles upstream of the pile are shown in Fig. A.5. It is clearly seen that a significant return flow is present in between the stones up to around 10 cm from the edge of the pile. This is consists very well with the results of the flow visualizations.

As mentioned previously, small horseshoe vortices were observed in front of the protection stones at the upstream side of the scour protection. This will, combined with the inflow in the gaps between the stones, cause edge scour. However, edge scour is not a problem as long as the scour protection is large enough and contains enough material. With the edge scour, the stones will slump down into the scour hole and form a protective slope.

The flow into the scour protection at the downstream side of the pile is very weak and is not able to carry any significant amount of sediment. The sediment bed tests showed a significant deposition of sediment in between the stone in the wake of the pile and only very little or no sinking at all at the downstream edge of the pile, contrary to the case of an unprotected pile, where the vortex shedding is responsible for the scour at the downstream side of the pile, see e.g. Sumer and Fredsøe (2002).

A.4.2 Live-Bed Results

The live-bed tests showed a clear correlation between the sinking of the scour protection, the stone size, the thickness of the scour protection and the pile diameter. The flow visualizations showed that the horseshoe vortex penetrated into the scour protection.

Based on the results of the flow visualizations and the velocity mea-

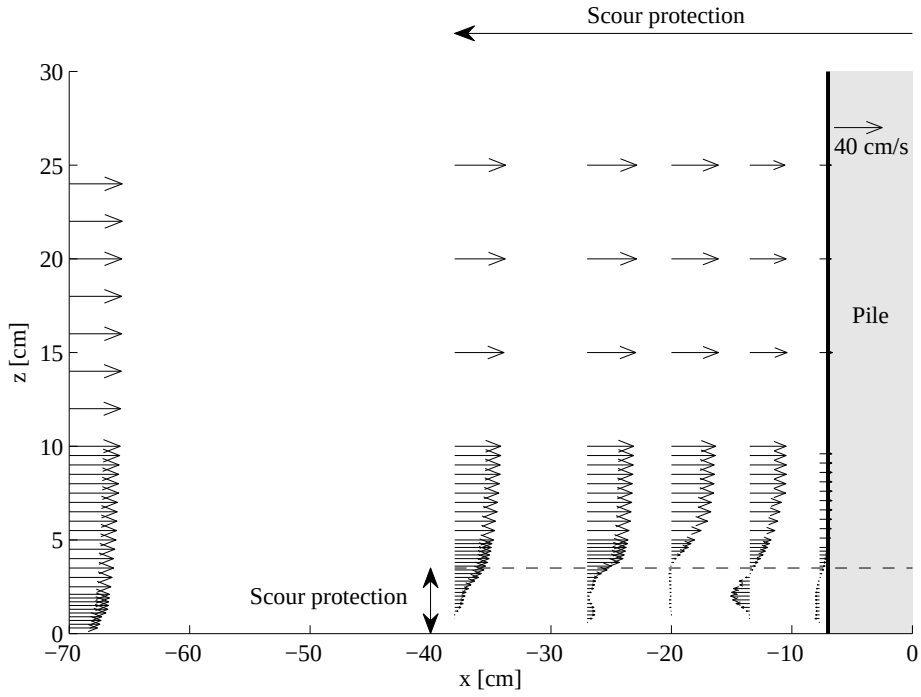

Figure A.5: *Velocity profiles at different distances to the mono-pile with one layer of 4 cm stones. The undisturbed velocity is 40 cm/s.*

surements the flow pattern around the pile causing the sinking of the scour protection can be described as follows: The horseshoe vortex caused by the pile penetrates into the scour protection and causes scouring adjacent to the upstream side of the pile. The scoured material is transported by the horseshoe vortex either upstream to the separation line or to the sides. The material will in both cases be deposited in between the stones, relatively far from the pile or, if the horseshoe vortex is strong enough, sucked/winnowed up into to the main body of the flow and transported downstream. The reason for the suction/winnowing of the sand out from the scour protection is a combination of suction by the main flow, as described in Sumer *et al.* (2001), and the upward directed flow at the separation line between the incoming flow and the horseshoe vortex. The tests have shown that the deposition inside the scour protection is very limited on the upstream side of the pile, and for this reason most of the sediment must be sucked out from the scour protection and transported away. Sumer *et al.* (2001) used the parameter e/D_{stone} as the non-dimensional parameter for the sinking of

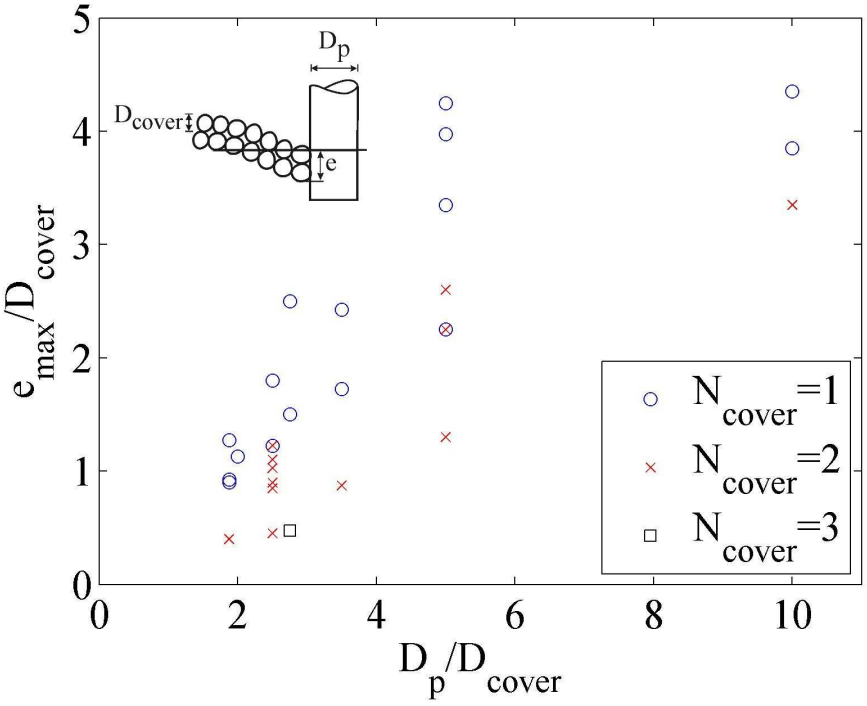

Figure A.6: *Results of the live-bed tests. The range of θ is $0.10<\theta<0.23$ and that of h/D_p is $1.5\leq h/D_p \leq 5.1$.*

an undisturbed protection layer. The process for a scour protection around a pile is in many ways similar to that described above and the parameter e/D_{cover} is also adopted for the present process as well.

The size and strength of the horseshoe vortex is determined by the flow velocity and the pile size. The velocity is indirectly included in the Shields parameter, while the pile diameter is not included in any of the other parameters above. The horseshoe vortex causes the removal of the sediment and a larger pile/horseshoe vortex will, in absolute terms, cause a larger sinking. On the other hand, for a given pile diameter, the larger the ratio D_p/D_{cover}, the larger the penetration of the agitating forces. Therefore the sinking, e_{max}/D_{cover}, should be larger for larger values of D_p/D_{cover}. If the ratio $D_p/D_{cover} = 0$ the situation is the undisturbed protection, Sumer *et al.* (2001). In this case Sumer *et al.* (2001) showed that the ratio $e_{max}/D_{cover} = 0.1$ for one layer of stones, in agreement with the trend seen in Fig. A.6.

Fig. A.6 shows the non-dimensional sinking relative to the non-dimensional pile size for $0.06<\theta<0.20$. There is a clear trend that the larger the pile di-

ameter, the larger the sinking. This is obviously linked to the horseshoe vortex; the larger the pile diameter, the larger the horseshoe vortex, and the larger the scour underneath the stones, and therefore the larger sinking. The sinking decreases for increasing number of layers. When the number of layers is increased from one to two the sinking is decreased with around a factor of two for D_p/D_{cover} smaller than around 5, however, the effect is much smaller for $D_p/D_{cover} = 10$. There have only been made one test with three layers and considering the scatter of the results with one and two layers it is not clear if the third layer provide any significant extra protection.

Regarding the scatter in the data in Fig. A.6, this may be attributed to the way in which the stones are laid around the model pile, considering the fact that the stone size in the tests was relatively large.

A.5 Conclusion

The mechanism causing sinking of the scour protection adjacent to the monopile has been identified as the horseshoe vortex penetrating into the scour protection. When the horseshoe vortex penetrates into the scour protection it transport the sediment adjacent to the pile upstream, where it is winnowed and transported away by the main flow.

It is found that a larger pile diameter relative to the size of the protection stones will cause a larger sinking. The maximum sinking is found to be approximately 4 to 4.5 times the diameter of the cover stones in case of one layer of stones and approximately 3 to 3.5 in case of two layers of stones.

Two layers of stones will decrease the sinking relative to one layer of stones with the same size. For values of D_p/D_{cover} smaller than approximately 5 the sinking seems to be reduced by a factor of two if the number of layers is increase from one to two.

Acknowledgement

This research was carried out as part of the Statkraft Ocean Energy Research Program, sponsored by Statkraft (www.statkraft.no). The study was partially supported by the Danish Council for Strategic Research (DSF)/Energy and Environment under the program Seabed Wind Farm Interaction (http://sbwi.dhigroup.com, sagsnr. 2104-07-0010) and DHI (www.dhigroup.com). The fixed-bottom experiments and a major part of the live-bed experiments were conducted by MSc Adriana Hudecz. A part of the live-bed experiments were conducted by François Roignant.

Appendix B

Surveys of Horns Rev I Wind Farm Area

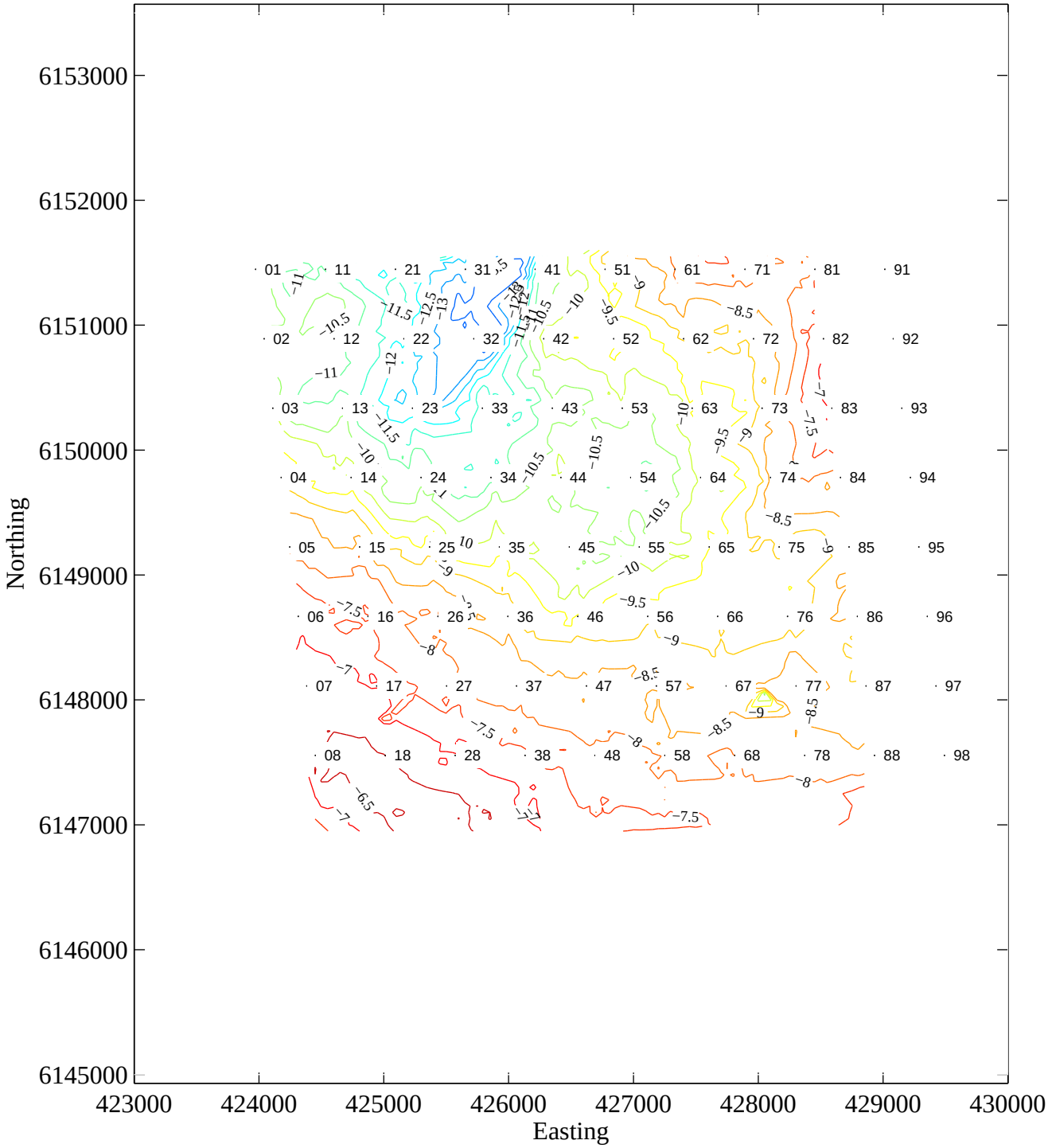

Figure B.1: *Bathymetry of the Horns Rev 1 Wind Farm area (1998 survey). The coordinates are UTM zone 32U. Adapted from Nielsen (2007). Courtesy of Vattenfall and Dong Energy.*

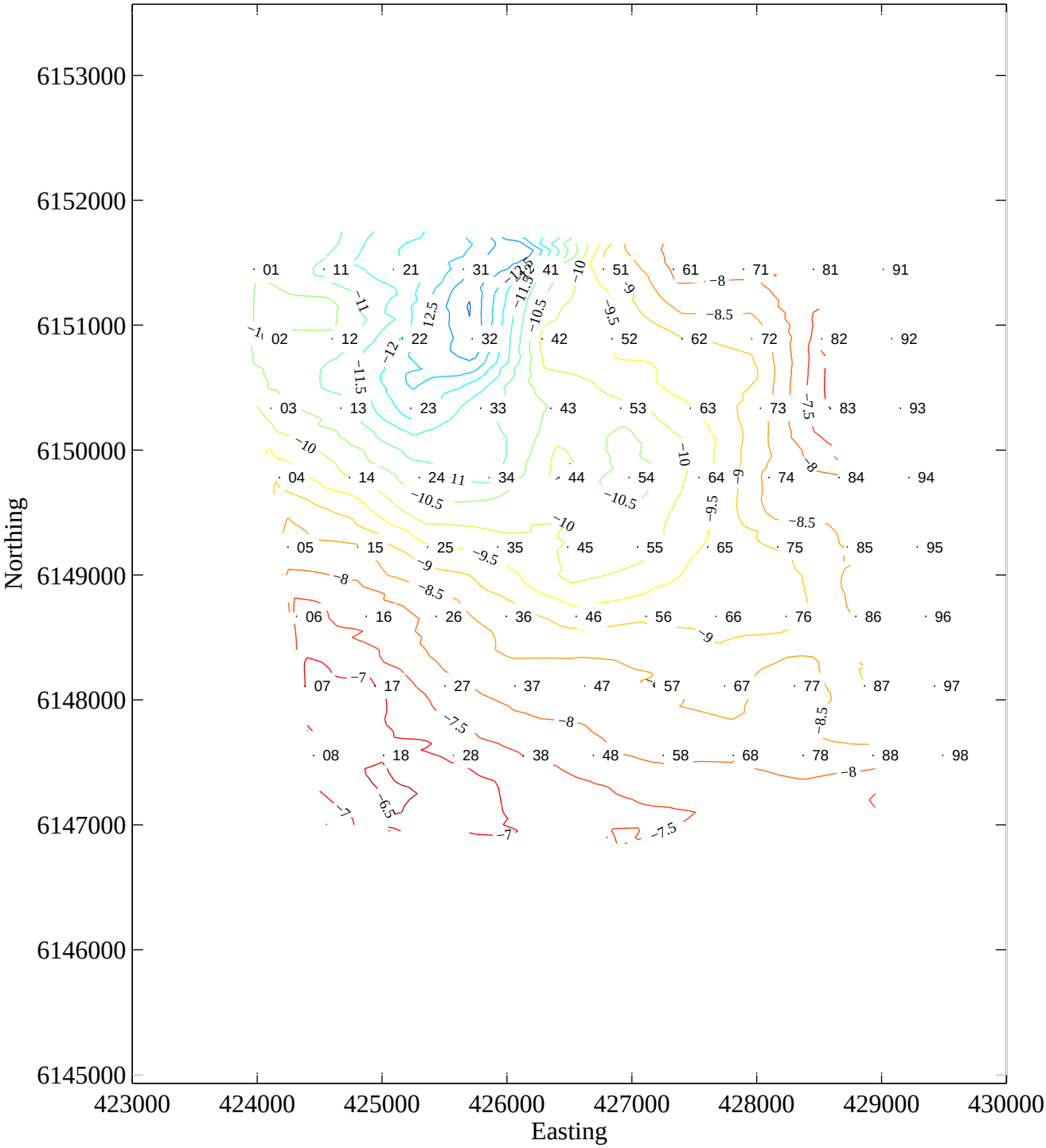

Figure B.2: *Bathymetry of the Horns Rev 1 Wind Farm area (1999 survey). The coordinates are UTM zone 32U. Adapted from Nielsen (2007). Courtesy of Vattenfall and Dong Energy.*

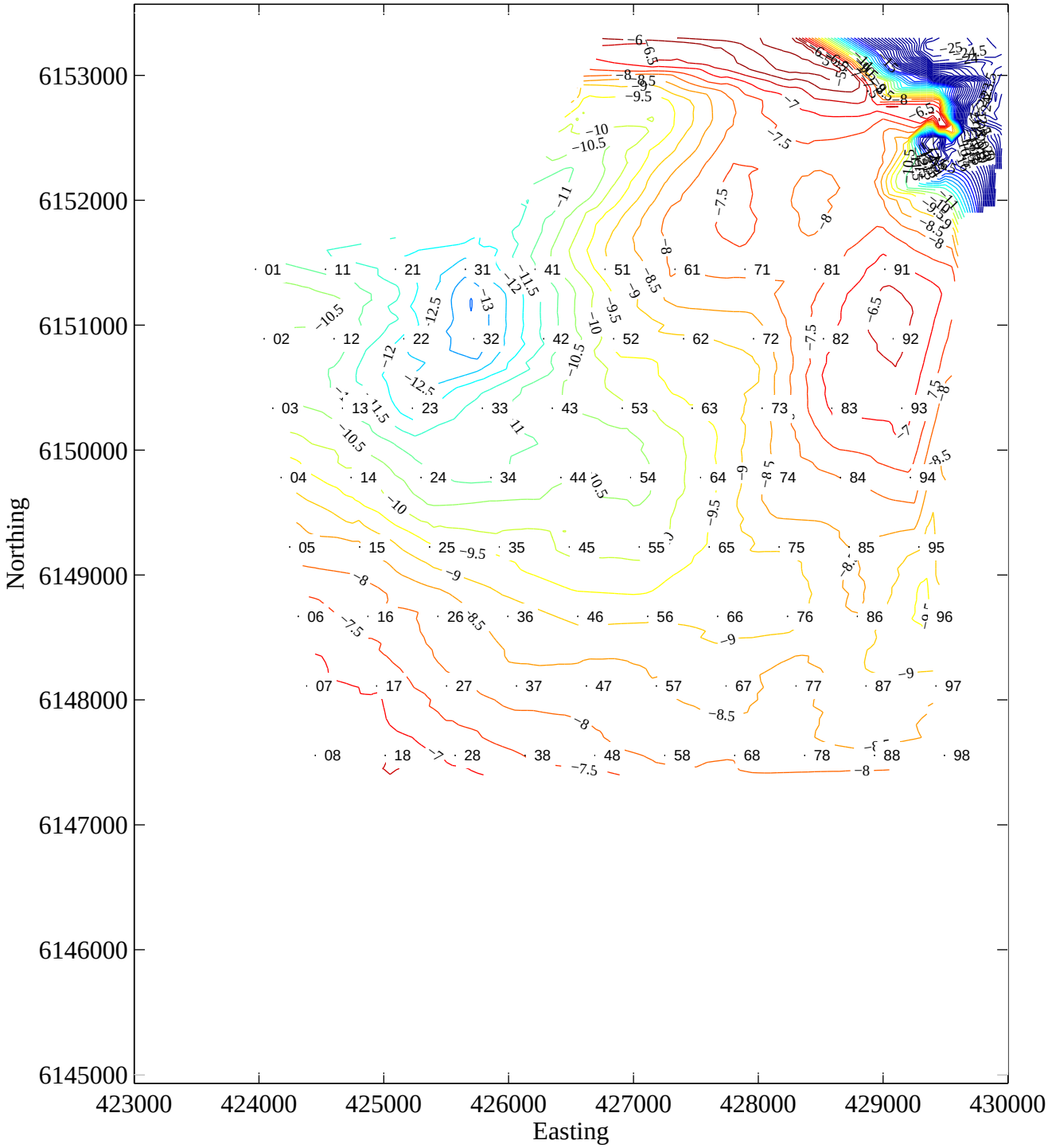

Figure B.3: *Bathymetry of the Horns Rev 1 Wind Farm area (2000 survey). The coordinates are UTM zone 32U. Adapted from Nielsen (2007). Courtesy of Vattenfall and Dong Energy.*

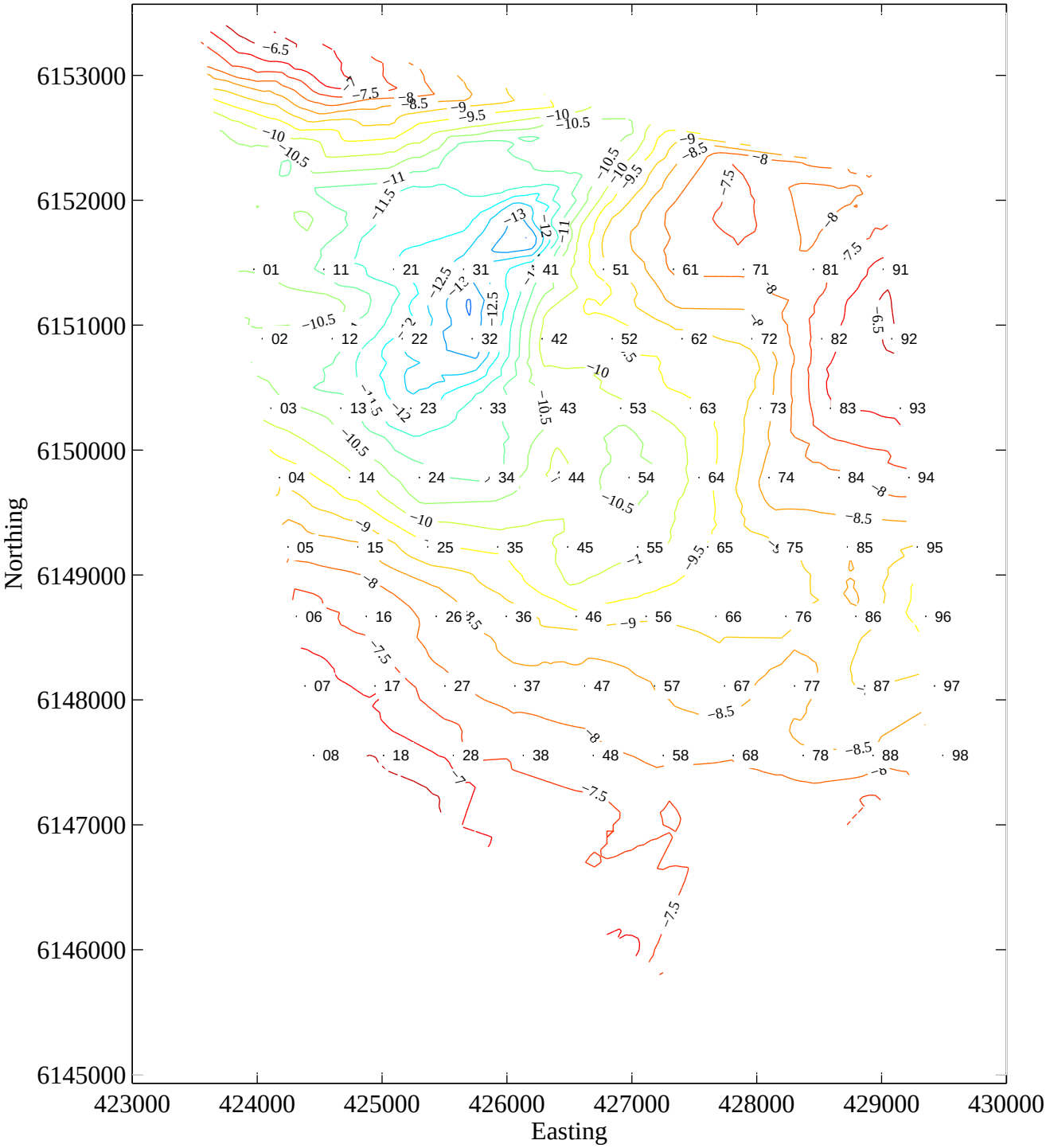

Figure B.4: *Bathymetry of the Horns Rev 1 Wind Farm area (2001 survey). The coordinates are UTM zone 32U. Adapted from Nielsen (2007). Courtesy of Vattenfall and Dong Energy.*